ELECTROCOAGULATION DRIVEN FABRICATION OF METAL-ION-CONTAINING GRAPHENE OXIDE FILMS

by

Clovis Weisbart

A Dissertation Submitted to the Faculty of the

DEPARTMENT OF MATERIALS SCIENCE AND ENGINEERING

In Partial Fulfillment of the Requirements

For the Degree of

DOCTOR OF PHILOSOPHY

In the Graduate College

THE UNIVERSITY OF ARIZONA

2018

THE UNIVERSITY OF ARIZONA
GRADUATE COLLEGE

As members of the Dissertation Committee, we certify that we have read the dissertation prepared by ***Clovis Weisbart***, titled ***Electrocoagulation Driven Fabrication of Metal-Ion-Containing Graphene Oxide Films*** and recommend that it be accepted as fulfilling the dissertation requirement for the Degree of Doctor of Philosophy.

Dr. Barrett G. Potter Jr. Date: (***05/29/2018***)

Dr. Krishna Muralidharan Date: (***05/29/2018***)

Dr. Srini Raghavan Date: (***05/29/2018***)

Final approval and acceptance of this dissertation is contingent upon the candidate's submission of the final copies of the dissertation to the Graduate College.

I hereby certify that I have read this dissertation prepared under my direction and recommend that it be accepted as fulfilling the dissertation requirement.

Dissertation Director: ***Dr. Barrett G. Potter Jr.*** Date: (***05/29/2018***)

Dissertation Director: ***Dr. Krishna Muralidharan*** Date: (***05/29/2018***)

STATEMENT BY AUTHOR

This dissertation has been submitted in partial fulfillment of the requirements for an advanced degree at the University of Arizona and is deposited in the University Library to be made available to borrowers under rules of the Library.

Brief quotations from this dissertation are allowable without special permission, provided that an accurate acknowledgement of the source is made. Requests for permission for extended quotation from or reproduction of this manuscript in whole or in part may be granted by the head of the major department or the Dean of the Graduate College when in his or her judgment the proposed use of the material is in the interests of scholarship. In all other instances, however, permission must be obtained from the author.

SIGNED: Clovis Weisbart

ACKNOWLEDGEMENTS

I would like to first and foremost express my deepest appreciation and gratitude to every member of my committee: Dr. Barrett G. Potter Jr., Dr. Krishna Muralidharan, and Dr. Srini Raghavan. They supported and mentored me throughout the entirety of my graduate career. They were patient, helpful, and caring. The combination of their expertise, broad knowledge, and creative thinking helped inspire me and was essential to my research accomplishments. Most importantly, they led by example and showed me how to become a good researcher and scholar.

I would like to thank multiple faculty members at the University of Arizona: Dr. Kelly Potter for accepting to be part of my Oral Comprehensive Exam committee, Dr. Pierre Deymier for allowing me to use his wave function generator, Mary Kay Amistadi for her help with the ICP-MS analysis, Paul Lee for his help with XPS analysis, Dr. Paul Wallace for his help with SEM analysis, Dr. Jerry Yang for his help with TEM analysis, and Dr. Reyes Sierra for allowing me to use her zetasizer. I would also like to acknowledge the colleagues who mentored or helped me throughout my research career: Wei-Jie Huang, Ryan Biggie, Dongni Ma, Bing Wu, Yusuke Watanabe, Ben Geller, Ryan O'Connell, Neil Jenkins, Deepak Sridhar, Tony Gnanaprakasa, and Jillian Grass. Finally, I would like to thank my family for their support and encouragement.

DEDICATION

I would like to dedicate this dissertation to my parents, Jon and Veronique, for their love, support, and encouragement.

Table of Contents

List of Figures

List of Tables

Abstract

The development of simple, solution-based techniques for the formation of graphene oxide (GO) films is of great interest to the materials community due to the potential application of these films in diverse areas such as filtration membranes and anticorrosion coatings. Further, the reduction of graphene oxide (GO) has been a reliable route to restore electrical conductivity and to obtain chemically modified graphene platelets in large scale and low cost for electronic and energy storage technologies.

The stability of GO films in aqueous systems (e.g. for coatings or membrane applications) is often driven by the presence of multivalent, cationic metal contaminants that serve as strong cross-linkers between GO platelets. However, the incorporation of the metal ions into GO suspensions used for film formation is often uncontrolled. In contrast, this work demonstrates the rapid formation of GO films containing metal ions that are introduced using an easily implemented, electrochemical approach that enables the metal ion content and resulting film properties to be tailored. Specifically, the method is based on the electrocoagulation of GO particles onto a Cu substrate/electrode. In this process, the Cu ions used to cross-link and form the GO film are electrochemically evolved from the Cu electrode itself.

Tuning of EC-driven GO film deposition was explored using a number of approaches, including size tuning of GO particles in suspension via chemical coagulation prior to deposition and the control of applied voltage, deposition time and suspension concentration. Moreover, the frequency dependence of AC-applied voltage on the resulting film evolution and resulting microstructure was also examined.

An electrochemical reduction of the resulting GO films was subsequently used to produce reduced graphene oxide. Cyclic voltammetry was successful in identifying the primary

reduction potentials for both the Cu^{2+} and GO present in the film offering a means to selectively reduce these individual constituents. With this information, a constant potential technique was applied to produce reduced graphene oxide films exhibiting greater conductivities than those typically observed in thermally or chemically reduced graphene oxide films (for example: up to 36% increase compared to hydrazine reduction and up to 200% increase compared to thermal exfoliation). These results offer new avenues for employing GO and reduced GO in a wide variety of technology, energy, and membrane applications.

Chapter 1: Introduction

Graphene has garnered significant attention from the scientific community due to its remarkable structure-property relations.[1–4] Graphene, an individual layer of graphite, is a monolayer sheet of sp^2 bonded carbon atoms with delocalized π-bonding states in a honeycomb crystal lattice. As a result of its structure, graphene has very promising properties, including excellent electrical conductivity, electron mobility, thermal conductivity, mechanical strength, and chemical stability. This combination of properties enables its use in numerous applications.[1–4] For example, it provides a new and effective avenue for fabricating electrochemical biosensing,[1] photovoltaic,[5] and supercapacitor[6] devices due its capability to promote electron transfer between electroactive species and electrodes.[1] Moreover, its high thermal conductivity, has enabled its application as a highly efficient thermal interface material (TIM) in semiconductor packaging.[7]

While graphene represents an attractive and important material from both a scientific and a technological perspective, there is still the need for new research to refine material synthesis and processing to not only enhance properties but to also to obtain graphene at large scale and low cost. [2,4]

Many techniques have been employed to synthesize graphene. These can be defined in terms of their primary paths toward the final structural form and are often referred to as bottom up and top down.[4] Mechanical exfoliation of graphite is an example of a top-down approach and is the earliest technique reported for the synthesis of graphene.[4] Exfoliation can be accomplished using a variety of agents (such as scotch tape[8] or ultrasonication[4]). However, the technique is very time consuming and it is not inherently scalable. Some of the most notable techniques used in the bottom-up approach include chemical vapor deposition on metal surfaces (such as copper)[9]

and epitaxial growth on silicon carbide[10]. The main disadvantage of these techniques is the very small production scale typically accessed.[4]

In this regard, graphene oxide (GO), the oxidized counterpart of graphene, has recently garnered significant attention from the scientific community. The reduction of GO has become a reliable route for obtaining chemically modified graphene platelets (also referred to as reduced graphene oxide (rGO)) in large scale and low cost. [11,12,13,14,6,15] Furthermore, GO has found uses where pristine graphene is not directly applicable, such as filtration membranes for water treatment [16] and anticorrosion applications[17].

Thin films of GO are of particular interest for applications requiring exceptional stability in aqueous media, e.g. as water desalination membranes. .[18] Their stability in water appears to be driven by the presence of multivalent metal ions within their matrix, that serve as strong cross-linkers.[18] In this context, GO has been found to be an effective absorber of multivalent metal ions.[19–23]

From a chemical perspective, GO has an abundant amount of oxygen atoms on its graphitic backbone in the form of epoxy, hydroxyl, and carboxyl groups.[24] These oxygen-containing functional groups are characterized by an isolated electron pair. By sharing an electron pair, the functional groups can efficiently bind a metal ion to form a metal complex.[19] However, metal cation integration within the material typically occurs during processing steps, such as vacuum filtration.[18] The integration is therefore accomplished in an uncontrolled and sometimes even unintentional fashion.

In this regard, “Project 1” of this dissertation focused on developing a new and improved method for the formation of GO films. The distinguishing feature of this project as compared to GO film synthesis approaches was the utilization of electrocoagulation (EC) as the driver for

rapidly depositing GO films on conductive substrates. This new method allowed for the controllable incorporation of multivalent metal ions within the GO film, which, as previously mentioned, has been shown to provide significant mechanical and structural stability of the GO films. Although the majority of the project focused on the formation of copper-ion containing GO films on copper substrates through the EC-assisted technique, varied material systems (such as stainless steel) were briefly explored. The effect of tuning applied voltage, deposition time, and initial GO suspension concentration on the film deposition rate and concentration of copper ions incorporated in the film was critically assessed.

As previously mentioned, graphene is capable of promoting high electrical conductivity. In distinction, GO is an electrically insulating material due to its disrupted sp^2 bonding networks. Through reduction, the electrical conductivity is capable of being enhanced by restoring the dominant sp^2 network and associated extended π-bond network.[25] GO reduction is therefore necessary for applications where high conductivities are needed (such as biosensors, photovoltaics, and supercapacitors). However, it is important to note that although rGO has very similar properties to pristine graphene, it still contains some oxygen functionalities.[3] It therefore does not reach the same levels of electrical conductivity as graphene.[3] GO reduction can be achieved through chemical, thermal, or electrochemical reduction pathways.[1,6,11,12,14,15,26–30]

Typically, the chemical reduction of GO involves the use of reducing agents, the most common being hydrazine. However, the excessive use of reducing agents could contaminate the resulting product and can be harmful to human health and the environment.[14] Thermal reduction involves the use of high temperature to remove the oxygen functionalities. This can result in significant volume loss.[3] In contrast, electrochemical reduction of GO is a relatively simple, low cost, and an environmentally benign method.

"Project 2" focused on preparing the EC-GO/Cu(II) films for use in applications where high conductivity is needed. Electrochemical reduction was chosen as the reduction method given its relative simplicity and the direct compatibility with the EC deposition process itself. Specifically, electrochemical reduction was done by two distinct techniques: Cyclic Voltammetry (CV) and DC constant potential reduction. The primary objectives of Project 2 were to survey the reduction processes as well provide a thorough electrochemical reduction of both the primary constituents in the system (i.e. GO and Cu^{2+}). This was intended to produce an enhanced conductivity closer to that of pristine graphene (values in order of 10^7 S/m have been reported)[12] relative to traditionally reduced GO films without Cu addition.

The EC-driven fabrication of GO films characteristic of Project 1 is a novel technique. The effect of its processing parameters on film structure, composition, and deposition rate has not been extensively studied, and remains relatively unknown. In this regard, "Project 3" specifically examined the effect of tuning GO particle size on the nature of the deposition process and the resulting film characteristics (deposition rate and concentration of copper incorporated). The particle size was tuned by two approaches. The first approach involved increasing the average particle size prior to electrocoagulation. This was accomplished by the agglomeration of GO particles upon the addition of Cu^{2+} ions to the suspension. The second approach involved applying an alternating current (AC)-field during the electro-deposition of the films. The frequency and duty cycle of the waveform were tuned in an attempt to control the size of the GO particles participating in the deposition.

This dissertation will be arranged in the following manner. Chapter 2 will provide the reader with the necessary background on the structure, synthesis, and reduction of GO as well as the theory and mechanisms behind electrocoagulation. Chapter 3 will focus Project 1, which is

based on an already published manuscript in *Carbon*.[31] Project 2 and Project 3 will be examined in Chapter 4 and Chapter 5 respectively. Finally, Chapter 6 will summarize the research outcomes and their impact and provide an outlook for future work based on the discussed projects.

Chapter 2: Background

2.1 Graphite oxide and Graphene oxide

2.1.1 History and Structure

Graphite, an allotrope of carbon, has a planar, layered atomic structure. Each individual layer of graphite is defined as graphene, a two-dimensional sheet of sp2-hybridized carbon. The extra valence electron not participating in the primary, sp2-based σ-bonding is delocalized within a p-based, π bond. Transient polarization associated with these pi-bonded electrons results in weak van der Waals forces between the graphene layers.[32] The crystal structure of graphite is shown in Fig. 2.1.1. In a similar manner to graphite, graphite oxide also exhibits a layered structure. However, in graphite oxide, the interlayer distance is expanded by the presence of oxygen-containing groups. The oxidized layers are hydrophilic and can be exfoliated in water under moderate ultrasonication or through mechanical stirring.[33] Graphene oxide (GO) is defined as the exfoliated sheets of graphite oxide, characterized by up to several layers of carbon-based sheets, similar to graphene.

Although graphene is regarded as a relatively novel material, the history of graphite oxide extends back to some of the earliest studies concerning the chemistry of graphite. Schafhaeutl first reported graphite oxide in 1840, followed by Brodie in 1859. [3,12] In recent years, graphite oxide and GO have re-emerged as strong research foci due to their roles as precursors for the cost-effective, mass production of graphene-based materials.

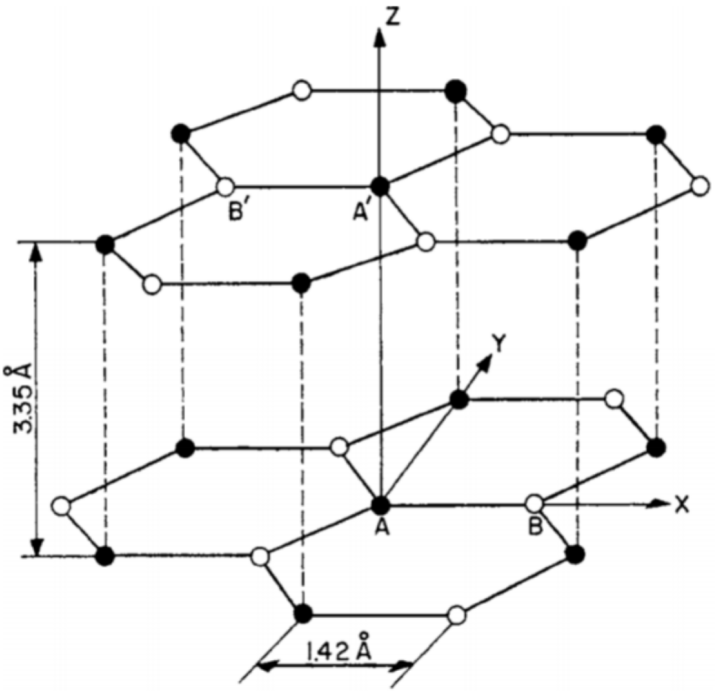

Fig. 2.1.1- The crystal structure of graphite. The primitive unit cell is hexagonal, with dimensions a = 2.46 Å and c = 6.71 Å. The in-plane bond length is 1.42 Å. There are four atoms per unit cell, namely A, A', B and B'. The atoms A and A', shown with full circles, have neighbors directly above and below in adjacent layer planes; the atoms B and B', shown with open circles, have neighbors directly above and below in layer planes 6.71 Å away.[32]

Although GO has been examined for over a century, the chemical structure remains a controversial issue and no unambiguous model exists. The high complexity of GO is due its amorphous character and nonstoichiometric atomic composition. In addition, there was a lack of precise analytical techniques for characterizing such materials. Numerous structural models of GO have been proposed in past decades, including early investigations proposing a regular lattice composed of discrete repeat units (see Fig. 2.1.2). [3,12,34,35] Hofmann and Holst's structure was comprised of epoxy groups spread across basal planes of graphite, with a net molecular formula of C_2O. Ruess' model in 1946 incorporated hydroxyl groups in the basal plane. The structure of the basal plane therefore incorporated sp^3 hybridization of carbon. Scholz and Boehm proposed a model in 1969 in which the epoxide and ether groups are substituted by quinoidal species in a

corrugated backbone. Nakajima and Matsuo later assumed a fourth model in which the lattice framework is similar poly(dicarbon monofluoride). [3,12,34,35]

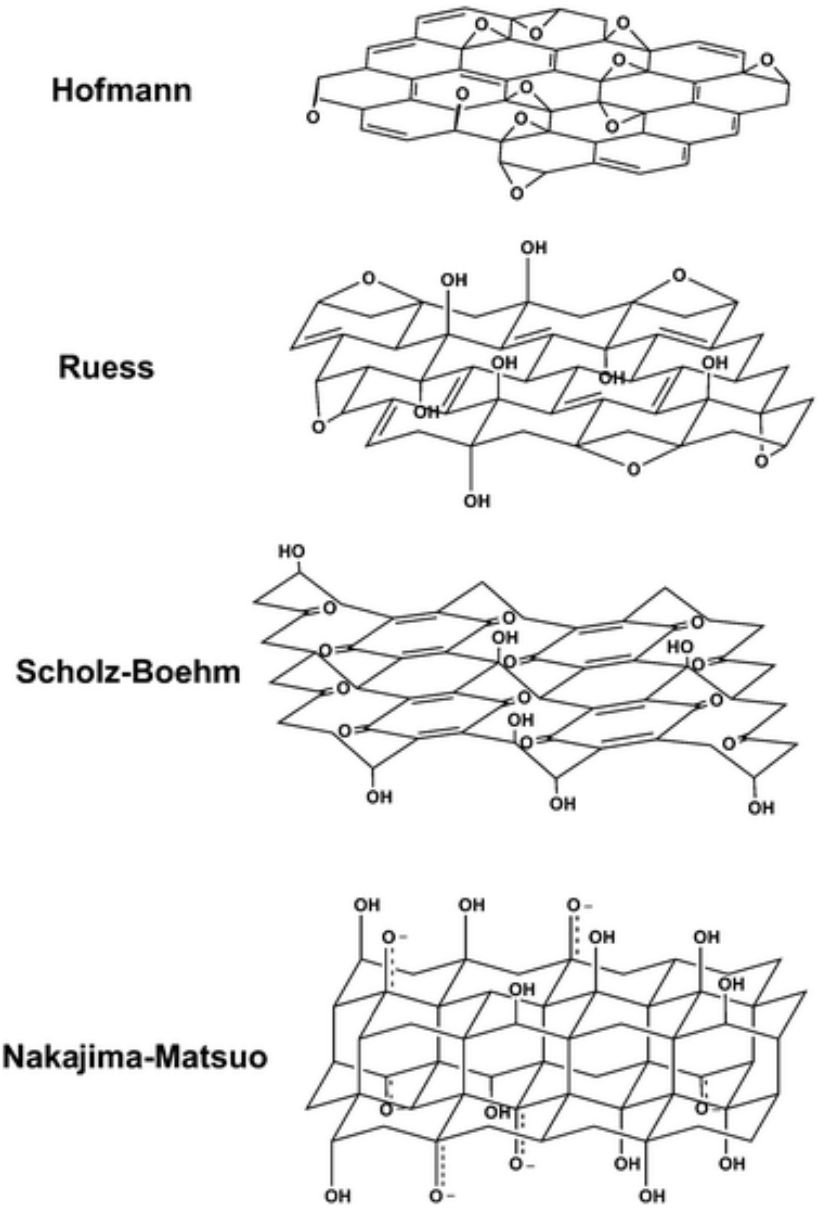

Fig 2.1.2- Summary of several older structural models of GO.[3]

However, most recent models reject the lattice-based model and have concentrated on nonstoichiometric and amorphous alternatives. The most well-known nonstochiometric model is that of Lerf and Klinowski, [3,12,34,35] wherein the carbon plane is decorated with hydroxyl and epoxy (1,2-ether) functional groups. Carbonyl groups are also present, most likely as carboxylic

acids along the sheet edge but also as organic carbonyl defects within the sheet. A proposed schematic is shown in Fig. 2.1.3. Though the Lerf–Klinowski model remains largely unchallenged in subsequent studies, others have made slight modifications to the proposed structure. One exception is the more recent the Dékány model, which assumes that GO is composed of two distinct domains. There are trans-linked cyclohexyl species interspersed with tertiary alcohols and 1,3-ethers, as well as a corrugated network of keto/quinoidal species.[3], [35]

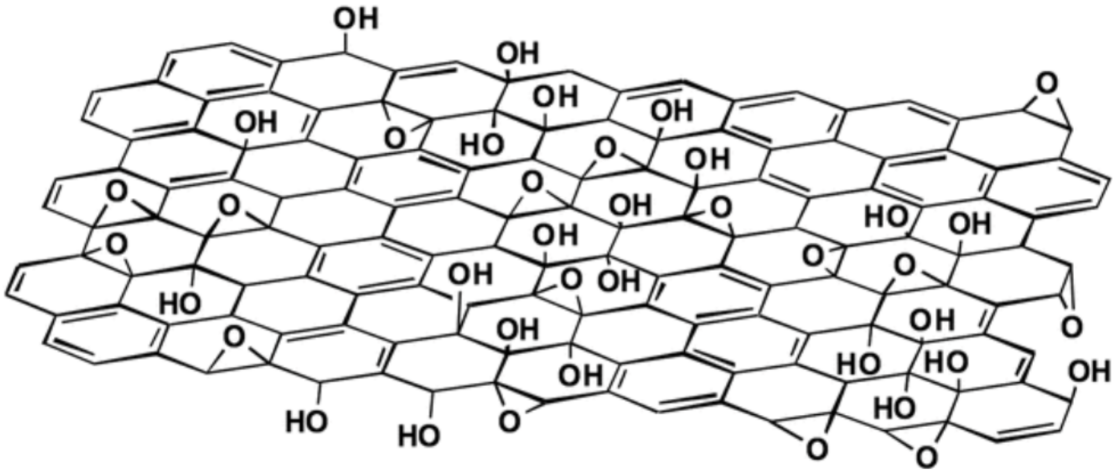

Fig. 2.1.3- A proposed schematic (Lerf-Klinowski model) of graphene oxide structure.[36]

2.1.2 Synthesis

While there are many GO models, no single model has successfully described the GO structure and composition fully. Furthermore, the various oxidation methods used to form GO from graphite not only result in varying degrees of oxidation, but also produce intrinsically different oxygen functionalities. This oxygen groups differ in terms of type, quantity and location along the basal plane of graphite. In this context, the effectiveness of an oxidation process is often evaluated by the carbon/oxygen ratios of the graphite oxide. Graphite oxide is

synthesized using numerous methods, notably: Staudenmaier, Hofmann, Brodie, Tour, and Hummers[37] methods. Many variations of these methods exist, with improvements constantly being explored to achieve better results and more inexpensive processes. [2,26,38]

Brodie was the first to report work on the synthesis of graphite oxide in 1859.[3,38,39] In his method, graphite was mixed with potassium chlorate ($KClO_3$) in a 1:3 ratio. The mixture reacted in fuming nitric acid (HNO_3) at 60°C for 4 days. Successive oxidative treatments resulted in a further increase in the oxygen content until a limit was reached. An elemental analysis revealed a composition of approximately 60 wt% C, 2 wt% H and 38 wt% O. The resulting product was soluble in neutral or basic aqueous solutions, but not acidic.[2], [38] In 1898, Staudenmaier added $KClO_3$ in multiple aliquots over the course of the reaction and replaced about two thirds of the fuming HNO_3 with concentrated sulfuric acid (H_2SO_4) to increase the acidity of the mixture. With this slight modification, he allowed the overall reaction to take place in a single vessel and by extension simplified the synthesis. However, the duration of the synthesis was unaffected and the extent of the oxidation was similar to Brodie's method (C:O was approximately 2:1 by atomic weight)[2,38]

Hummers and Offerman developed the most widely applied synthesis method 60 years later.[3] In the Hummers method, 100g of graphite powder, 50g of sodium nitrate ($NaNO_3$), 2.3L of concentrated H_2SO_4, and 300g of potassium permanganate ($KMnO_4$) are used in the oxidation process. The reaction occurs between graphite and H_2SO_4, while $KMnO_4$ and $NaNO_3$ act as catalysts. The Hummers method has several advantages over earlier techniques. The reaction time is significantly decreased. Indeed, the reaction is completed in a matter of hours instead of days. Furthermore, the replacement of $KClO_3$ with $KMnO_4$ allows for increased reaction safety. $KClO_3$ can evolve into chlorine dioxide (ClO_2), which may explosively decompose into chlorine

and oxygen. In addition, the fuming HNO_3 used in the previous methods is replaced with $NaNO_3$, thereby eliminating the formation of acid fog. [2,26,38–41]

However, the Hummers method still suffers from several flaws. Notably, the oxidation procedure releases toxic gasses such as NO_2 and N_2O_4. Additionally, the residual Na+ and NO3 ions are difficult to remove from the wastewater formed from the GO synthesis and purification processes. There have been many modifications and improvements to the Hummers method over the years.[2,39] Chen et al. found that the removal of $NaNO_3$ does not affect the yield or the degree of oxidation in the resultant graphite oxide. From this finding, they demonstrate an improved Hummers method for the eco-friendly synthesis of GO.[2,39] The work presented in this manuscript uses Chen et al.'s method for the synthesis of its GO.

2.1.3 Reduction

Unlike graphene, GO is an electrically insulating material due to its disrupted sp2 bonding networks. However, electrical conductivity can be recovered by restoring the π-bond network through reduction.[3] Reduction of GO has been a reliable route for obtaining chemically modified graphene platelets in large scale and at low cost.[1,6,11,13,14] GO reduction to reduced graphene oxide (rGO) can be achieved through variety of means, the most common involving chemical, thermal, or electrochemical reduction pathways.[1,6,11,13,14] All techniques lead to products that resemble pristine graphene to varying degrees based on their electrical, thermal, and mechanical properties and their film surface morphology.[3] Fig. 2.1.4 illustrates the main steps involved in synthesizing rGO from graphite. Graphite needs to be oxidized to graphite oxide, which then needs to be exfoliated and reduced (steps can happen simultaneously). It is important to note that the term "reduction" in the graphene community is a colloquial term used and not a rigorous use of reduction in terms of oxidation state change of the carbon atoms. The

term chemical converted graphene (CCG) is sometimes used instead of rGO for the reason stated above.

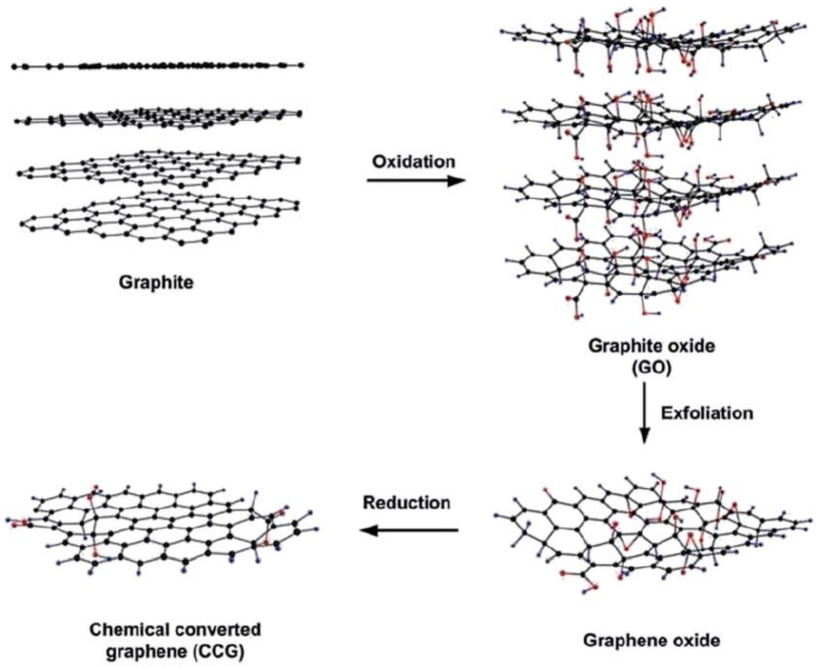

Fig. 2.1.4- Preparation of RGO.[26]

Thermal reduction

Graphite oxide can be reduced by heat treatment. This process is called thermal annealing reduction and is usually carried out in a vacuum, inert, or reducing atmosphere. In the early stages of graphene research, it was shown that rapidly heating graphite oxide (above 2000 °C/min) would allow for exfoliation. The exfoliation occurs by a sudden expansion of carbon monoxide (CO) or carbon dioxide (CO_2) evolved from the spaces between graphene sheets during the rapid heating of the graphite oxide. The rapid temperature increase allows for functional groups containing oxygen to decompose into gases. [3,12,26] The decomposition leads to a high enough pressure between the stacked carbon layers to induce separation. The Hamaker

constant A can be defined for a Van der Waals body-body interaction by: $A=\pi^2.C.\rho_1.\rho_2$, where ρ_1 and ρ_2 are the number densities of the two interacting particles and C is the coefficient from the Van der Waals pair potential. Evaluation of the Hamaker constant predicts that a pressure of only 2.5 MPa is necessary to separate two stacked GO platelets, and based on state equations, 40 MPa is generated at 300 °C and 130 MPa is generated at 1000 °C. [3,12,26]

The rapid heating process therefore has a dual effect. Not only does it exfoliate graphite oxide, but it also reduces the density of oxygen-based functional groups. However, this procedure is known to cause structural damage to the platelets during the release of CO_2. Approximately 30% of the mass of graphite oxide is lost during the exfoliation, which leaves behind lattice defects throughout the graphene sheet.[3,12] The defects affect the electronic properties of the rGO product by diminishing the ballistic carrier transport path length and forming scattering sites. Electrical bulk conductivities ranging from 10 to 23 S/cm have still been measured, demonstrating the potential for effective reduction and restoration of the planes' electronic structure via appropriate process control.[3,12,26]

It is important to note that unconventional heating sources such as microwave irradiation (MWI) and photo-irradiation have been used to accomplish thermal reduction. These unconventional methods offer certain advantages over the conventional anneal method. MWI allows for a rapid and uniform heating of graphite oxide. In a commercial microwave oven, rGO can be readily obtained within 1 min under ambient pressure.[12,26] Photo-irradiation of GO is a additive free, facile, clean, and versatile approach to reduce GO. High-quality rGO has been prepared by irradiating GO with sunlight, ultraviolet light, xenon flash lamps and KrF excimer lasers. In addition, rGO patterns can be easily fabricated with photomasks, which facilitates the direct fabrication of electronic devices based on rGO films.[12,26,28,42] Fig. 2.1.5 illustrates an rGO

pattern created by flash reduction and by femtosecond laser reduction.

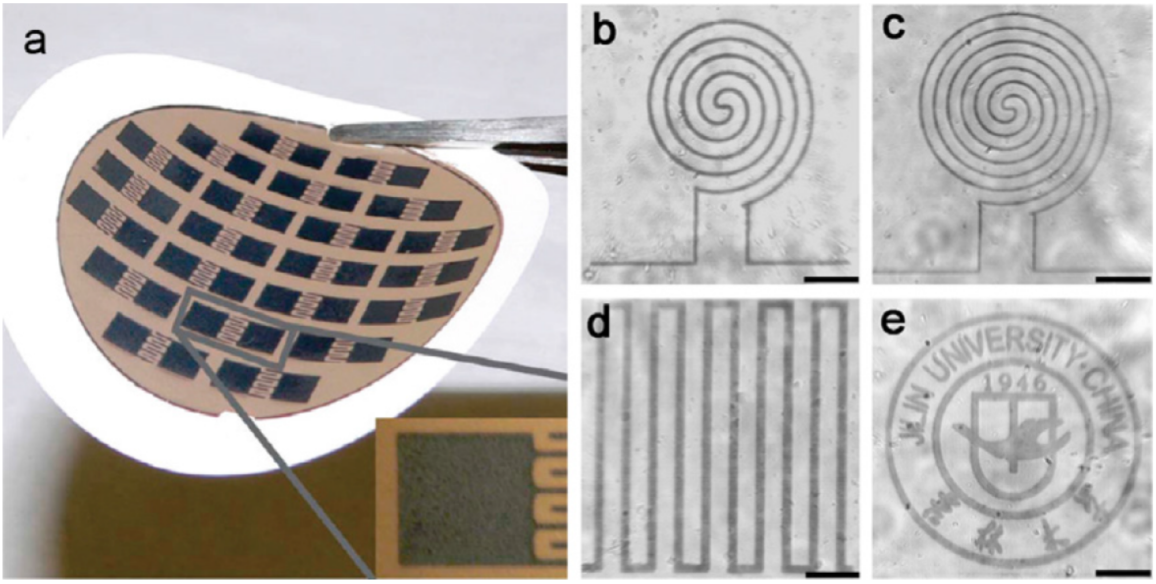

Fig. 2.1.5- Patterned rGO film obtained by (a) flash reduction [42] (Copyright 2009 ACS) and (b–e) femtosecond laser reduction [28]. Scale bars, 10 lm (Copyright 2009 Elsevier). The black parts in the films are the reduced GO patterns.[12]

Chemical reduction

Chemical reduction of GO is the most widely used technique for the preparation of rGO. When GO is colloidally dispersed, it can be reduced by a variety of chemical means. Chemical reductions can usually be realized at room temperature or by moderate heating.[12] Chemical reductions therefore ljmit the need for equipment and have fewer environmental constraints than thermal annealing reduction. This makes chemical reduction a cheaper alternative to thermal annealing. As described earlier the rGO formed resembles graphene but contains residual oxygen and other hetero atoms, as well as structural defects.[26]

Reducing GO with very strong reducing agents can be problematic since most strong reductants have varying degrees of reactivity with water, commonly used for dispersing GO. Hydrazine monohydrate does not have reactivity with water, making it an often used method for

reducing aqueous dispersions of graphene oxide.[3] However, the use of hydrazine (N_2H_4) introduces heteroatomic impurities. Nitrogen is very effective at removing oxygen functionality, but usually stays covalently bound to the surface of GO, likely in the form of hydrazones, amines, aziridines or other similar structures. There is no facile approach as of now to remove these impurities.[3,12] Sodium borohydride (NaBH4) has been shown to function more effectively than hydrazine as a reductant of GO. However, NaBH4 is slowly hydrolyzed by water and the scalability of such an approach remains questionable.[3,12] Other reducing agents such as phenyl hydrazine, hydrazine hydrate, sodium borohydride, ascorbic acid, glucose, hydroxylamine, hydroquinone, pyrrole, amino acids, strongly alkaline solutions and urea have been explored for the chemical reduction of GO.[13–15,26,27]

Electrochemical reduction

Electrochemical reduction of GO can be accomplished in a typical electrochemical cell using an aqueous buffer solution under ambient conditions. It does not require chemical agents and is mainly caused by the electron exchange between GO and electrodes. It is a route, which avoids the high production costs and environmental constraints of thermal annealing reduction and avoids the use of dangerous and toxic reductants (such as hydrazine) and by-products in chemical reduction.[1,3,12,14] Electrochemical reduction of GO can be carried out through two different routes: a one-step approach and a two-step approach (see Fig. 2.1.6). In the one-step approach, GO sheets from an aqueous colloidal suspension are simultaneously reduced and deposited as an rGO film on an electrode surface in the presence of buffer electrolyte. On the other hand, in the two-step approach, a film of GO is first deposited onto the surface of an electrode, and then the GO-coated electrode is electrochemically reduced on the electrode

surface to form rGO. [14] The work presented in this manuscript primarily focuses on the two-step reduction approach.

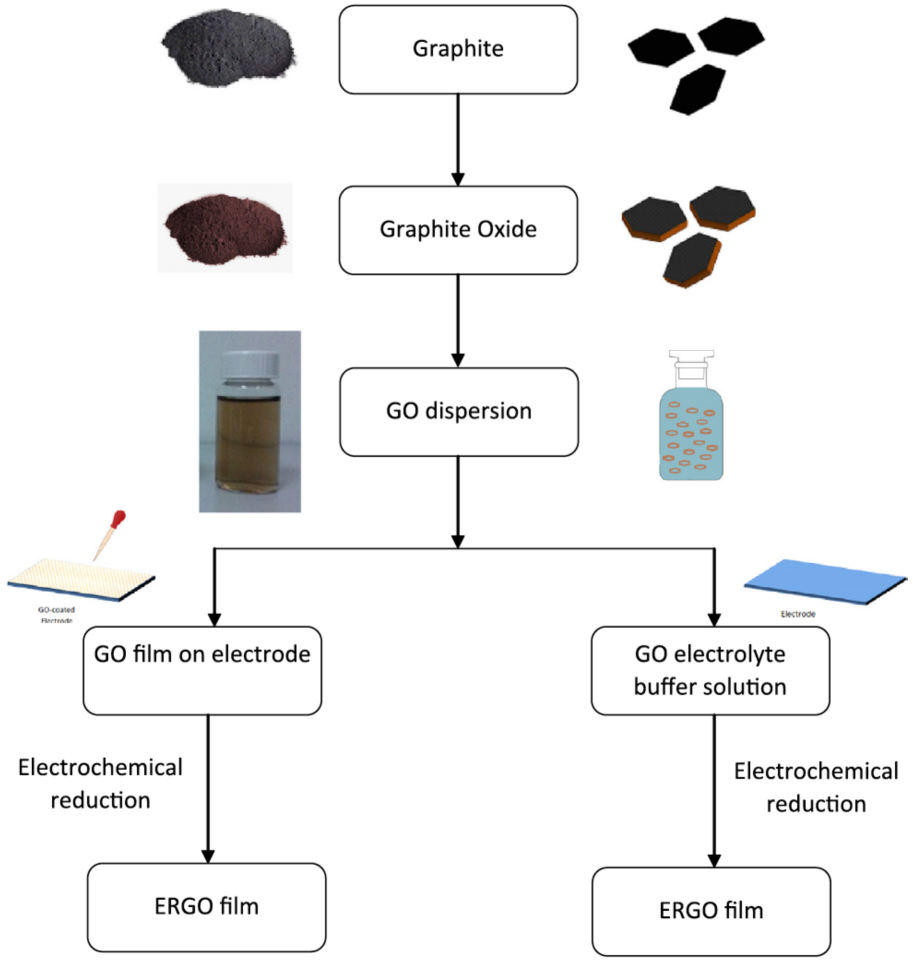

Fig. 2.1.6- Schematic illustration of electrochemical reduction approach to production of electrochemically reduced GO (ERGO).[14]

In the two-step approach, an electrochemical setup with a standard three-electrode electrochemical system in the presence of a buffer or supporting electrolyte is used. The working electrode is the GO-coated substrate, which can be conducting or insulating.[12,14] However, if the substrate is insulating, there is a need of an additional conductive electrode to be in contact with the substrate. If the substrate is conductive, it can act as the working electrode independently.[14]

Typically some form of platinum is used as the counter electrode and either a silver chloride or saturated calomel is used as the reference electrode.[12,14], [43] Supporting electrolytes such as phosphate buffer solutions (PBS), potassium chloride (KCl), potassium nitrate (KNO_3), and sodium chloride (NaCl) have been used.[29,30,43–45] A near neutral or low pH value is favorable to the reduction of GO. Since low pH mediums favor hydrogen ions, it has been proposed that hydrogen ions participate in the reaction.[12,14,46] As with many of the aforementioned methods, the reduction mechanism remains unclear. [3,12,14]

The two-step reduction process is typically performed with cyclic voltammetry (CV), or at a constant potential mode.[14,29,30,43–45] CV is based on linearly varying the potential over a fixed potential range. After the set potential has been reached, the potential is ramped linearly in the opposite direction until the initial potential has been reached. It provides information on the reversibility of the reaction and a survey of the present redox potentials.[47] A typical cyclic voltammogram is shown in Fig. 2.1.7. The first CV scanning cycle of a GO-coated electrode exhibits one cathodic current peak at a negative potential range. The peak position varies widely depending on the reference electrode system and the electrolyte medium used. However, the cathodic peak is shown to decrease significantly and disappear after several subsequent scanning cycles, indicating an irreversible process.[14,29,44] In the constant potential mode, selection of the proper applied reduction potential and time is vital to the degree of reduction. The applied potential is usually determined by the location of a potential peak observed in the CV voltammogram or a linear sweep voltammogram. The voltage used for reduction is chosen to provide a more negative potential than the peak potential observed in the CV scan. When the applied potential is less negative than the observed peak potential, the resulting rGO still holds onto some oxygen functional groups even with increased reduction time.[14]

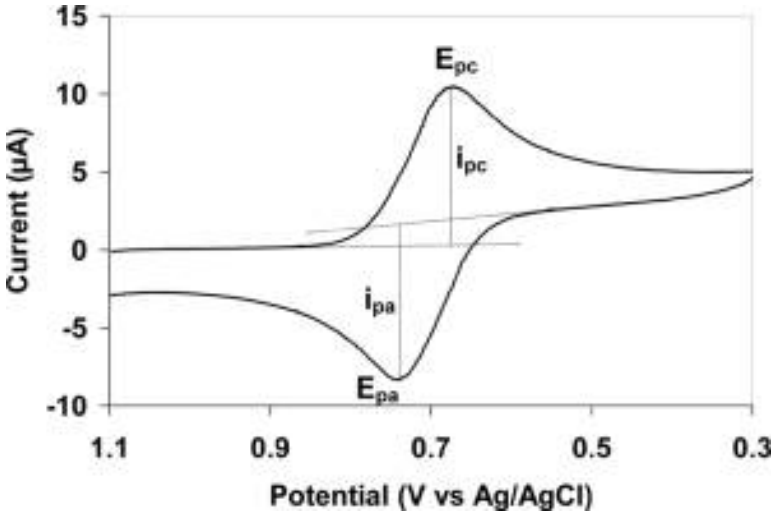

Fig. 2.1.7- Typical cyclic voltammogram where i_{pc} and i_{ac} and show the cathodic and anodic current peaks respectively for a reversible reaction. (public domain)

2.2 Electrocoagulation

Electrocoagulation (EC) has been traditionally used as a method to separate ions and colloidal particles from wastewater. The following sections will introduce the theory and mechanisms behind the EC process. Given the central role this process plays in the electrochemical deposition of the Cu-GO films in the present dissertation, the discussion below will provide an important context for the results to be described later.

2.2.1 Particle surface charge, electrophoresis, and zeta potential

A colloid suspension is a mixture in which microscopic, insoluble particles of one substance are suspended throughout a solution or solvent. The stability of colloidal dispersion is dependent on the colloidal particle surface charge. In an aqueous system, solid surfaces can develop an electrostatic charge by various means, including ion adsorption and surface group ionization. The surface charge is balanced by the adsorption of ions of opposite charge (counter

ions) to the surface by electrostatic and van der Waals forces. This compact layer of counter ions, called the Stern layer, is itself surrounded by a diffuse layer of ions whose dynamics are driven by thermal agitation. The structure described above provides the basis for the electric double layer (EDL).[48,49] Fig. 2.2.1 is a schematic illustrating the EDL structure.

Within the diffuse layer, there is a theoretical boundary, called the surface of shear or slipping plane, inside which the ions and particles form a stable entity. If solid particles are placed into an electrolyte solution, the slipping plane is an imaginary surface, which is considered to lie close to the particle surface and within which the fluid is stationary. The particles are capable of being induced to move by the application of electric field across the system. This is called electrophoresis. When a particle undergoes electrophoresis, the surface of shear forms a casing, which envelops the particle. Everything inside that casing is considered to be the kinetic unit. The ions beyond the slipping plane are not part of the kinetic unit. Therefore, under electrophoresis, the particle along with the quantity of the surrounding electrolyte within the surface of shear and its contained charge travel together. The potential at the surface of shear is measurable and is called the zeta potential. [48–50]

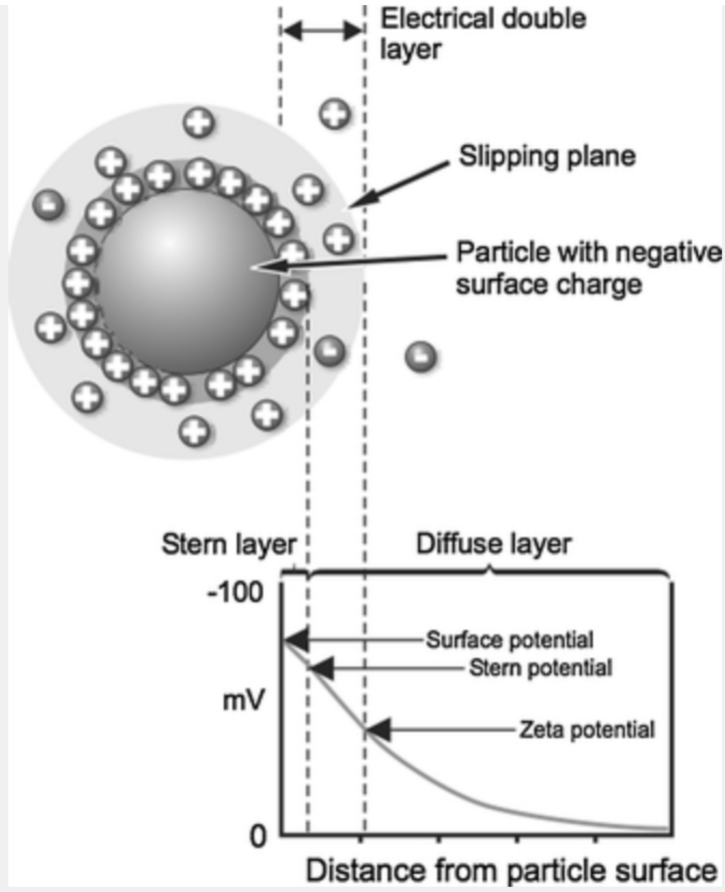

Fig. 2.2.1- Schematic representation of the double layer that surrounds a particle in aqueous medium. The potential that exists at the slipping plane is known as the ζ-potential.[51]

Theoretically, the zeta potential is the potential difference between the stationary fluid attached to the particle and the dispersion medium. The zeta potential is the main source of colloidal system stability, since it indicates the extent of repulsion between adjacent and similarly charged colloidal particles. A greater magnitude in the zeta potential leads to a more stable the colloidal system since the extent of repulsion between particles is greater. In practice, colloidal suspensions with zeta potentials of ±30mV are considered stable. As suspensions are destabilized, the zeta potential approaches zero.[49]

2.2.2 DLVO Theory and Coagulation

Understanding the Derjaguin-Landua-Verwey-Overbeek (DLVO) theory is essential to the description of colloid stability. DLVO theory considers that the net interaction energy (V_{Tot}) of two particles is the sum of their van der Waals attraction energy (V_A) and their electrostatic repulsion energy (V_R) (See Fig. 2.2.2). As two surfaces of similar charge approach each other, their electric double layers interact causing an electrostatic repulsion.[52] The electrostatic repulsion is countered by van der Waals forces producing an energy barrier containing two minima (primary minimum and secondary minimum) and a maximum.[49]

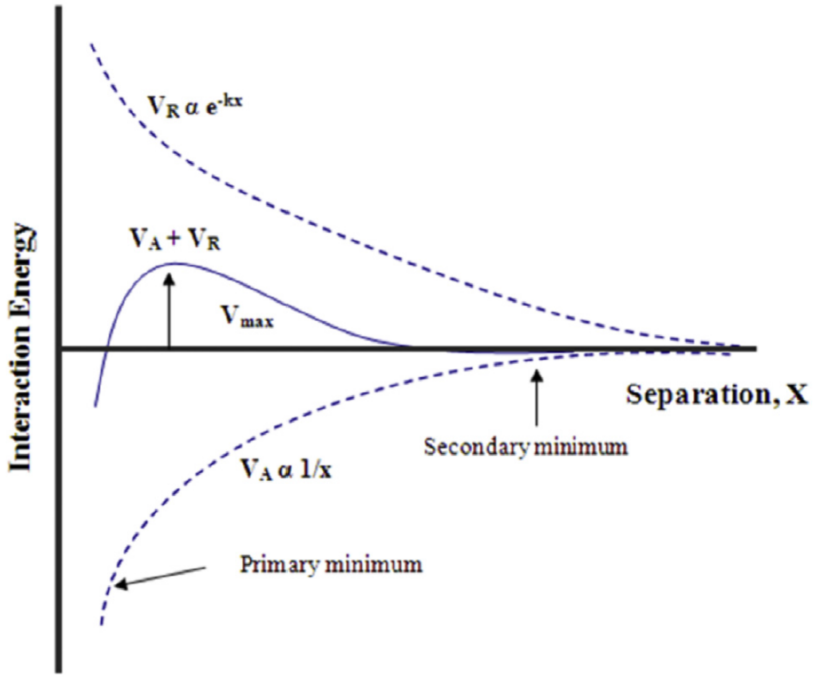

Fig. 2.2.2- Typical particle interaction versus particle separation curve.[49]

All the energies vary as a function of the distance between the two particles, as illustrated by the following equations describing the classical DLVO theory:[52]

$$V_{Tot} = V_A + V_R \qquad \text{(Eq. 2.2.1)}$$

$$V_A = -\frac{Ar}{6d} \quad \text{(Eq. 2.2.2)}$$

where it is assumed that a particle is spherical with radius r and is interacting with a planar surface of particles, A is the Hamaker constant, d is the distance between the sphere and the surface.

$$V_R \propto \psi^2 e^{-\kappa d} \quad \text{(Eq. 2.2.3)}$$

where ψ is the surface potential (if the surfaces have different potentials $\psi_1\psi_2$ is used), and the Debye length κ^{-1} (thickness of the diffuse double layer).

$$\kappa = \sqrt{\frac{2000e^2 N_A c}{\varepsilon\varepsilon_0 kT}} \quad \text{(Eq. 2.2.4)}$$

where e is electronic charge, N_A is Avogadro's constant, c the concentration (in mol/L) of the ions in the electrolyte, k is the Boltzmann constant, T the temperature, ε is the dielectric constant of the solution, and ε_0 is the dielectric permittivity of free space.

Coagulation occurs when the charged particles in colloidal suspensions are neutralized by collision with counter ions, resulting in the agglomeration of the particles. As previously mentioned, colloidal particles are stabilized by electrostatic repulsion. It is believed that coagulation is caused by particles capable of approaching each other close enough for van der Waal forces to hold them together and allow aggregation.[53]

2.2.3 Electrocoagulation (EC) mechanisms

Theory

The EC process can be divided into three main successive stages (see Fig. 2.2.3). It first involves the presence of a coagulant. These species are generated *in-situ* by electrolytic oxidation of a sacrificial anode through the application of an electric field between the electrodes. The colloidal particle suspension is then destabilized followed by an aggregation of colloidal substituents to form destabilized flocs.[53–55]

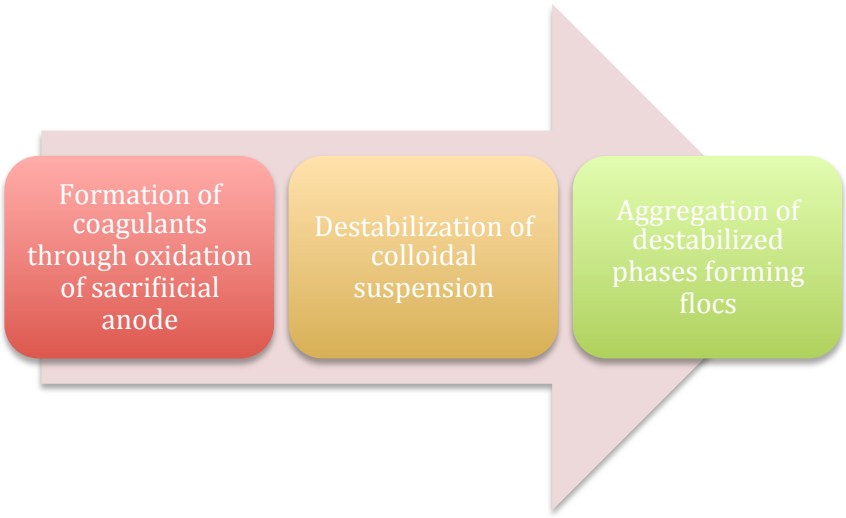

Fig. 2.2.3- The main stages present in electrocoagulation.

At the anode, metal from the sacrificial material is oxidized to form cations and water may be oxidized. The reactions at the anode can be summarized by the following equations:[53–55]

$$M(s) \rightarrow M^{n+}(aq) + ne^{-} \qquad \text{(Eq. 2.2.5)}$$

$$2H_2O \rightarrow O_2 + 4H^{+} + 4e^{-} \ (E^{o} = 1.23\ V\ vs.NHE) \qquad \text{(Eq. 2.2.6)}$$

where M is the metal species, n is the number of electrons transferred in the oxidation process per mole of metal, and NHE is the normal hydrogen electrode. At the cathode, water is reduced to form hydrogen gas and hydroxyl anions. The reaction can be summarized by the following equation: [53–55]

$$3H_2O(l) + 3e^{-} \rightarrow \frac{3}{2}H_2 + 3OH^{-} \ (E^{o} = 0.00\ V\ vs.NHE) \qquad \text{(Eq. 2.2.7)}$$

In the EC experimental setup, the electrode assembly is typically connected to a DC power supply. The amount of metal dissolved (w (g of $M.cm^{-2}$)) by anodic oxidation is dependent on the current density (i ($A.cm^{-2}$)) and electrolysis time t (s). A simple relationship can be derived using Faraday's law:[54,55]

$$w = \phi \frac{itM}{nF} \qquad \text{(Eq. 2.2.8)}$$

where M is the relative molar mass of the material, ϕ the current efficiency or faradic yield (equal to 1 in theoretical case), and F is Faraday's constant (96,500 $C.mol^{-1}$)

When not all the electrons in the system contribute to the metal dissociation reaction, a correction factor or faradic yield, ϕ, which is different than 1 is introduced to account for the gap between theoretical and experimental dissolution of the sacrificial electrode. The faradic yield is typically less than 1.[55]

Destabilization Mechanisms

There are four main colloidal suspension destabilization mechanisms in the EC process: compression of diffuse layer, charge neutralization, enmeshment, and interparticle bridging.

Compression of diffuse layer:

The compression of the diffuse layer around charged species is one of the main mechanisms for destabilization. Indeed, the thickness of the double layer affects the degree of repulsion between particles and, by extension, their stability. As the thickness decreases, the repulsive forces are also diminished. Compression of the double layer is caused by interactions with ions generated by the oxidation of the sacrificial anode. These metal cations diffuse through the double layer, which increases the counter ion concentration around the colloidal particle and, by extension, decreases the double layer thickness.[49,53–56]

Charge Neutralization:

Charge neutralization of the surface of colloidal particles is another common destabilization mechanism. Charge neutralization is achieved by adsorption of metal ions produced by the sacrificial electrode. The counter ions reduce the electrostatic interparticle repulsion and allow van der Waal forces to dominate, causing coagulation. The process results in a zero net charge. [49,53–56]

Enmeshment and Interparticle Bridging:

The enmeshment and interparticle bridging mechanisms are less common. The enmeshment mechanism occurs when coagulants such as metal hydroxides or metal salts are added at high concentration to the suspension. Precipitation of metal hydroxides or metal hydrates can occur forming a sludge blanket, which can entrap colloidal particles. Destabilization by bridging typically occurs when metal coagulants are polymerized forming a polymer with high molecular weight. Through adsorption, these polymers are capable of entrapping particles forming an interparticle bridge. Polymers must have chain lengths sufficient to extend beyond the double layer. In addition, colloidal particles must have sites available for polymer adsorption for mechanism to occur.[49,55,56]

It is important to note that the selection of the sacrificial electrode is vital to the destabilization mechanism in the EC process, since different metal ions have different coagulating powers. According to Schultze-Hardly rule,[49,57,58] the coagulating power increases with the valency of the counter metal ion. Therefore, divalent and trivalent metal ions have a higher destabilization capacity than monovalent ones

Chapter 3: Electrocoagulation Driven Fabrication of Graphene Oxide films

The majority of the text and images present in Chapter 3 were taken and adapted from the following published work:
Weisbart, C., Raghavan, S., Muralidharan, K. & Potter, B. G. Electrocoagulation driven fabrication of graphene oxide films. *Carbon.* **116,** (2017)

3.1 Motivation and Objective

Graphene oxide (GO), the oxidized counterpart of graphene, has found considerable application as an important constituent in electrodes [59–61] as well as in optoelectronic and photonic devices.[5,62] In addition, it has been shown to act as a strong barrier for oxidizing molecules, enabling anti-corrosion applications.[63,64] Further, reduction of GO has been a reliable route for obtaining chemically modified graphene platelets in large scale and low cost.[6,11–15] Recently, there has been significant interest in the utilization of GO thin films as filtration membranes underlined by their exceptional stability in water.[18] Their stability in water appears to be driven by the presence of multivalent metal ions within their matrix, that serve as strong cross-linkers.[18] While the focus of this work examined the effect of the metal cations on the stability of the GO matrix in water, the underlying procedure for the cation integration within the GO film was accomplished in an uncontrolled and sometimes unintentional fashion.

In contrast, the present work demonstrates for the first time, the controlled and rapid formation of metal-ion-containing GO films from GO dispersions. Specifically, the method employed in this work is based on copper-ion-assisted electrocoagulation (EC) and deposition of GO particles on copper electrodes. Importantly, the thickness and the rate of deposition are controlled by varying the applied voltage and the concentration of GO particles under acidic conditions in the suspension. The EC-based method developed in this work has far-reaching

technological implications and it provides a new avenue for obtaining stable metal-ion-containing GO films.

Electrocoagulation has been traditionally used as a method to separate ions and colloidal particles from wastewater.[65] In the classic EC process, metal cations are produced by electrochemical oxidation of a soluble anode. The multivalent metal ions can induce coagulation of particles in the suspension either by neutralizing the surface charge of the colloidal particles (if they are negatively charged) or by simply reducing the double layer thickness around the particles.[66–68] Much of the EC literature deals with coagulation of particles in the bulk of the dispersion. For the formation of films via the EC process, it is critical to selectively induce the coagulation very near the electrode surface.

In aqueous dispersions containing positively charged ceramic particles, film deposition at a cathode utilizing a combination of coagulation via cathodically generated hydroxide ions and electrophoretic (EP) migration has been reported.[69] The hydroxide ions, by their univalent state, are highly unlikely to be as effective as higher-valent cations in their coagulation power.[57,58] In contrast, the present technique utilizes bivalent copper ions generated near a copper anode to drive the anodic deposition of GO films from GO dispersions. On a related note, while previous work [19] has demonstrated that copper ions adsorb onto negatively surface-charged GO particles under acidic pH conditions, the ability to utilize EC-driven deposition of GO has not been demonstrated before. Additionally, in comparison to previous EP based deposition of GO films on conductive substrates,[70,71] the method developed here allows the incorporation of metal ions that are essential to enhancing the mechanical and chemical stability of GO films.[18] Further, this method represents a readily scalable technique for the formation of GO films that can be carried out under ambient pressure and temperature conditions.

3.2 Experimental Methods

3.2.1 Material synthesis

Suspension: Graphene oxide was synthesized from natural graphite flakes (99.35% purity, 325 mesh, Asbury Carbons) based on a modified Hummers'method.[2] The graphite flakes (3g, average diameter size 44 micrometers) and concentrated H_2SO_4 (69mL, Honeywell, 96%, VLSI) were mixed in a beaker with magnetic stirring. Potassium permanganate ($KMnO_4$, 9g, E.S.P. Chemicals, A.C.S reagent, Crystal) was then added to the graphite dispersion slowly over 30 minutes, while the beaker was in an ice bath. The dispersion was then kept at 40 °C for 30 minutes while being stirred vigorously. Deionized (DI) water (150 mL) was then added and the dispersion was stirred for 15 minutes at 95°C. After being brought down to room temperature, more DI water (450 mL) was added, followed by a drop-wise addition of H_2O_2 (15 mL, Sigma-Aldrich, 30 weight % in H_2O, ACS reagent) to remove excess $KMnO_4$. Afterward, the dispersion was centrifuged at 6000 r.p.m. for one hour. The resulting solids were sonicated with 2 ml dilute HCl (2mL of HCl purchased from Sigma-Aldrich as 37%, ACS reagent) in 250 mL of DI water. The dispersion was then centrifuged under the previously stated conditions. The settled solids were dispersed in water and centrifuged under the same conditions a final time. The resulting supernatant liquid was kept, while the settled solids were discarded. The supernatant liquid was then ultrasonicated for 90 minutes to produce the final suspension with a concentration of 13.5 mg/mL, a pH of 2, and a conductivity of 8.2 mS/cm. Other suspensions with varying concentrations of GO and resulting conductivities were also examined to evaluate the effect of dispersion properties on the ensuing quality of GO films produced in the EC process.

Thin films: GO films were deposited onto copper foil substrates (0.127 mm thick, annealed, 99.9%). After pre-cleaning in 0.1 M HCl, the copper substrates were electrochemically

etched at 10V in dilute sulfuric acid (pH ~2) to roughen the surface and promote film adhesion. In addition, the substrates were coated on the backside and the sides with epoxy (3M, Scotch-Weld, DP 270 Clear) to eliminate deposition on the back of the substrate as well as gas evolution on the substrate edge. The copper substrate serves as the anode in the electrochemical cell, while platinum served as the cathode material. Electrocoagulation was performed by applying a potential across the electrodes using a Hewlett Packard 6334A power supply. Deposition voltages ranged from 2 to 10V and deposition times ranged from 2 to 60 sec. The distance between the cathode and anode was fixed at 0.015 m. Acidic conditions were used in order to ensure the presence and stability of solubilized copper ions in the GO dispersion.[72]

The GO films formed on the anodes were removed from the deposition bath, rinsed immediately with DI water, and dried on a hot plate at 55 °C under flowing nitrogen. The thickness of the films was measured with a profilometer (Dektak 6M, Veeco) with a scan length of 2000 microns and a stylus force of 3 mg. The thickness was measured at 5 to 10 different locations on a given sample, then averaged.

3.2.2 Characterization Techniques

X-ray photoelectron spectroscopy

X-ray photoelectron spectroscopy (XPS) spectra are obtained by exciting a material surface with a beam of X-rays under high-vacuum conditions allowing photoelectrons to be emitted from the sample surface. An electron energy analyzer is used to simultaneously measure the number of electrons that are emitted as well as their corresponding kinetic energy. For every chemical element, there is a characteristic set of binding energies associated with each core atomic orbital. The appearance of peaks at specific binding energies can be used to ascertain the

presence of a specific element in the sample under study.[73] The binding energy can be determined by the following equation:

$$E_{Binding} = E_{Photon} - (E_{Kinetic} + \varphi) \quad \text{(Eq. 3.2.1)}$$

where $E_{Binding}$ is the binding energy of the electron, $E_{kinetic}$ is the kinetic energy of the electron, ϕ is the work function which is an adjustable instrumental correction factor accounting for photoelectron being absorbed by the instrument's detector. Furthermore, the concentration of the element is related to the intensity of the peaks.[73]

In addition, shifts in the binding energy observed can be associated with variations in the oxidation state of atoms and the local chemical environment. Atoms of higher positive oxidation state exhibit a higher binding energy because of the extra coulombic interaction between the emitted photoelectron and the nucleus. XPS is a quantitative technique that can determine elemental composition as well as oxidation states of materials.[73]

From the electron energy analyzer, a spectrum is capable of being formed where the y-axis is intensity (arbitrary units) and x-axis is binding energy (eV). From the binding energy and intensity of the photoelectron peak, the elemental identity and chemical state of a detected element can be established. The standard analysis depth resolution for an XPS measurement is about 5 nm. XPS is therefore considered a surface analysis technique. However, depth distribution information can be acquired by joining XPS measurements with sputter ion cleaning and angle resolved work.[74]

In this work, a Kratos Axis 165 Ultra X-ray photoelectron spectrometer is used to determine the prevalent oxidation state of copper ions present in the GO film. The measurements were taken with a monochromatic Al Kα source. The XPS instrument used employed a hybrid active lens mode and a charge neutralizer.

Raman spectroscopy

Light propagating through a medium is capable of being scattered. Depending on the energy and momentum changes of the incident photon, the scattering may be termed elastic or inelastic. For elastic scattering, there is a momentum transfer between the incident light and the scattering species. However, the kinetic energy is conserved during the scattering process. In contrast, for inelastic scattering, there is both a momentum and energy transfer. Raman scattering is a type of inelastic scattering where the change in energy or frequency is associated with the formation or loss of an optical phonon. The strength of interaction between the incident EM field and the atomic structure of the material under study in Raman scattering is dependent upon the nature of the vibrational mode involved. Only structural elements or molecules, which experience changes in their polarizability with respect to the vibrational coordinate, will produce a Raman effect.[75]

Raman scattering can lead to two possible outcomes. Figure 3.2.1 depicts different scattering outcomes associated with Raman that use the concept of a "virtual" state into which the incident photon excites the system. The virtual state is not a stationary state for the system but represents a rapid, transient disturbance in the material polarization. When the emitted (scattered) photon has a lower energy than the incident (excitation) photon, the process is called "Stokes" scattering. Referring to the Figure, this corresponds to the "relaxation" of the photon to a higher vibrational state. Physically, this process is associated with the formation of a phonon whose energy is equal the energy lost by the scattered photon. In contrast, anti-Stokes Raman scattering is indicated by an emitted photon with a higher energy than that used for excitation photon. This scenario occurs when the system already exists in an excited vibrational energy

state. After excitation to the virtual state, relaxation terminates at a lower vibrational state. Thus, the process can be thought of as consuming phonons during the scattering process. Anti-Stokes scattering is typically less intense than Stokes scattering due to the decreased probability of finding the system at a higher excited energy state (Boltzmann distribution). Figure 3.2.1 depicts both forms of Raman scattering as well the more common elastic Rayleigh scattering in which the initial and final vibrational states are the same after the scattering process.[75]

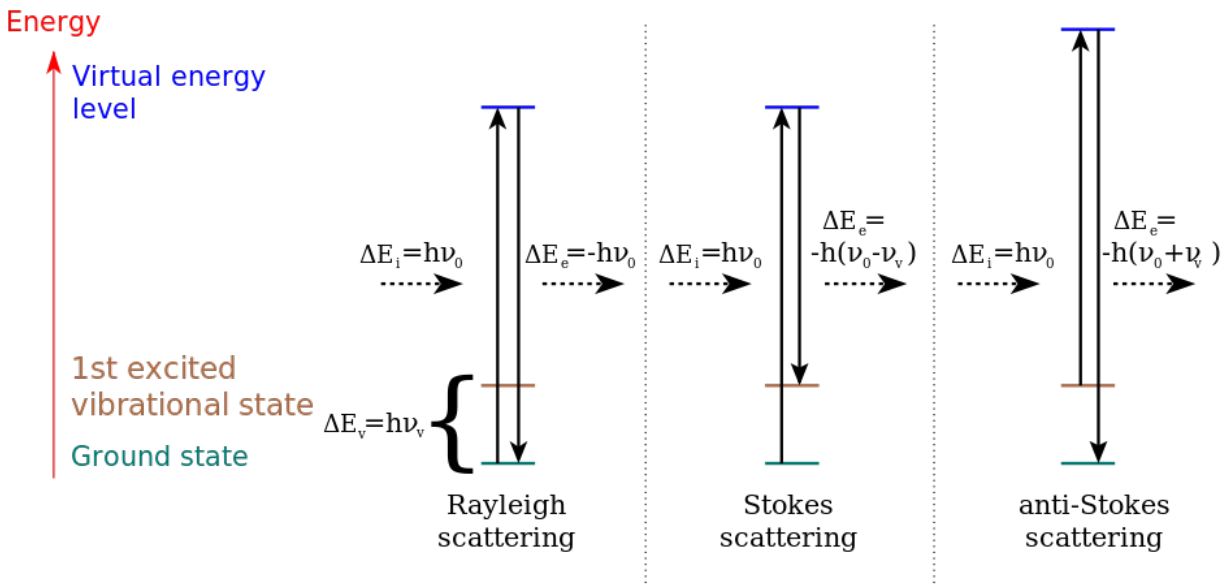

Fig. 3.2.1- Schematic representation of Stokes scattering, anti-Stokes scattering, and Rayleigh scattering.[76]

In Raman spectroscopy the frequency shift of the scattered photons directly provide the vibrational energy of the characteristics vibrational modes involved in the scattering process. By identifying the optical phonon modes participating the inelastic scattering process, the atomic structure of the material can be examined.

In this work, a Jobin–Yvon Horiba Lab-Ram HR800 micro-Raman spectrometer equipped with a thermoelectrically cooled CCD array detector was used with an Argon ion laser

for excitation of the sample (514.5 nm). The beam was focused with a 100x microscope objective with a corresponding 10 μm spot size and 100 mW incident power at the sample surface. Stokes-scattered spectra were collected over the 1000-3000 cm^{-1} Raman shift range (resolution: 5 cm^{-1}). Collection integration time was 20s and 10 scans were collected and averaged to provide improved signal-to-noise ratio in the final spectra.

X-ray diffraction

A powder X-ray diffractometer (Bruker Kappa APEX II Duo) was used in this work to gain additional insight into the structure of GO. In an X-ray tube, electrons are accelerated and collide with a Cu target ejecting K shell electrons and forming vacancies. Electrons from the L shell fill the vacancy and, by extension, generate Cu Kα X-rays. The X-rays are then filtered to form monochromatic radiation, which is guided towards the GO powder. However, constructive interference between the incident ray and periodic atomic arrangements in the sample can be produced when scattering conditions satisfy Bragg's Law[77]:

$$n\lambda = 2dsin(\theta) \qquad \text{(Eq. 3.2.2)}$$

where n is a positive integer, d is the spacing between two atomic planes, θ is the angle of the incident beam on the sample, λ is the wavelength of the incident beam.

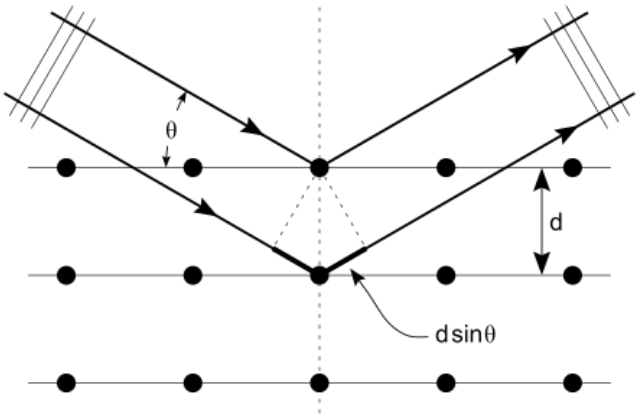

Fig. 3.2.2- Schematic representation of Bragg's law for two incident beams, where d is the interplanar spacing and θ is the incident angle. [78]

Scattering 2θ angles were scanned from 5° to 70°. Powdered GO specimens were used for all measurements. Each peak in the resulting diffractogram corresponds to a specific value of d-spacing (Eq 3.2.2) and by extension a particular family of atomic planes. A crystalline structure has a specific collection of d-spacings and atomic planes unique to that particular structure. XRD spectra therefore allow for the identification and characterization of crystal structures.[77]

Zeta potential measurement

A Malvern Zetasizer NS equipped with a disposable capillary cell and 633 nm (HeNe) laser source, was used to determine the zeta potential and size distribution of the suspended GO particles in solution. The Zetasizer incorporates two main techniques: dynamic light scattering (DLS) and laser doppler micro-electrophoresis.[79] DLS measures the diffusion of particles moving under Brownian motion. Using the Stokes-Einstein relationship, DLS allows for the calculation of particle size and size distribution.[80] For laser Doppler micro-electrophoresis, an electric field is applied to the dispersion. A laser beam irradiates the particles and is scattered by the particles. The frequency shift of the incident laser beam is correlated to the particle mobility

caused by the electric field. The electrophoretic mobility is related to the zeta potential. Doppler micro-electrophoresis therefore enables calculation of zeta potential and zeta potential distribution.[81]

Inductively coupled plasma-mass spectroscopy (ICP-MS)

The plasma in ICP discharge is formed by streaming argon gas through an assembly of three concentric quartz tubes (referred to as plasma torch). The plasma torch is bordered by an induction coil connected to an RF generator. The RF current through the induction coil generates a magnetic field, which induces a current in the gas stream. An argon plasma is subsequently formed, capable of exciting and ionizing a wide range of metals. Ions from the plasma are then extracted into a quadrupole mass spectrometer and separated relative to their mass to charge ratio. A detector collects an ion signal, which is proportional to the concentration of the metal. The argon ICP allows for concurrent detection of multi-element concentrations.[82]

For ICP analysis, sections of GO films that were successfully deposited on to copper were scored and delaminated from the substrate using a nitrogen gas stream. The films were thoroughly washed in DI water and isopropyl alcohol (IPA) in order to minimize copper contamination from the underlying substrate. Prior to ICP-MS analysis, the delaminated films were bleached in nitric acid for metal dissolution and stabilization. The sections were analyzed using an Inductively Coupled Plasma-Mass Spectrometer (Agilent 7700x ICP-MS) to determine the concentration of copper incorporated in the film. The ICP-MS employed an RF power of 1550W, a plasma gas flow of 15 L/min, a carrier gas flow of 0.85 L/min, and a makeup gas flow of 0.15 L/min. In addition, the corrosion of copper (with an exposed area of approximately 2 cm^2 on only one side) was measured by ICP-MS in dilute sulfuric acid solutions at a pH of 2 and a

conductivity of 8.2 mS/cm (conditions representing EC experiments). This experiment was performed to provide a control for comparison and to correlate amount of copper going into solution with the amount of GO deposited (i.e. the efficiency of the EC process)

Scanning Electron Microscopy (SEM)

An SEM scans a sample surface with a focused beam of electrons. The electrons interact with the atoms in the sample, producing various signals, which reveal information about the sample's surface topography and composition. While the beam is scanned in a raster pattern, images are produced by combination of the beam's position and the signal detected.[77] The various signals produced include secondary electrons (SE), back-scattered electrons (BSE), characteristic X-rays, visible light, heat, etc. The SE and BSE modes are typically used for SEM imaging.[83] In this work the SE mode was used over the BSE mode in order to produce higher resolution images of topography and morphology. In the SE mode, secondary electrons are emitted from very close to the sample surface. In the BSE mode, electrons are reflected by elastic scattering (defined in Raman spectroscopy section). They arise from deeper locations within the sample compared to secondary electrons.[83] The SE mode therefore produces higher resolution images compared to those in the BSE mode. For an assessment of the film structure, fracture surface cross-sections were produced in some specimens and analyzed using a FEI Inspect S SEM at 30 kV. In addition, top-plan view images of the GO-coated copper substrates were produced on a Hitachi TM3000 tabletop SEM at 15 kV with maximum resolution of 30nm.

3.3 Results

3.3.1 Starting Material Characterization

An assessment of the as-prepared GO material was pursued to confirm the anticipated material structure and provide a basis for comparison with EC-derived film characteristics. Graphene oxide dispersions were vacuum dried at 50°C for 24 hours and characterized in the form of powder compact by XRD and Raman spectroscopy.

Fig. 3.3.1 contains a characteristic XRD pattern of the as-prepared (and dried) GO material. The peak located at a 2θ =11.46° with a full width half maximum (FWHM) of 2.03° corresponds to the (001) reflection of GO.[17,84,85]

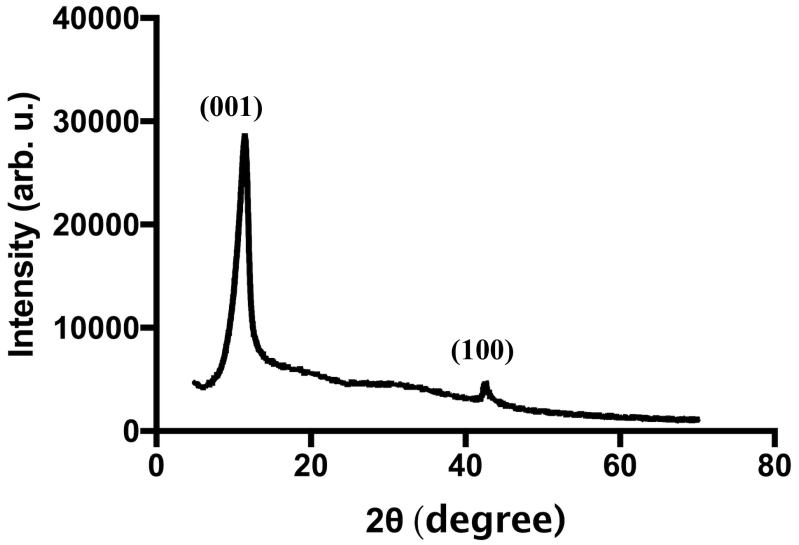

Fig. 3.3.1 - Representative XRD spectrum of the graphene oxide produced using the modified Hummer's process prior to film deposition. Adapted.[31]

A characteristic Raman spectrum of GO starting material produced by the Hummer's process is shown in Figure 3.3.2. This spectrum is in good agreement with published spectra for GO.[17,39] The peak centered at approximately 1350 cm^{-1} is the D band, which is associated with

the breathing modes of six membered carbon rings that are activated by defects. The G-band, located in the range of 1590 to 1600 cm^{-1} is attributed to E_{2g} phonons at the Brillouin zone center.[39] Two peaks, also present and centered at approximately 2700 and 2900 cm^{-1}, represent the 2D band and the D+G band respectively.

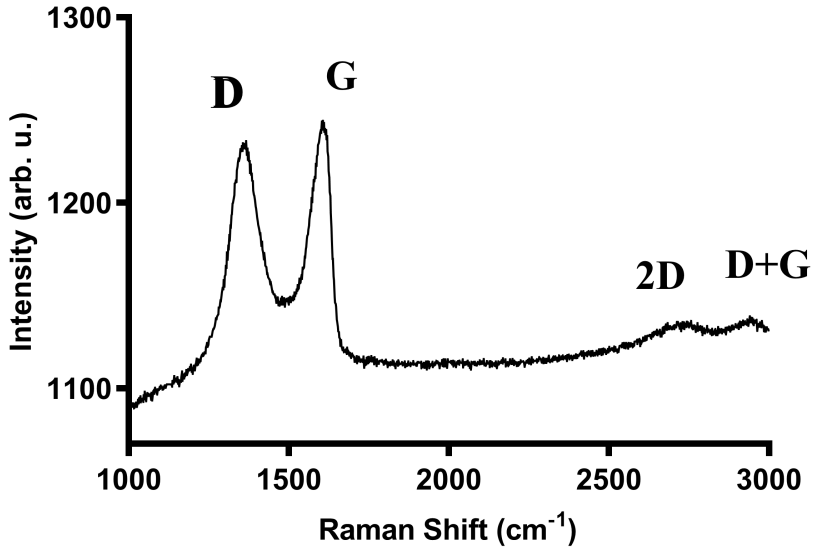

Fig. 3.3.2 - Representative Raman spectra of as synthesized graphene oxide particles. Adapted.[31]

The measured zeta potential distribution of GO particles in suspension at two different dilutions is displayed in Fig 3.3.3. The dilution of the suspension (< 10 mg/mL) avoided the effect of increased optical scattering during the measurement and a corresponding distortion in the particle size distribution obtained. The mean value of zeta potential was approximately -49 mV and -46 mV for 0.5mg/mL and 7.2 mg/mL respectively. The negative zeta potential can be attributed to the presence of ionizable carboxyl (-COOH) groups at the GO edges.[86] A published study has reported that GO particles are characterized by a negative zeta potential in the pH range 2 to 11.[86] These results clearly indicate a propensity for the electrophoretic migration of particles towards the copper anode.

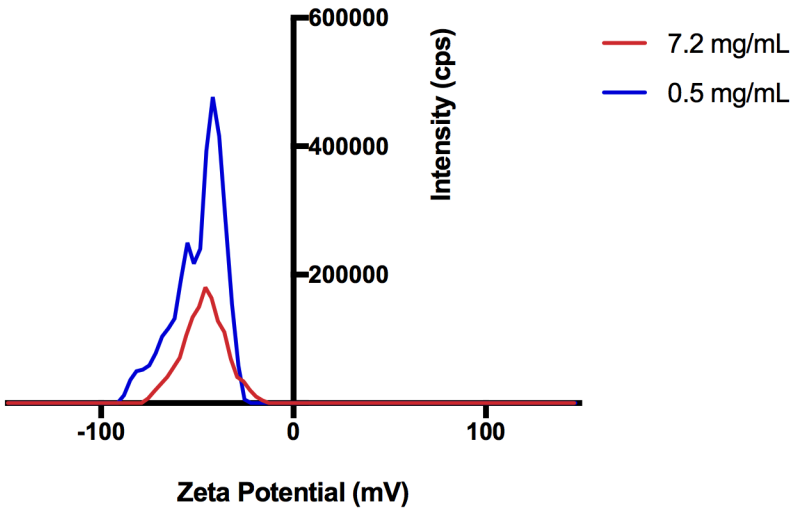

Fig. 3.3.3 – Zeta potential distribution of GO particles in Suspension A at two different dilutions (0.5 and 7.2 mg/mL).[31]

3.3.2 Graphene Oxide Thin Films Characterization

Deposition rate:

The dependence of the GO film-thickness on the applied voltage and deposition time is shown in Fig. 3.3.4. As evident in the Figure, the film thickness was strongly dependent on the magnitude of the applied voltage as well as on the deposition time. Thicker films were deposited at higher applied voltages and/or higher deposition times showing that the electrochemical deposition method provides a ready path for controlling GO film-thicknesses in a reliable fashion.

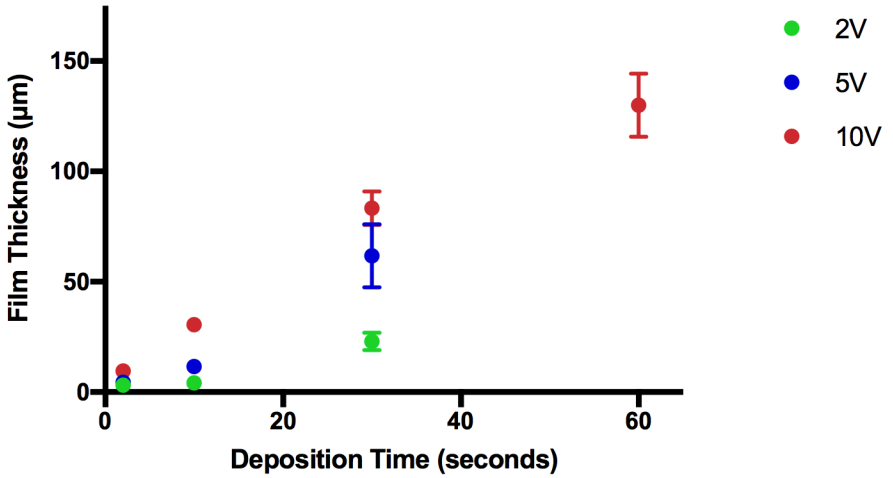

Fig. 3.3.4 – Thickness measurements for films deposited from 13.5 mg/mL GO suspension vs. deposition time for various applied voltages. [31]

To demonstrate the versatility of the EC-driven deposition process, other suspensions were created with lower concentrations of GO particles (3-8 mg/mL). With these suspensions, EC-driven deposition of GO films onto copper substrates was successfully accomplished. It is important to note that the concentration of GO had a direct effect on the thickness of the coating produced under a given set of conditions. More specifically, a decrease in thickness under the same deposition conditions (voltage, time) was shown for suspensions with a lower GO concentration. Fig. 3.3.5 shows the results of a detailed study of GO film thicknesses as a function of time at various voltages from a 8 mg/mL GO suspension. If compared to Fig. 3.3.4 (13.5 mg/mL GO suspension), a notable decrease in deposition rate and thickness can be observed for the films deposited from the suspension with the lower concentration. Table 3.3.1 lists deposition rates from films deposited from two different suspension concentrations.

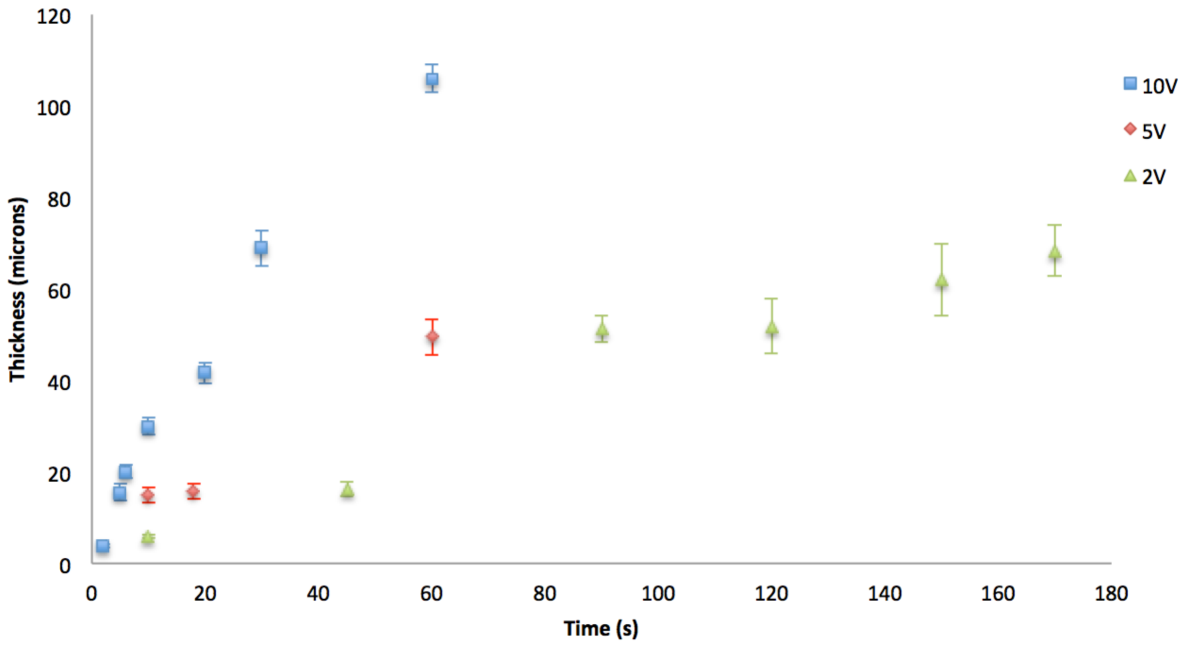

Fig. 3.3.5 –Thickness measurements for films deposited from 8 mg/mL GO suspension vs. deposition time for various applied voltages.

Table 3.3.1 –Deposition rate for films deposited from GO suspensions with different concentrations.

	Deposition rate (μm/s)	
Voltage	13.5 mg/mL	8 mg/mL
2V	0.76	0.42
5V	1.97	0.85
10V	2.31	1.92

Microstructure:

In addition, a cross-sectional and a plan-view view examination of GO coating surfaces were performed by scanning electron microscopy. A representative cross-sectional image, shown in Fig. 3.3.6, exhibits a layered microstructure. A representative plan-view (electrolyte side) image, shown in Fig. 3.3.7, exhibits a wrinkled surface. This characteristic surface morphology is commonly reported for GO films.[87] A more detailed structural analysis performed by microscopic techniques (i.e. FIB, SEM, and TEM) will be present in Chapter 4 to further elucidate the film formation process and resulting microstructural evolution.

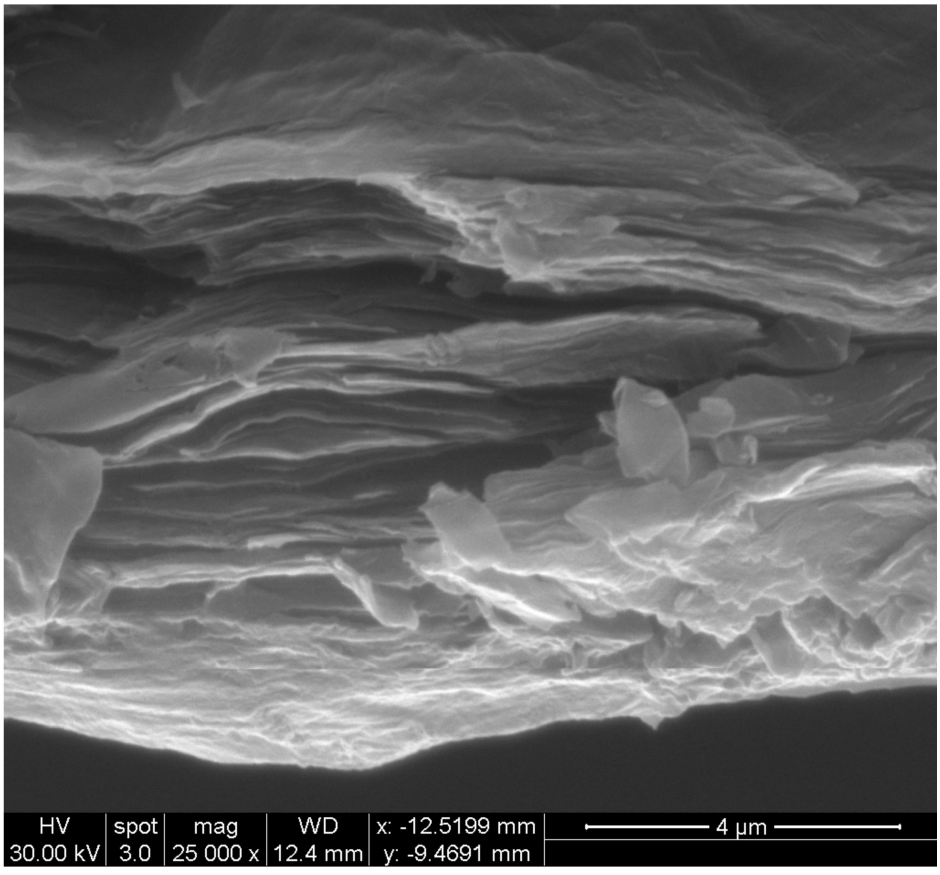

Fig. 3.3.6 – Cross-sectional image of GO film (10V 60 sec) performed by scanning electron microscopy. [31]

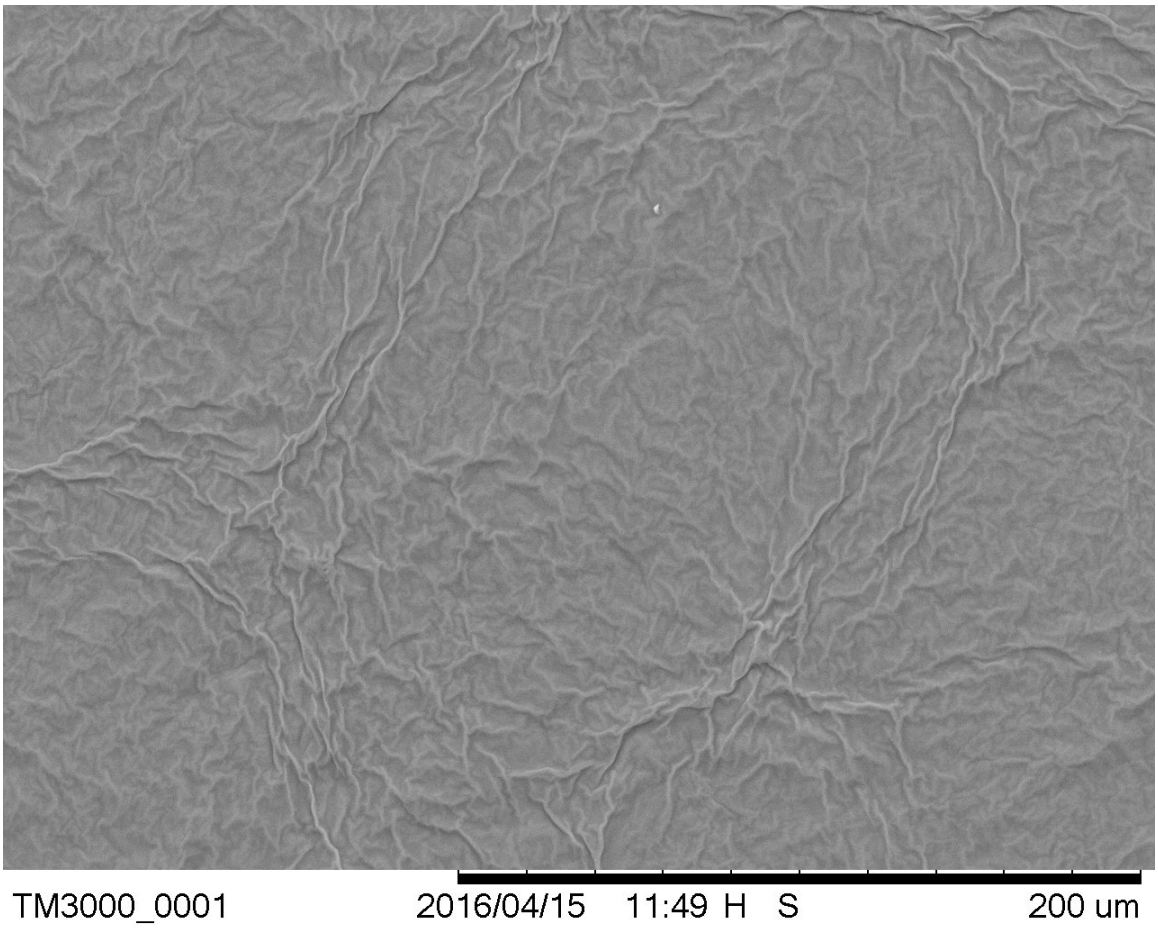

Fig. 3.3.6 – Top-plan view image of GO film (10V 60 sec) performed by scanning electron microscopy.

The representative Raman spectrum of GO films deposited on copper anodes at an applied potential ranging from 2 to 10 volts for a deposition time ranging from 2 to 30 sec is shown in Figure 3.3.8. A comparison of the data in this figure with that in Figures 3.3.2 clearly shows that the location and number of peaks are unaffected after deposition.

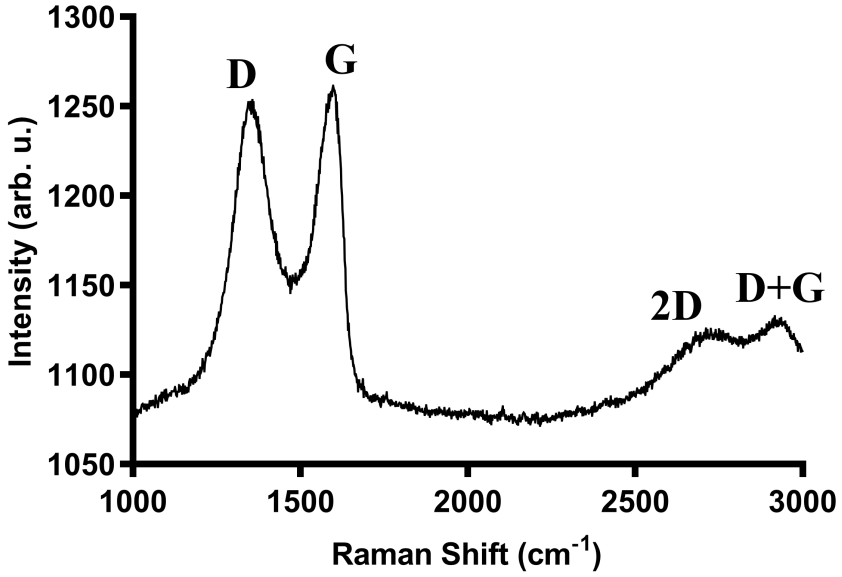

Fig. 3.3.8 - Representative Raman spectra of GO coatings formed via EC. Adapted. [31]

Film chemistry:

The extent of incorporation of copper ions in the films was characterized using ICP-MS. The ICP-MS analysis was carried out on several sets of films. Films for the analysis were obtained by careful mechanical separation from the substrate and were then thoroughly washed in DI water and IPA. Sections of the films were digested in nitric acid prior to ICP- MS analysis. Two sets of films prepared under two different conditions, namely 2V for 30s and 10V for 30s, were used to determine the effect of applied voltage on copper incorporation. The copper concentration was found to be approximately 34 mg/g for the 2V 30s film and 82 mg/g for the 10V 30s film, indicating a strong correlation between the applied voltage and concentration of incorporated copper ions in the deposited material.

The effect of deposition time on copper incorporation was also studied for 8 mg/mL GO suspensions. Fig. 3.3.8 illustrates the concentration of copper incorporated in GO films at two voltages (2V and 10V) as a function of time. Specifically at a given applied voltage, films with

16 +/- 3 µm thicknesses and lower deposition times (10V 5s and 2V 45s) were compared to films with 69 +/- 10 µm thicknesses and greater deposition times (10V 30s and 2V 170s). It was shown that longer deposition times led to a decrease in the concentration of copper incorporated in the GO films. These results demonstrate the ability of the EC based procedure to drive both the deposition of the GO films as well as the controllable incorporation of copper ions within the film.

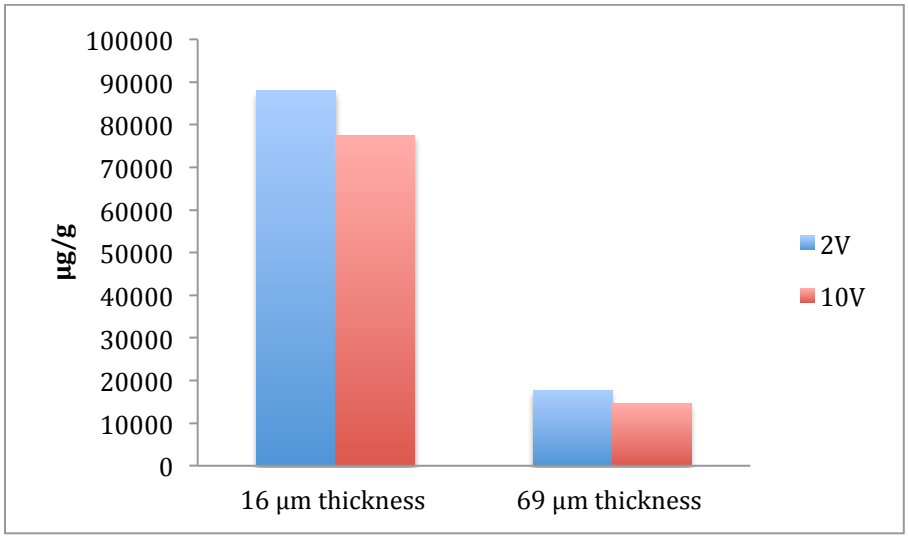

Fig. 3.3.9 – Concentration of copper incorporated in the GO film at 2V and 10V as a function of time (lower deposition times were used to obtain 16 µm and longer deposition times were used to obtain 69 µm).

To correlate the amount of copper going into solution with the amount of GO deposited (i.e. the efficiency of the EC process), the corrosion of copper (with an exposed area of approximately 2 cm^2 on only one side) was measured in dilute sulfuric acid solutions at a pH of 2 and a conductivity of 8.2 mS/cm (conditions representing EC experiments). The tests were carried out at 2V for 30s resulting in a copper concentration in solution of 4.7 ppm (ICP-MS). Based on this value, it was estimated that the ratio amount of GO deposited to copper dissolved into the deposition bath was approximately 30:1 (by mass ratio).

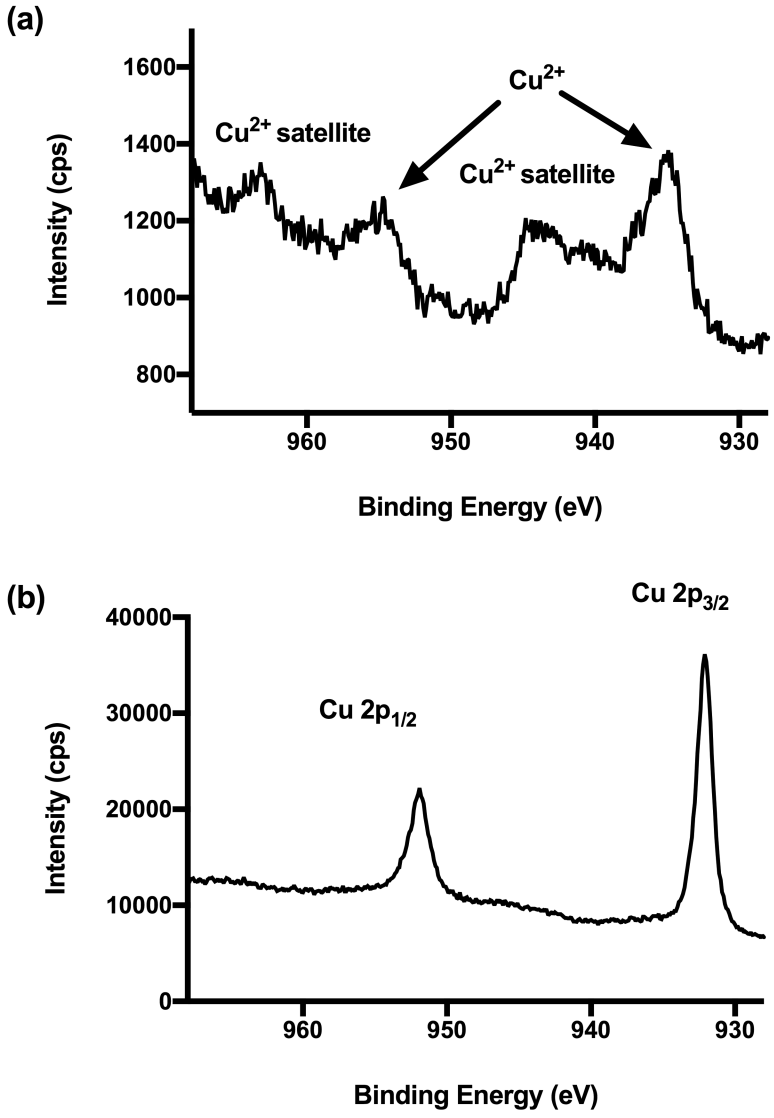

Fig. 3.3.10– Copper region of the XPS spectrum of (a) graphene oxide coating and (b) bare copper. [31]

In order to study the charge-state of the incorporated copper ions, the deposited material was examined using X-ray Photoelectron Spectrometry (XPS). All specimens examined exhibited similar XPS spectra, irrespective of deposition conditions. A representative XPS spectrum is shown in Fig. 3.3.10 (a) and indicates that the copper ions had a predominant

oxidation state of 2+. Specifically, the presence of Cu^{2+} can be identified by two binding energy peaks at approximately 934.5 and 954.5 eV and by shakeup satellite peaks at approximately 944 and 963 eV. The XPS spectrum of cleaned, bare copper used as the anode is also shown in Fig. 3.3.10 (b) for comparison. This spectrum displays binding energy peaks at 952 eV and 932 eV, which can be attributed to Cu $2p_{1/2}$ and Cu $2p_{3/2}$ peaks of bare Cu and Cu_2O.

3.4 Discussion

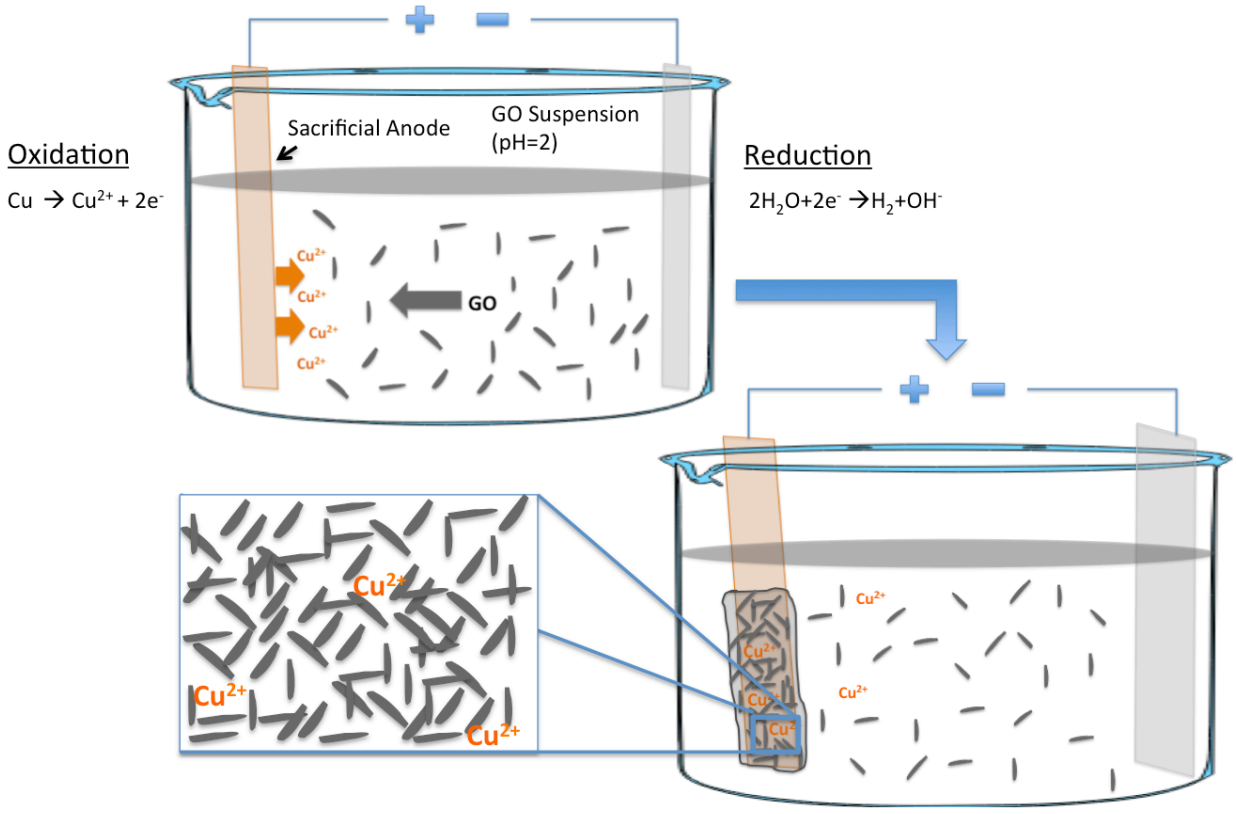

Fig. 3.3.11– Schematic of proposed EC-Driven deposition process. [31]

The above observations provide fundamental scientific insight into the underlying basis for the EC-driven deposition procedure. A simple schematic of the proposed film formation

process is illustrated in Fig. 3.3.11. Under the deposition conditions explored, partial dissolution of the copper anode generates copper ions at the anode/liquid interface. The concentration of the solubilized copper ions increased with increasing applied voltage. These doubly charged copper ions serve as an effective reagent to coagulate electrophoretically migrating GO particles close to the anode via adsorption, double layer compression, and surface charge reduction/neutralization as explained by classical DLVO theory.[19] This interpretation is also consistent with the reported observation of the strong adsorption of copper ions onto GO in the pH range 2-8.[19] Oxygen-containing GO functional groups contain a lone electron pair. By sharing an electron pair, they are capable of efficiently binding a metal ion and forming a metal complex.[19] Fig. 3.3.12 illustrates how copper is incorporated into the GO matrix through binding to the oxygen functional groups.

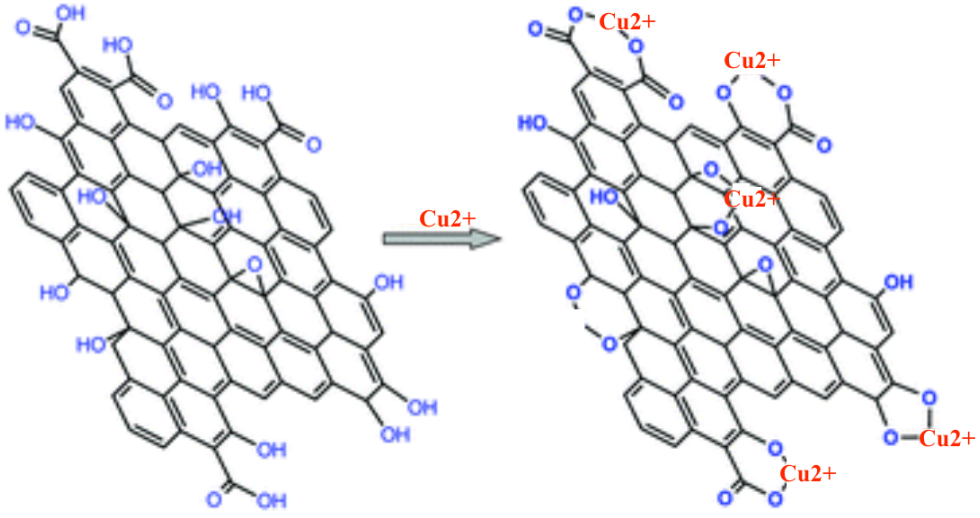

Fig. 3.3.12– Schematic of Cu^{2+} binding to oxygen-containing functional groups in GO matrix. Adapted from Sitko et al.[19]

The combination of electrophoresis and electrocoagulation allows for the ready deposition of the coagulated GO particles and Cu^{2+} ions onto the copper anode. Increasing the applied voltage leads to an increase in the migration rate of the GO particle, in the concentration of the copper ions near the anode, and hence the electrocoagulation rate. By extension, this leads to thicker GO films for a given deposition time. It was also shown that shorter deposition times and larger applied voltages led to an increase in the concentration of copper incorporated in the GO films and that larger applied. Therefore, variation of applied voltage and deposition time allow for tunable incorporation of copper in the deposited material.

In addition, successful EC deposition was not limited to copper substrates. It was also found possible to deposit GO films via EC onto SS 304 stainless steel substrates with a deposition potential of 10V and time of 90 sec, establishing the viability of the approach using alternative anode materials. Raman spectroscopy again confirmed the anticipated GO structure in these films while XPS showed the presence of Fe ions on the GO film coating. In a similar manner to the Cu-anode systems, the iron ions would come from the dissolution of the SS anode, which would lead to electrocoagulation of GO particles as a film on the anode. More detailed studies focusing on a generalized investigation of the EC process and the role of anode identity will be pursued in the future.

3.4 Conclusion

This facile formation approach enables the rapid, controllable development of GO films ranging in thickness from 3 to 130 microns in a matter of seconds to minutes. While this study focused on the use of a copper substrate, it can be extended to other conductive substrates that can generate higher-valent cations (such as aluminum and stainless steel). This strategy opens up new avenues for the production of electrode and filtration membrane materials offering enhanced

performance. For applications where high conductivities are needed (such as biosensors, photovoltaics, and supercapacitors), reduction of the GO/Cu(II) film is needed. Due to the additional presence of copper ions incorporated in the films, there is opportunity for enhanced conductivities compared to traditional rGO conductivities.

Chapter 4: Highly Conductive, Electrocoagulated, Reduced Graphene Oxide/Copper(II) films

4.1 Motivation and Objectives

Graphene is a sheet of sp^2 bonded carbon atoms in a honeycomb crystal lattice. It has very promising properties such as excellent electrical conductivity, mechanical strength, and chemical stability enabling its use in various applications.[1] It provides a new and effective avenue for fabricating electrochemical biosensing,[1] photovoltaic,[5] and supercapacitor[6] devices due its capability for promoting the electron transfer between electroactive species and electrodes.[1]

Many techniques have been introduced to synthesize graphene. Among them, the reduction of graphene oxide (GO), is believed to be one of the most promising methods since it has become a reliable route for obtaining chemically modified graphene platelets in large scale and low cost and temperature. [11,12,13,14,6,15] In addition, both GO and reduced graphene oxide (rGO) have found uses where pristine graphene is not directly applicable, such as filtration membranes for water treatment.[16]

The first study in this work demonstrated controlled and rapid formation of binder-free metal-ion-containing GO films from GO dispersions through an electrochemical method.[31] Specifically, the method is based on copper-ion-assisted electrocoagulation (EC) of GO particles from an aqueous dispersion onto Cu electrodes. The Cu ions are electrochemically released from the Cu electrode itself. This method is carried out at ambient pressure and temperature conditions, and allows the controllable incorporation of Cu^{2+} ions into the graphene matrix, which is essential to ensuring the mechanical and chemical stability of GO films.[18,31]

Graphene exhibits complete, sp^2 hybridized bonding with delocalized π-bonding states that promote the high electrical conductivity characteristic of this material. In contrast, GO is an

electrically insulating material due to its disrupted sp^2 bonding networks. However, electrical conductivity can be recovered by restoring the dominant sp2 network and associated π-bond states through reduction.[25] GO reduction is therefore necessary for applications where high conductivities are needed (such as biosensors, photovoltaics, and supercapacitors). GO reduction can be achieved through chemical, thermal, or electrochemical reduction pathways.[1,6,11,12,14,15,26–30]

Typically, the chemical reduction of GO involves the use of reducing agents, the most common being hydrazine. However, the excessive use of reducing agents could contaminate the resulting product and can be harmful to human health and the environment.[14] Thermal reduction involves the use of high temperature to remove the oxygen functionalities. This can result in significant volume loss.[3] In contrast, electrochemical reduction of GO is a relatively simple, low cost, and an environmentally benign method.

The primary goal of this study was to prepare EC-GO/Cu(II) films for use in applications where high conductivity is needed. Electrochemical reduction was chosen as the reduction method given its relative simplicity and the direct compatibility with the EC deposition process itself. To be more precise, electrochemical reduction was performed by a DC constant potential technique and confirmed by a cyclic sweep.

The objective of CV was to survey reduction processes in the GO/Cu material, provide insight on the reversibility of the action, and determine if there were distinct reduction potentials which can be attributed to each of the primary constituents (i.e. GO and Cu^{2+}) present in the system. By having distinct reduction potentials for each of the constituents, selective reduction of different constituents can be achieved. By extension, this provides an opportunity for enhanced control of the conductivity of the film.

The objective of the DC constant potential technique was to provide a more thorough reduction of both of the primary electrochemically active constituents present in system throughout the entirety of the film. This is intended to produce enhanced conductivity relative to traditionally reduced GO films without Cu addition. X-ray photoelectron and Raman spectroscopy were used to determine if both the primary constituents of the GO/Cu(II) films were reduced throughout the entirety of film and a four point-probe was used to calculate the sheet resistance and conductivity of the films.

4.2 Experimental Methods

4.2.1 Material Synthesis

A GO suspension was created through the modified Hummers' method described in the Experimental Methods section of chapter 3. The primary suspension had a GO concentration of approximately 8 mg/mL, a pH of 2, and a conductivity of 7.2 mS/cm. Films were deposited on copper substrates by the EC technique describe in the Experimental Methods section of chapter 3. An applied potential of 5V *(*field strength of approximately 3.3 V/cm*)* for 10 seconds was used, leading to film thicknesses of approximately 15 microns.

4.2.2 Characterization Techniques

Electrochemical Reduction

Electrocoagulated GO/Cu(II) films were electrochemically reduced under both potentiodynamic and potentiostatic conditions. In both cases, a standard three-electrode electrochemical cell containing a buffer or supporting electrolyte was used. Silver/silver chloride (Ag/AgCl) was used as the reference electrode, platinum as the counter electrode, and GO/Cu(II)

was deposited on a copper substrate that served as the working electrode. It has been shown that a near neutral or low pH value is favored for the reduction of GO.[14] Therefore, 0.5M sodium chloride (NaCl, Sigma Aldrich, ≥ 99.5%) with a pH of approximately 6 was used as the supporting electrolyte.

Cyclic voltammetry (CV) is a type of potentiodynamic electrochemical measurement. In this case, the working electrode potential is varied linearly over a fixed range. After the final potential has been reached, the potential is ramped linearly in the opposite direction until the initial potential has been reached. In this work, CV was performed through 5 scans over an applied potential range of 0.1 to -1.1 V and a scan rate of 50 mV/s on a Potientiostat/Galvanostat (Gamry Instrument). Voltammograms were created where the current of the working electrode was plotted versus the potential of the working electrode.

The CV experiment provides information on redox potentials of electro-active couples by the presence of positive or negative peaks in the current (typically due to mass transport and/or surface depletion effects) at specific potentials. Negative shifts in the current from 0.1 to -1.1 V correspond to reduction, while positive shifts from -1.1 to 0.1 V correspond to oxidation. The CV experiment also provides information on the reversibility of the electrochemical reactions taking place in the cell. If a current shift associated with a redox reaction occurs in one direction of the scan, but not the opposite, then the reaction is considered irreversible since only reduction or only oxidation is occurring.

The CV analysis of the primary EC GO/Cu(II) films provided reduction potential values, however there is no indication of which constituent(s) (i.e. GO or Cu^{2+}) of the system are being reduced at the specific reduction potentials found. In order to attribute the reduction potentials to specific constituents, additional CV scans were performed. Both Cu^{2+} and GO were individually

examined in order to determine their associated reduction behavior. In the case where no Cu^{2+} was present, the working electrode described above was replaced by a Pt substrate with a dip coated GO film. In the case, in which only Cu was to be examined, a platinum electrode was used as the working electrode and 1000ppm of Cu^{2+} was added to the 0.5M NaCl electrolyte.

In another experiment, potentiostatic electrochemical process conditions, i.e. one where the potential is held constant over time, were pursued. Here, a more thorough reduction of both GO and Cu^{2+} was sought when compared to the 50 mV/s potential sweep used in the CV scans. In this case, the GO/Cu film was exposed to a constant -0.9V potential for 15 hours using a Potientiostat/Galvanostat (PAR 273A) while the current was measured.

Using the CV scans of the GO/Cu(II) system and the corroborating, individual constituent studies above for guidance, an applied potential of 0.9V (with respect to Ag/AgCl reference electrode) was chosen to be more negative than both the GO and Cu2+ reduction potentials. This ensured that both species were subjected to reducing conditions. The reduced film was then carefully delaminated by a nitrogen gas stream and thoroughly washed in DI water and IPA. In future discussion, the "front side" of the film corresponds to that surface in contact with the electrolyte, while the "back side" of the film corresponds to that in contact with the copper substrate.

X-ray Photoelectron Spectroscopy (XPS), Raman Spectroscopy, and Inductively Coupled Plasma-Mass Spectroscopy (ICP-MS)

The theoretical basis for XPS, ICP-MS, and Raman Spectroscopy was described in the experimental methods section of Chapter 3.

In this study, a Kratos Axis 165 Ultra X-ray photoelectron spectrometer was used to determine the prevalent oxidation state of copper ions and GO species (e.g. C-O bonds) present

in the films before and after electrochemical reduction processing. Measurements were taken with a monochromatic Al Kα excitation source and used a hybrid active lens mode and charge neutralizer. Argon-ion sputter cleaning and an angle-resolved collection geometry were used to obtain depth profiles of the chemical species of interest.

A Jobin–Yvon Horiba Lab-Ram HR800 micro-Raman spectrometer was used with an Argon ion laser (514.5 nm) to determine the effect of reduction on the GO structure through an examination of primary vibrational resonances described in Section 3.2.2. The beam was focused with a 100X microscope objective with a corresponding 10 μm spot size and 100 mW incident power at the sample surface. Stokes-scattered spectra were collected over of a spectral range of 1000-3000 cm^{-1} (5 $cm^{-}1$ resolution). The spectra were collected with a thermoelectrically cooled CCD array using an integration time of 20s and signal averaging over 10 scans.

In addition, Inductively Coupled Plasma-Mass Spectrometer (Agilent 7700x ICP-MS) to determine the concentration of copper and sodium incorporated in EC GO/Cu(II) and reduced EC GO/Cu(II) films. The ICP-MS employed an RF power of 1550W, a plasma gas flow of 15 L/min, a carrier gas flow of 0.85 L/min, and a makeup gas flow of 0.15 L/min. The films were prepared identically to those in section 3.2 prior to the ICP-MS analysis.

Four-point Probe

The four-point probe technique allows the measurement of sheet resistance (and corresponding conductivity) of the rGO thin films.. The probes are set up into separate pairs of current-supplying and voltage-sensing electrodes. Fig. 4.2.1 illustrates the electronic setup of the four-point probe. A high impedance current source is supplied through the outer probes and voltage is measured between the inner probes by a voltammeter. For low resistance values, it is

advantageous to separate current and voltage electrodes, since this removes the lead and contact resistance from the measurements.

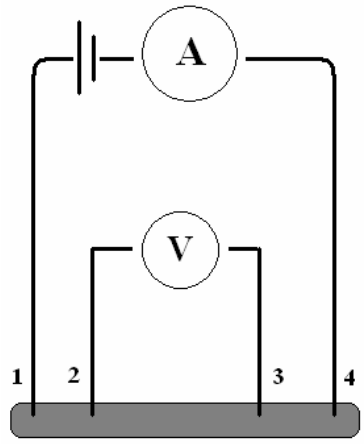

Fig. 4.2.1- Schematic representation of four-point probe electronic setup. Current is supplied through connections 1 and 4 and voltage is measured between connections 2 and 3. (Public domain)

In a three-dimensional sample, resistance can be expressed by the following equations:

$$R = \rho \frac{L}{A} = \frac{\rho}{t} \times \frac{L}{W} = R_S \times \frac{L}{W} \qquad \text{(Eq. 4.2.1)}$$

Where R is the resistance, R_S is the sheet resistance, ρ is the resistivity, L is the length, and A is the cross-sectional area, which is the product of the sheet thickness (t) and the width (W). The sheet resistance represents the quotient of the resistivity and sheet thickness. It can be directly measured by the four-point probe method with units Ω/□.[88]

A Jandel Model RM3 four-point probe station with a probe spacing of 1 mm was used in this work to determine the sheet resistance of the rGO samples. For very thin films, where the thickness is significantly smaller than the probe spacing, one can assume a current ring emanating from the outer probe tips. The sheet resistance can then be mathematically defined by the following equation:

$$R_S = \frac{\pi}{\ln(2)} \times \frac{V}{I} \qquad \text{(Eq. 4.2.2)}$$

Where V is the voltage and I is the current. The bulk resistivity of sample can simply be calculated by taking the product of the sheet resistance and thickness, and the conductivity can then be determined by taking the inverse of the resistivity:

$$\sigma = \frac{1}{\rho} = \frac{1}{R_S \times t} \quad \text{(Eq. 4.2.3)}$$

where ρ is the bulk resistivity measured in Ω.cm, and σ is the conductivity measured in S/cm.[88] The conductivity values determined by the four-point probe were used to quantify the extent of the electrochemical reduction on the GO-based samples.

Transmission Electron Microscopy

In this work, scanning transmission electron microscopy (STEM) was used to study the structure of the GO and rGO films fabricated through electrocoagulation. In this form of electron microscopy, an electron beam passes through the specimen that has been made electron-transparent. The material nanostructure can be examined through an analysis of different beam-sample interaction mechanisms contributing to image contrast. The contrast mechanisms address such issues as beam scattering or diffraction created by various elements of the microstructure, including crystalline structure and defects. This method allowed for the characterization of the GO-based structure as well as the distribution and size of copper-based particles embedded in the matrix. A more detailed description of sample preparation, STEM operation, contrast mechanisms, and elemental analysis is present below.

Focused-Ion Beam:

Appropriate sample preparation is key to obtaining high-resolution STEM images. In this study, the specimen thickness needed to be sufficiently thin to allow proper electron transparency

and imaging contrast development.[89,90] Cross-sectional GO and rGO samples were prepared with a method known as focused ion beam (FIB) using a FEI Helios DualBeam SEM/FIB. Specifically, a lift-out technique was used, where the electron transparent thin film is removed from the bulk sample and analyzed directly by STEM. An area of interest was first selected visually with the microscope's imaging capabilities. A rectangular carbon-platinum-carbon layer was then deposited through assisted chemical vapor deposition over the area of interest to prevent damage and spurious sputtering of the top portion of the sample. The layer was also used as a mask to delineate the area of interest. A focused beam of gallium atoms with a voltage of 30 kV then milled trenches around the area of interest. Specifically, rough cuts were made at front, back, and bottom of the region of interest. Another probe was then placed near mask and is welded to area of interest through FIB platinum deposition. The section is then cut away from the bulk sample by further milling, lifted out and transferred to a molybdenum STEM grid. The weld on the probe is then cut and the specimen is thinned further with the ion beam until the thickness was satisfactory for high-resolution imaging. The final specimen sizes were approximately 7 μm × 8 μm x 600 nm. It is important to note that the films used in this study had a total thickness of 15 μm. Therefore, only about half the thickness of the deposited material was capable of being analyzed by STEM. The STEM analysis was performed from the surface of the film initially in contact with the copper electrode to a distance of about 7 μm into the film.

STEM operation and imaging modes:

The molybdenum grid was then transferred and inserted into a Hitachi HF 5000 STEM for microstructural imaging. The STEM was operated at an acceleration voltage of 60 kV to ensure as little damage as possible to the rGO/GO film. A focused electron beam is scanned over

the GO/rGO samples. The interaction of the electrons with the sample as the beam is transmitted through forms an image, which is then magnified and focused onto a fluorescent screen. Fig. 4.2.2. shows a schematic of a STEM instrument.

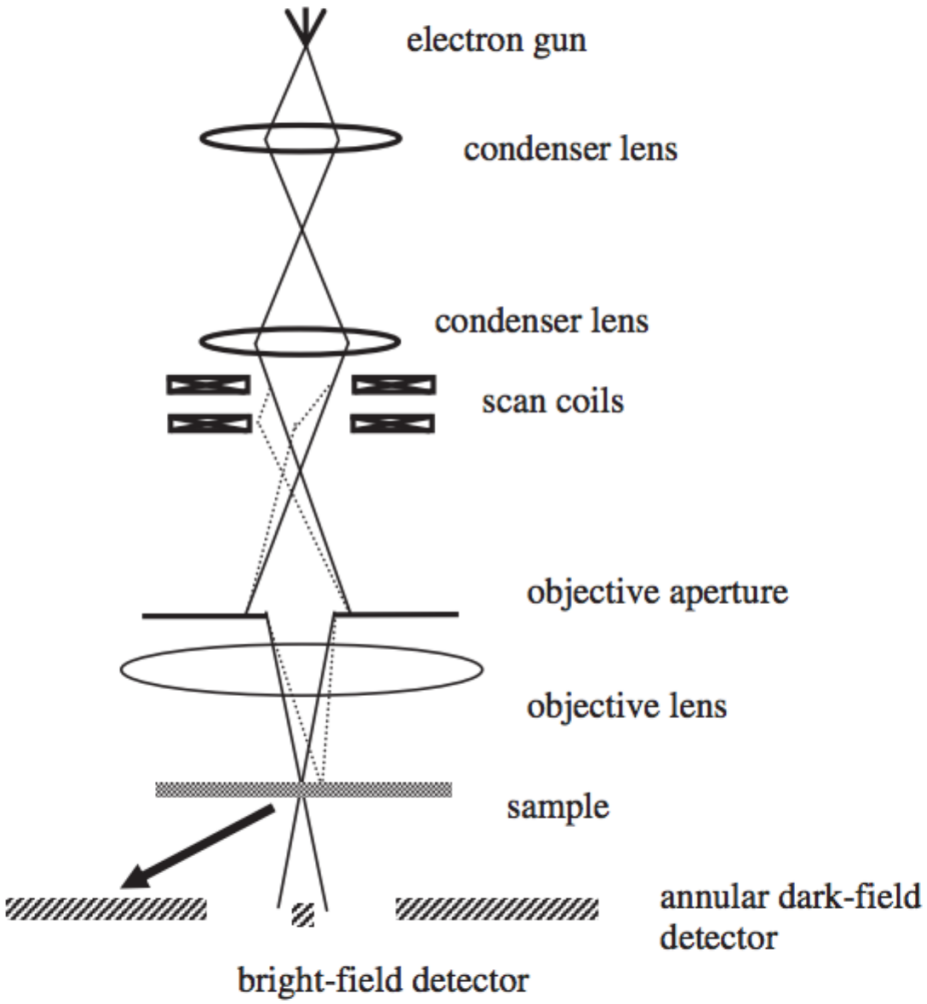

Fig. 4.2.2- Schematic diagram of STEM instrument.[91]

In this work, the STEM was operated through an annular dark field (ADF) imaging mode among others. In the ADF mode, images are formed by collecting fore-scattered electrons with an annular dark field detector, which lies outside of the path of the directly transmitted beam (as

evident in Fig.4.2.2).[91] One of the main advantages of this mode is that the scattered electrons are most strongly influenced by atomic number. Indeed, the strength of scattering increases with atomic number Z. The ADF mode therefore provides atomic number contrast images, where a brighter contrast corresponds to a higher atomic number.[90,91]

The STEM was also operated in a bright field (BF) imaging mode. In the BF mode, detectors are positioned in the path of the direct beam (as evident in Fig. 4.2.2). The BF detectors receive transmitted electrons that exit the sample at angles smaller than the incident beam convergence angle with respect to the optic axis.[91] The image is a result of the weakening of the electron beam and its interaction with the sample. The image produced is a function of mass-thickness and diffraction contrast. This signifies that areas with heavy atoms are enriched with higher intensity, while crystalline areas appear dark by contrast.[90,91]

The STEM was finally operated in a secondary electron (SE) imaging mode. During the electron beam scan, secondary electrons are also produced. The secondary electrons originate from the surface regions of the samples and typically occur due to inelastic interactions between the electron beam and the sample. This mode is beneficial for the inspection of the topography of the sample's surface.[90,91]

Energy Dispersive X-Ray Spectroscopy:

Energy dispersive X-ray spectroscopy (EDS) is an elemental analysis technique, which can be used in conjunction with STEM. The EDS technique in the Hitachi HF 5000 was primarily used to determine presence and spatial distribution of elements such as copper (among others) in the graphene matrix. As the STEM's electron beam is focused on the sample, it may excite and eject electrons from inner shells. This generates electron vacancies, which are then

filled by electrons from a higher-energy shell. The difference in energy between the two shells may be released in the form of x-ray emission. Fig. 4.2.3 depicts the energy levels of atomic electrons and species of characteristic x-rays. An x-ray detector measures the amount of x-rays emitted from the sample and their corresponding energy. The emitted x-rays have a wavelength (or energy) characteristic and unique to the element from which it came.[92] Therefore, EDS measures the elemental composition of a sample as well as the elemental distribution.

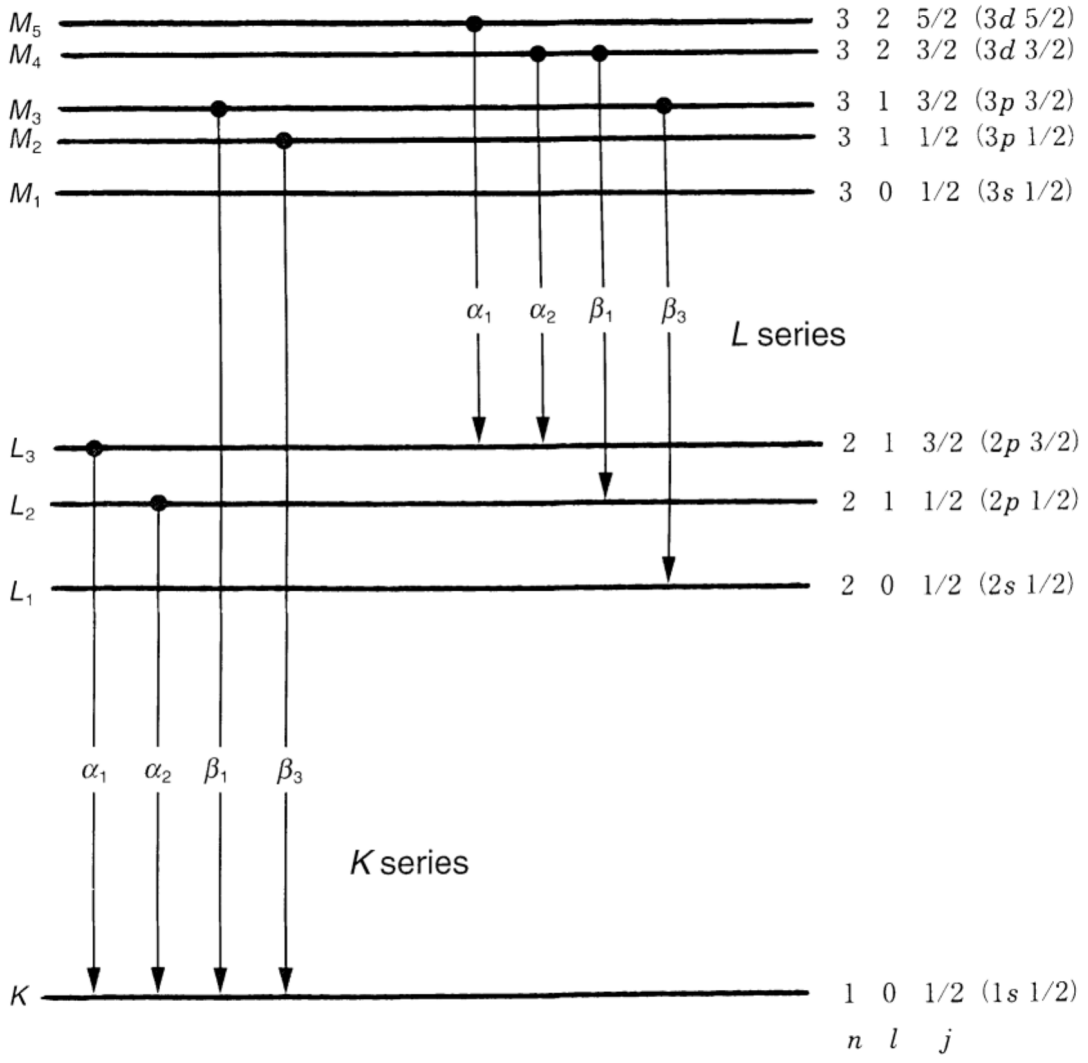

Fig. 4.2.3- Energy levels of atomic electrons and species of characteristic x-rays. [92]

4.3 Results and Discussion

4.3.1 Cyclic Voltammetry

Cyclic voltammetry (CV) was performed on the GO/Cu(II) films deposited on the copper substrate in a potential range from 0.1 to -1.1 V. Fig. 4.3.1 illustrates the first 5 CV scans at a scan rate of 50 mV/s. During the first scan, the presence of a large reduction current peak (i.e. local minima in current) centered at a potential of approximately -0.6 V is visible. In subsequent scans, the reduction current peak decreases in amplitude and is shifted towards -0.2 V. The lack of oxidation potential peaks (i.e. local maxima in current) indicates the irreversibility of the reactions.

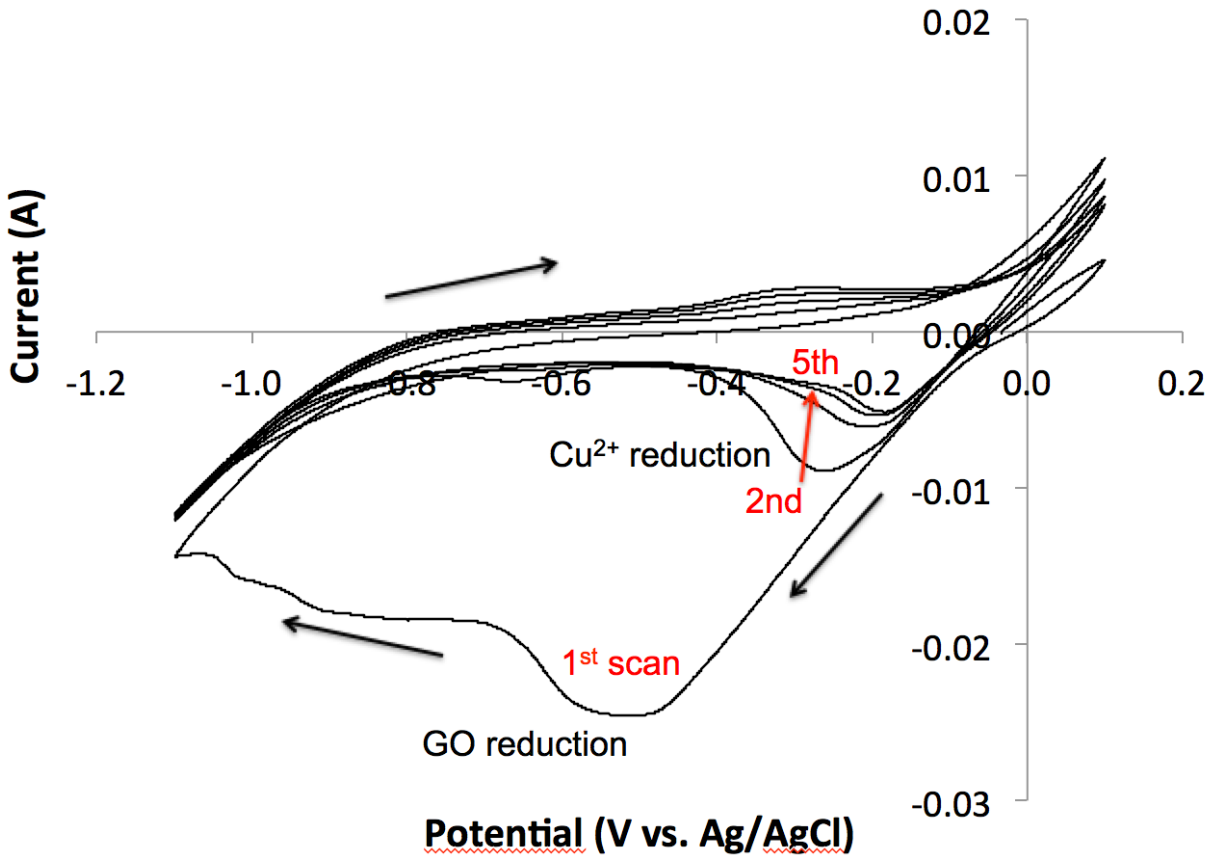

Fig. 4.3.1- CV scans of EC GO/Cu(II) film. Black arrows indicate voltage sweep direction.

The preliminary results validate that reduction is occurring, however there is no indication of which constituent(s) (i.e. GO or Cu^{2+}) of the system are being reduced at the specific reduction potentials found. There is the possibility of only one constituent being reduced, having a CV reduction potential at -0.6V (with respect to Ag/AgCl) on the first scan, which then shifts to more positive reduction potentials at subsequent scans. But there is also the possibility of both constituents being reduced, one being reduced at -0.6V (only on first scan) and the other being reduced at approximately -0.2V (on all scans). In order to determine if the reduction potentials at -0.6V and -0.2V were associated to different constituents of the films, additional CV studies were needed. As described earlier, different electrochemical systems in which only Cu^{2+} and only GO were present were produced and tested. Fig. 4.3.2 depicts the cyclic voltammograms of a system where no Cu^{2+} is present (i.e. the GO system). The figure shows a reduction current peak centered at approximately -0.6V on the first scan. In subsequent scans, no further reduction is visible. Fig. 4.3.3 depicts the cyclic voltammograms of a system where Cu^{2+} ions are present and GO is absent in the system. The figure illustrates a reduction current peak situated at approximately -0.2V. After each subsequent scan, the reduction potential is shifted to a slightly more positive value. The results from both of the isolation experiments suggest that the reduction potentials at -0.6V and at -0.2V in Fig. 4.3.1 are, in fact, attributable to GO and Cu^{2+}, respectively.

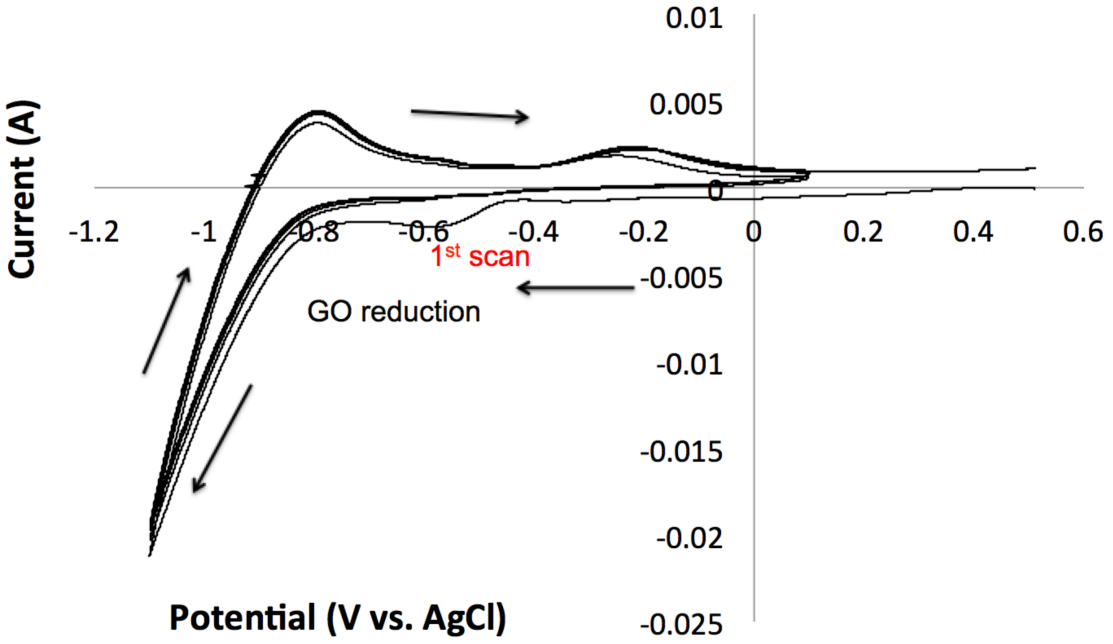

Fig. 4.3.2- CV scans using Pt dip-coated with GO working electrode without presence of Cu^{2+}. Black arrows indicate voltage sweep direction.

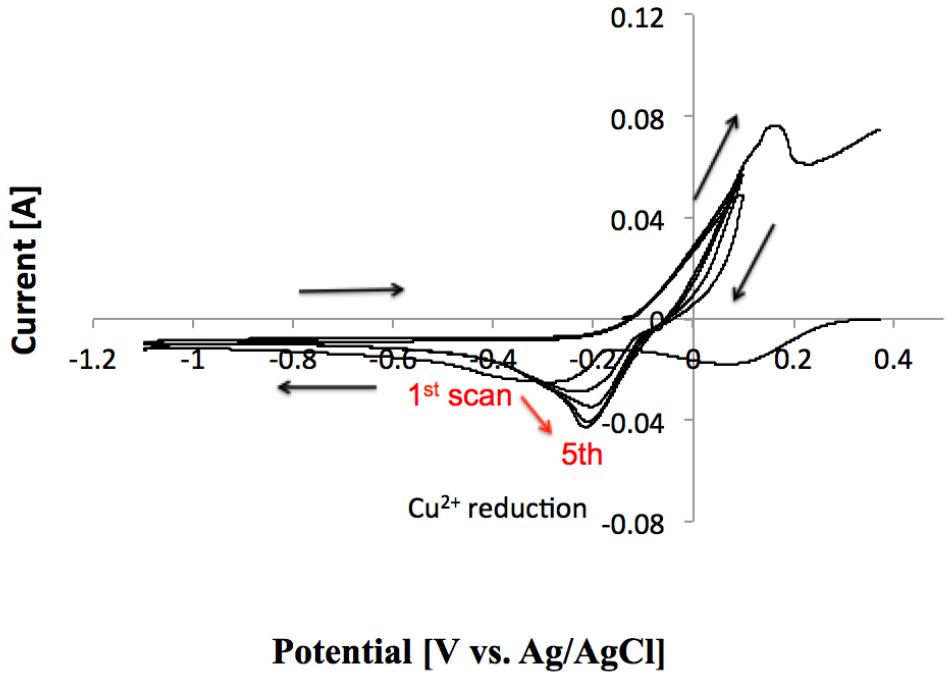

Fig. 4.3.3- CV scans using Pt working electrode in 1000 ppm Cu^{2+} containing 0.5M NaCl solution (no GO present). Black arrows indicate voltage sweep direction.

4.3.2 Constant Potential Reduction

To ensure complete reduction, the potential value during DC potential experiments was chosen to be slightly more negative than the GO reduction potential indicated by the CV experiment. The relative reduction potentials for Cu and GO provided by the CV studies above imply that either Cu^{2+} and GO together or Cu^{2+} separately can be reduced through selection of a single potential value. Indeed, a potential more positive than the GO CV reduction potential, but more negative than the Cu^{2+} CV reduction potential would only reduce Cu^{2+}, while a reduction potential more negative than the GO CV reduction potential would reduce both constituents. In this case, a potential of -0.9V was chosen to ensure reduction of both constituents in the EC GO/Cu(II) films as described in Section 4.2.

The EC GO/Cu(II) film on the Cu substrate was examined using X-ray Photoelectron Spectrometry (XPS), before and after the DC reduction test, in order to provide evidence for GO reduction (i.e. the loss of oxygen-related species) on the surface of the film. A representative XPS C1s spectrum before DC potential exposure is shown in Fig. 4.3.4(a) and the spectrum is in good agreement with published spectra for GO.[2,12,26] The peak centered at approximately 287 eV is associated to C-O and the peak centered at approximately 285 eV is associated with sp^3 carbon. Fig. 4.3.4(b) illustrates the spectrum after application of the constant potential and is also in good agreement with published spectra for rGO.[12,26] There is a significant decrease in the peak associated to C-O, indicating considerable deoxygenation of GO. In addition, the peak that was centered at 285 eV has shifted by 1 eV to approximately 284 eV implying a transition from sp^3 to sp^2 carbon. The GO after the reduction test is therefore shifted to an sp^2 hybridized chemistry more similar to graphene. The C1s spectrum analysis demonstrates GO reduction on the surface

of the EC GO/Cu(II) film.

XPS was also used in order to confirm a shift in the charge-state of the incorporated copper ions before and after the applied constant potential. A representative XPS Cu2p spectrum before reduction is shown in Fig. 4.3.4(c) and confirms that the copper ions had a predominant oxidation state of 2+. Specifically, the presence of Cu^{2+} can be identified by two binding energy peaks at approximately 934.5 and 954.5 eV and by shakeup satellite peaks at approximately 944 and 963 eV. After the applied constant potential treatment, no copper was detected on surface of the film in contact with the electrolyte. Through angle-resolved measurements and after only 20 min of sputtering, copper was detected at a depth of less than 100 nm. This is consistent with Cu^{2+} electromigration further into the film towards the copper electrode during the application of the negative potential. The representative Cu2p XPS spectrum after reduction is shown in Fig. 4.3.4(d). This spectrum displays binding energy peaks at 952 eV and 932 eV, which can be attributed to Cu $2p_{1/2}$ and Cu $2p_{3/2}$ peaks of bare Cu and Cu_2O. The Cu^{2+} has therefore been reduced to either Cu or Cu^{+}.

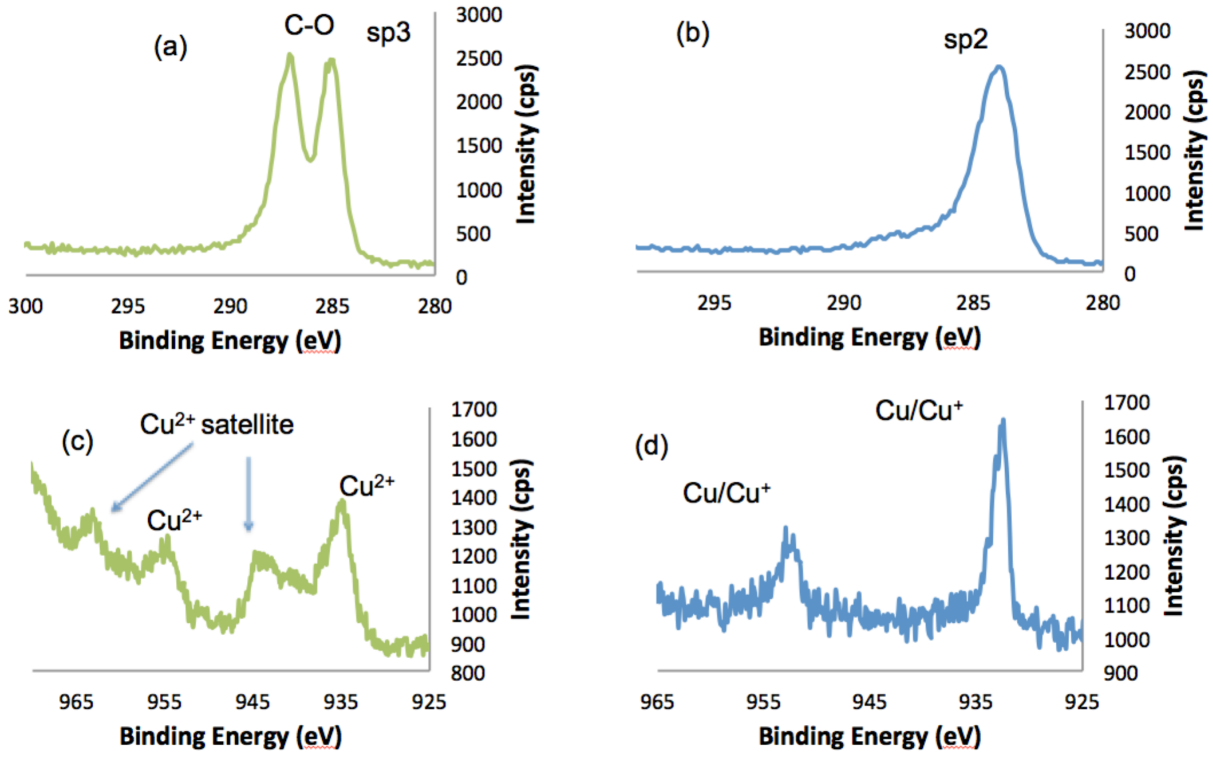

Fig. 4.3.4- XPS: C1s spectrum before (a) and after (b) electrochemical reduction, and Cu2p spectrum before (c) and after (d) electrochemical reduction

The same films were then delaminated from the Cu substrate and Raman spectroscopy was performed to confirm the reduction of GO and gain insight on the extent of reduction. Fig. 4.3.5 demonstrates the characteristic Raman spectra before and after the constant potential reduction on the front and back sides. The spectrum before reduction is in good agreement with published spectra for GO. The peak centered at approximately 1350 cm^{-1} is the D band, which is associated with the breathing modes of six membered carbon rings that are activated by defects. The G-band, located in the range of 1590 to 1600 cm^{-1} is attributed to E_{2g} phonons at the Brillouin zone center. Two peaks, also present and centered at approximately 2700 and 2900 cm^{-1}, represent the 2D band and the D+G band respectively. After the constant potential reduction, there is a noticeable increase in the intensity of the D band to that of the G band (I_D/I_G

ratio) after removal of background, which is commonly observed for rGO.[13,15] It represents the restoration of sp^2 carbon and a decrease in the average size of the sp^2 domains upon reduction. In addition, the spectra from the back and front sides of the film match implying a GO reduction throughout the entirety of the film. It is important to also note that the Raman spectrum for the surface of the film after the CV reduction matches the spectra of the front and back sides of the films after constant potential reduction. The CV reduction was therefore also capable of reducing GO on the surface of the EC GO/Cu(II) film.

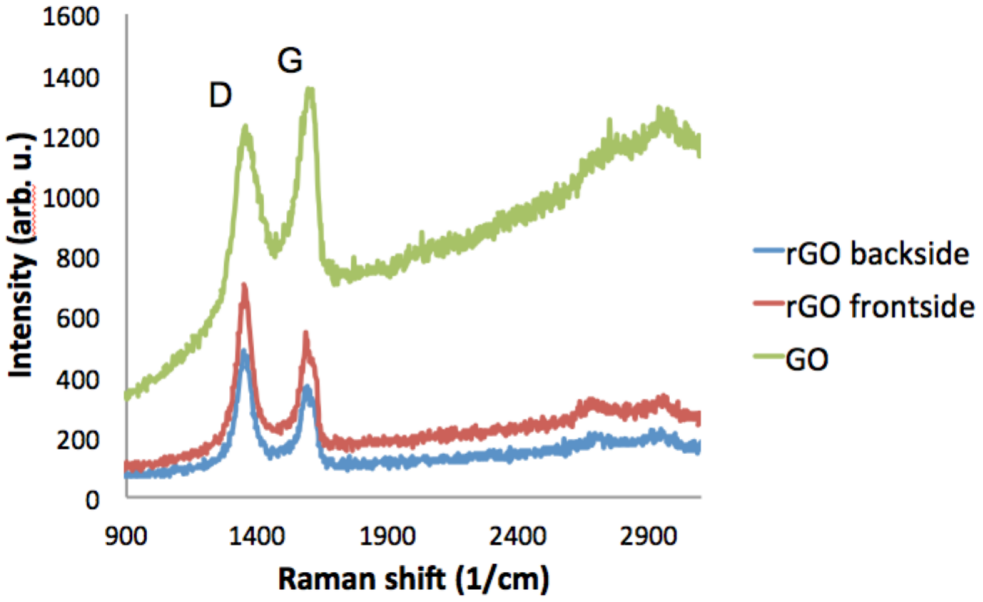

Fig. 4.3.5- Raman spectra of film before reduction (green curve) and after constant potential reduction (red and blue curves)

The sheet resistance of the EC GO/Cu(II) films was greater than the MΩ/sq range. However, after going through a constant potential reduction and washing process in DI water and IPA, the sheet resistance was significantly reduced to 22+/-4 Ω/sq on the back side and 24+/-3 Ω/sq on the front side of the film. The sheet resistances correspond to conductivity values ranging from 2800-3300 S/m. These reduced GO/Cu(II) conductivities are comparable and even greater than the rGO conductivities from some of the most common reduction techniques

(Hydrazine: 2420 S/m,[13] L-ascorbic acid: 800 S/m,[15] Al/HCl: 2100 S/m,[93] Thermal exfoliation:1000-2300 S/m,[94] etc.). The EC GO/Cu(II) films were therefore not only made conductive, but their conductivity was also enhanced compared to Cu-free rGO films.

4.3.3 Cross-Sectional Microscopy and Mass Spectroscopy Characterization

A cross-sectional examination of an EC GO/Cu(II) film was performed by FIB and STEM. As described earlier, the FIB was only capable of creating a cross-section extending approximately 6 microns into the 15 micron thickness of the film. Fig. 4.3.6 is a simple schematic illustrating the FIB process and subsequent orientation of the GO film. A representative STEM image in SE mode, shown in Fig. 4.3.7, exhibits a layered microstructure containing cracks and voids. The surface of GO in contact with the mask used for FIB was the surface in contact with the copper electrode before delamination. The white dots present throughout film are a mixture of copper oxide particles and crevices of about 20 nm in diameter. Corresponding STEM images in ADF and BF modes are present in the Appendix A. Fig. 4.3.8 (a) and (b) offer a higher magnification comparison of the microstructure between the crevices and copper oxide particles.

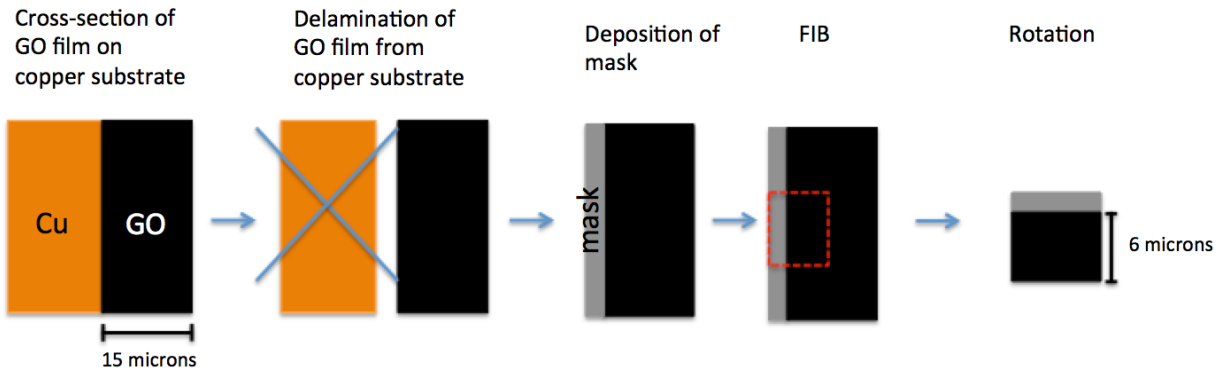

Fig. 4.3.6- Simple schematic of FIB process and subsequent GO film orientation.

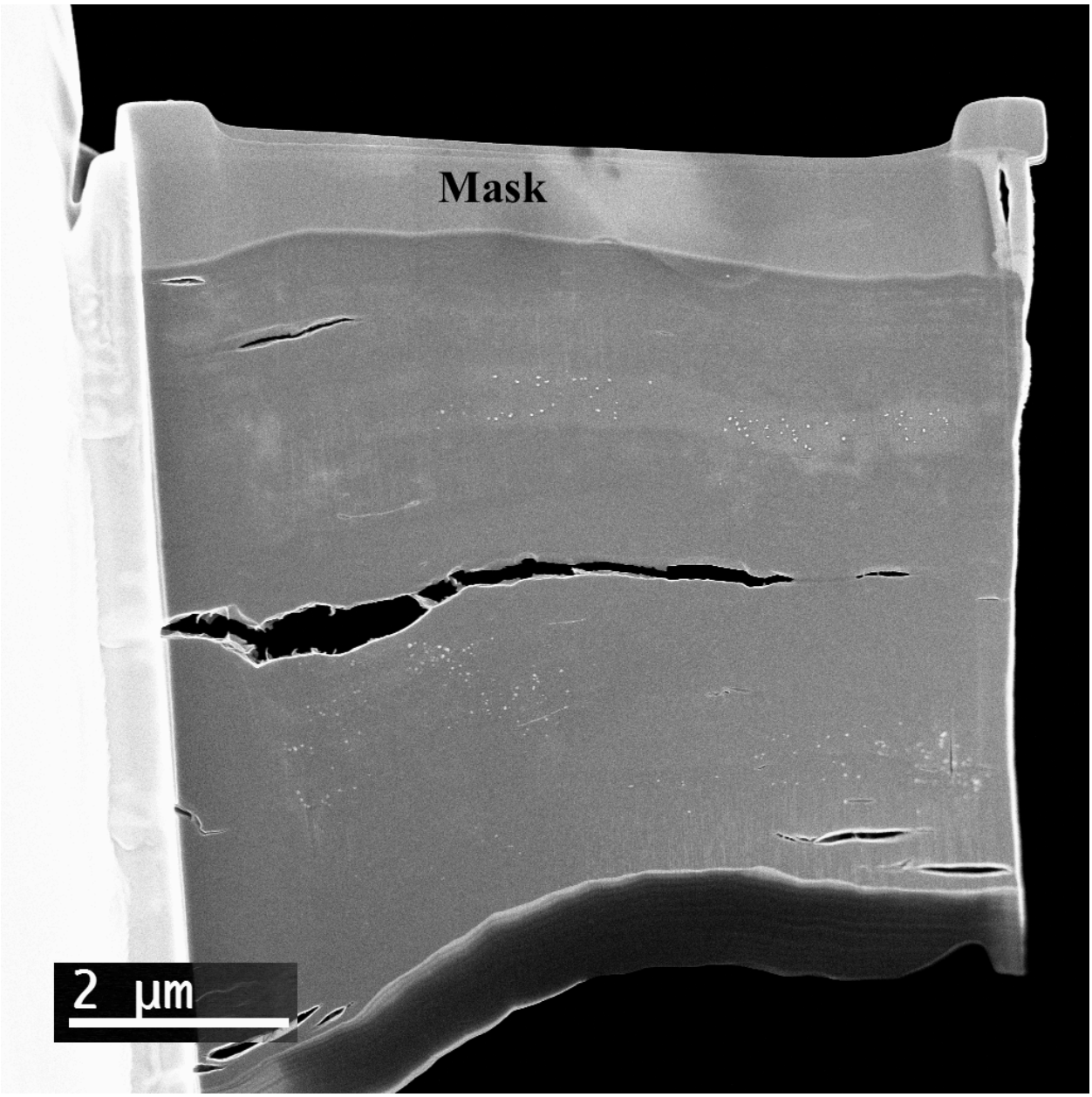

Fig. 4.3.7- Cross-sectional STEM image of EC GO/Cu(II) under secondary electron (SE) mode. The surface of GO in contact with the mask was GO surface in contact with the copper electrode before delamination. Towards bottom of image (darker area) there is re-deposition from the ion beam. (2000x magnification)

Copper ions are present throughout the entire portion of film as demonstrated by the EDS map of Fig. 4.3.9. However, it is important to note that there is a greater presence of copper closer to the surface in contact with the mask (originally in contact with the copper electrode). As the distance from that surface increases, the concentration of copper incorporated decreases.

This observation is in good agreement with the ICP-MS data present in Chapter 3, which showed that concentration of copper incorporation decreases with increasing film thickness, implying that most of the copper is incorporated near the anode surface during electrocoagulation. ICP-MS was performed on another EC GO/Cu(II) film created under same experimental conditions as the film undergoing STEM analysis. The concentration of copper incorporated into the GO film was approximately 92 mg/g.

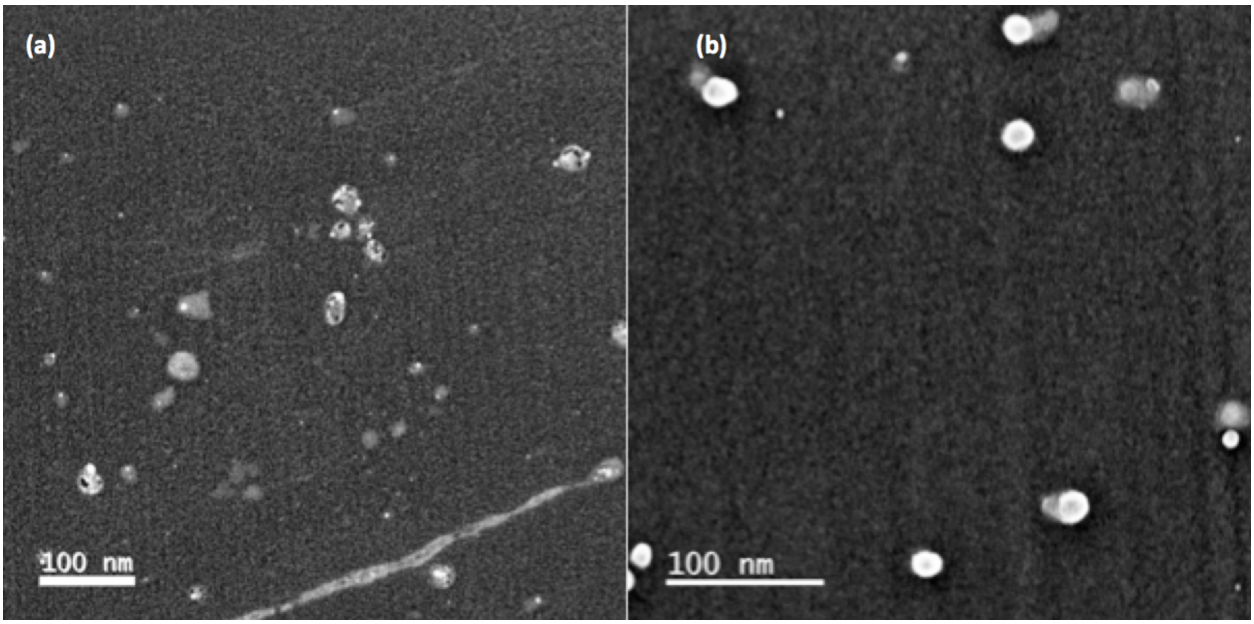

Fig. 4.3.8- STEM in SE mode: (a) higher magnification (30kx) image of crevices present throughout film. (b) higher magnification (50kx) image of copper oxide particles present throughout film.

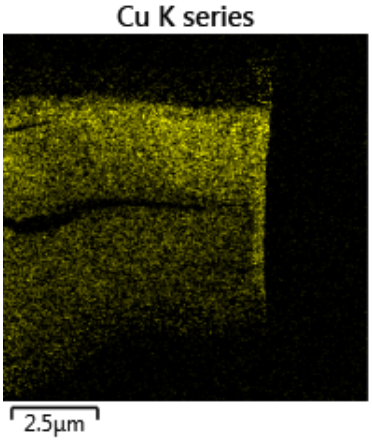

Fig. 4.3.9- EDS: Copper distribution throughout the film removed by FIB in Fig. 4.3.6.

Additionally, a cross-sectional examination of the EC GO/Cu(II) after the constant potential reduction was performed by FIB, SEM and STEM. With the FIB, approximately 7 microns out of the 15 micron thickness were removed and examined. Similarly to the unreduced film, the surface of rGO in contact with the mask was the surface in contact with the copper electrode before delamination (see Fig. 4.3.6 as reminder). A representative SEM image shown in Fig. 4.3.10 exhibits a similar layered microstructure to that of the film before reduction. However, most of the voids, fissures, and crevices have been expanded and filled with NaCl (confirmed via EDS) originating from the 0.5M NaCl electrolyte used in the electrochemical reduction setup. In addition, EDS analysis (Fig. 4.3.11) of the sample shows a noticeable decrease in the presence of copper throughout the first 7 microns of the film starting from the surface, which was in contact with the copper electrode.

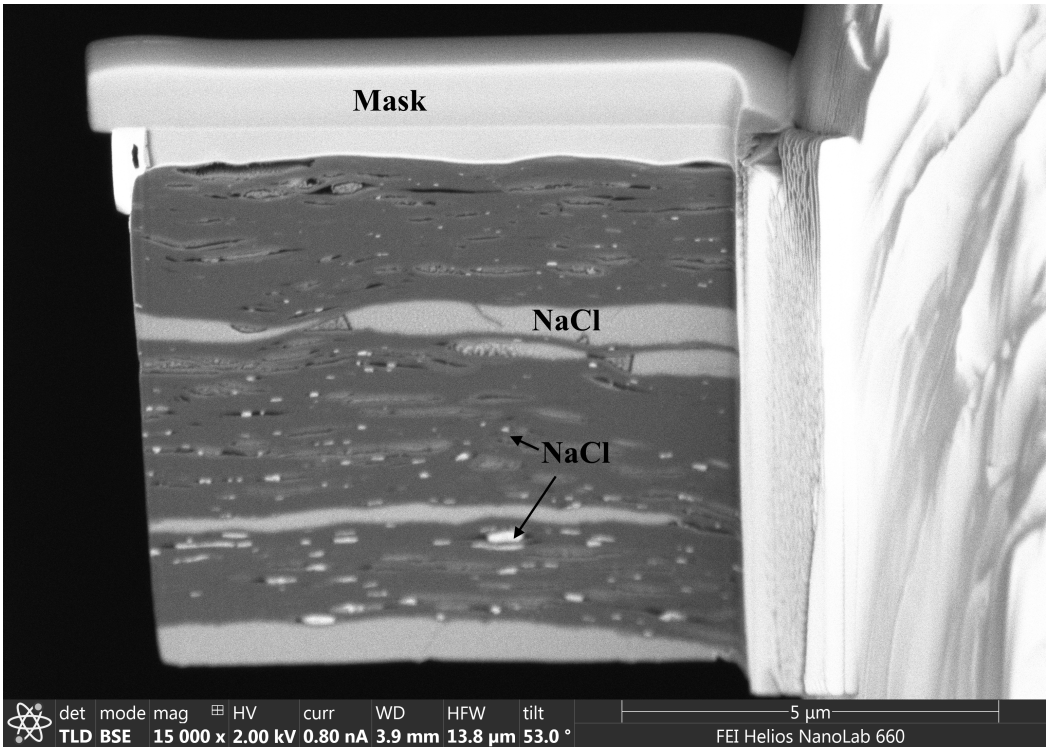

Fig. 4.3.10- Cross-sectional SEM image of reduced EC GO/Cu(II) film under back-scatter electron (BSE) mode. The surface of film in contact with the mask was GO surface in contact with the copper electrode before delamination. NaCl incorporation also shown.

Fig. 4.3.12 offers a higher magnification (8000x) STEM image (in SE mode) of a location on the film where copper is present. Corresponding STEM images in ADF and BF modes are present in the Appendix B. Fig. 4.3.13 is the corresponding EDS analysis of the higher-magnification location. The analysis shows that copper is bonded to oxygen as well as chlorine in some locations. The copper is present in the form of agglomerated particles ranging 100-200 nm in diameter. NaCl is also present in the form of agglomerated particles, but with a diameter ranging 20-40 nm. NaCl is in the form of an ionic solid; its presence should therefore not greatly contribute to the previously reported conductivity values.

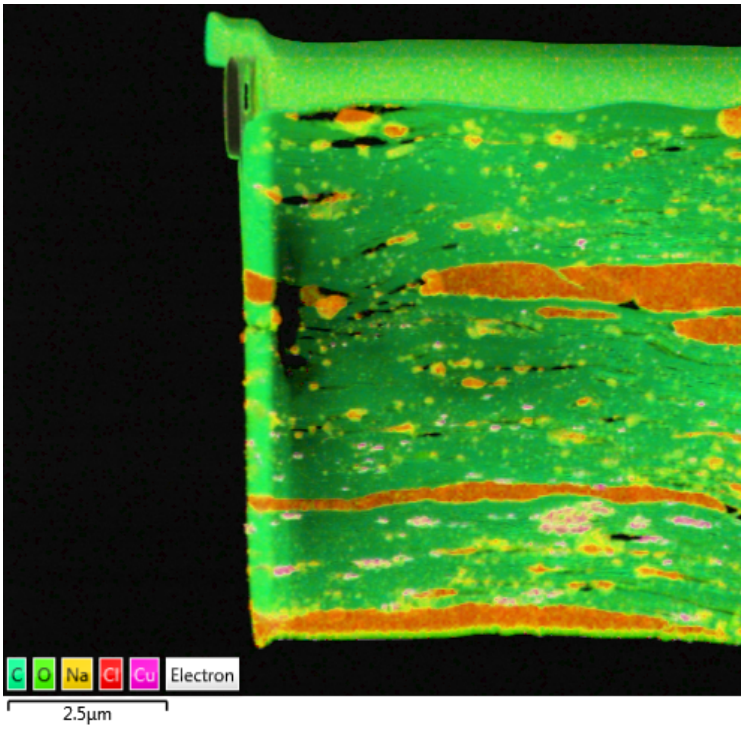

Fig. 4.3.11- EDS analysis of reduced EC GO/Cu(II) film

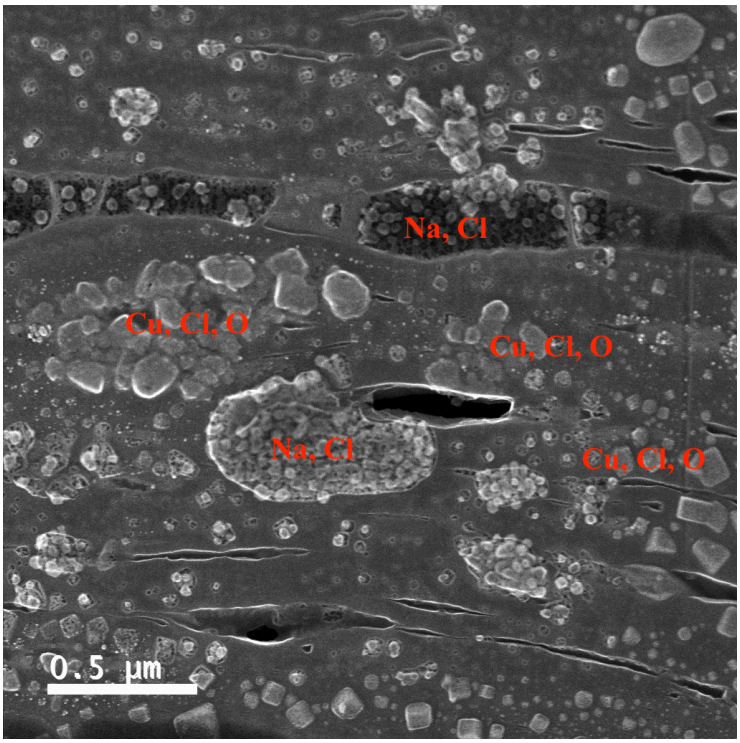

Fig. 4.3.12- Higher magnification (8000x) STEM image in SE mode of location on reduced EC GO/Cu(II) film where copper is present.

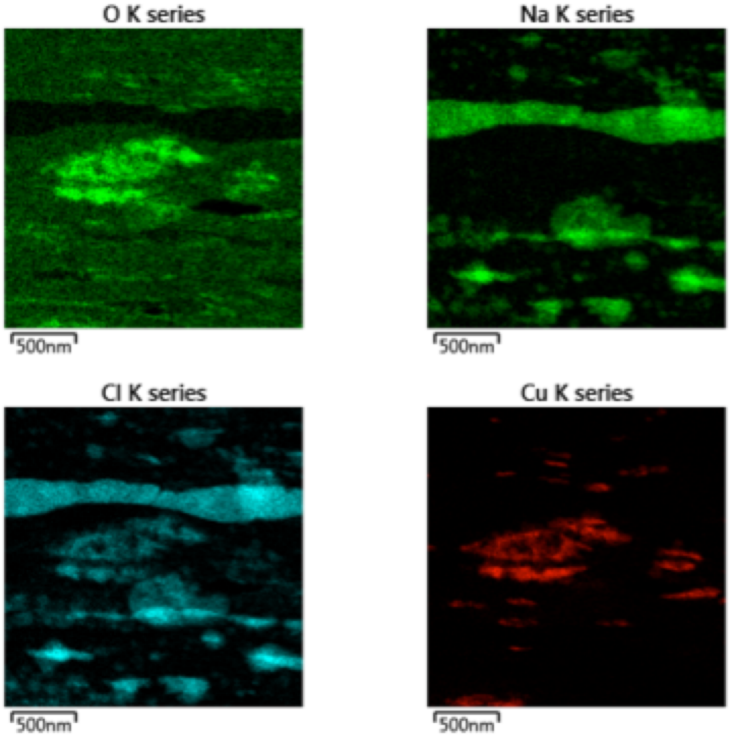

Fig. 4.3.13- EDS analysis of section of film present in Fig.4.3.11.

ICP-MS was performed on another reduced EC GO/Cu(II) film created under same experimental conditions as the film that was subjected to STEM analysis in order to determine the concentration of Na and Cu incorporated in the film. The concentration of Cu incorporated was approximately 67 mg/g and the concentration of Na was approximately 58 mg/g. As previously mentioned, the EDS analysis in Fig. 4.3.11 shows little to no presence of copper throughout the first 7 microns of the film starting from the surface that was initially in contact with the copper substrate. However, there is still a relatively high concentration of copper incorporated in the film. The copper must be present in the other half of the film (containing the surface that was in contact with electrolyte), which was not removed and analyzed by the FIB. This implies that the copper electro-migrated away from the copper substrate and towards the electrolyte. Cu^{+} ions are known to be highly complexed by Cl^{-} ions.[95] It is plausible that the Cu^{2+} was reduced to Cu^{+} during the electrochemical process. The copper ions might then have a stronger attraction to the Cl^{-} ions in the electrolyte than the copper substrate. In this case, the complexed Cu^{+} ions would then electro-migrate towards the electrolyte. The concentration of Cu incorporated actually decreased upon reduction, indicating that some of the copper might have gone into the electrolyte from the attraction to Cl^{-} ions. From the STEM images, it seems that NaCl is incorporated into the GO film from the sides. The GO film then, upon reduction, acted as an efficient "absorber" of sodium and chloride ions, which eventually precipitate out through a salting out effect.

4.4 Conclusions

Cyclic voltammetry (CV) was used to characterize the feasibility of reduction of GO and

Cu^{2+} ions in the EC film. The technique allowed distinct reduction potentials for the different primary constituents (i.e. GO and Cu2+) present in the system to be determined. Cyclic voltammetry demonstrated the irreversibility of the reduction reactions involved and that Cu^{2+} and GO were capable of being reduced at two distinct redox potentials (-0.2V and -0.6V respectively). In addition, by applying a more negative constant potential than the redox potentials found in the CV scans over the course of several hours, both constituents of the GO/Cu(II) films were reduced throughout the entirety of film. Sheet resistances as low as 22 Ω/□ were measured when both constituents were reduced, demonstrating efficient electron transport in the material. The deposition and reduction processes are rapid, simple, low cost, and environmentally benign, which creates opportunity for commercialization of EC-GO/Cu(II) films in high conductivity applications. However, during the reduction process, the voids in the EC film were filled with NaCl particulates.

Chapter 5: Effect of Particle Aggregation on Field-Assisted Formation of GO Films through Electrocoagulation

5.1 Motivation and Objectives

Recently, graphene oxide (GO) has garnered significant attention from the scientific community as a possible material for wastewater treatment due to its strong promise as an effective absorbent of multivalent metal ions.[19–23] From a chemical perspective, GO has an abundant amount of oxygen atoms on its graphitic backbone in the forms of epoxy, hydroxyl, and carboxyl groups.[24] The oxygen containing functional groups have an isolated electron pair, which can efficiently bind a metal ion to form a metal complex.[19]

In Chapter 3, the electrocoagulation (EC) process was described. The presence of multivalent metal cations (i.e. Cu^{2+}) was shown to lead to GO particle aggregation near an electrode surface. This electrocoagulation in aqueous media was caused by adsorption, double layer compression, and surface charge reduction/neutralization in accordance to classical DLVO theory.[19] The introduction of Cu^{2+} ions into GO suspensions was accomplished by electrochemical oxidation of a sacrificial Cu electrode.

However, controllable amounts of Cu^{2+} ions can be introduced to the system without the presence of an electric field and activate a bulk coagulation process. Indeed, Yang et al.[21] demonstrated that the addition of Cu^{2+} to a GO suspension induced aggregation of the GO particles through adsorption. In the context of the EC deposition process, the pre-coagulation of GO in suspension prior to electrochemical deposition was anticipated to have a significant effect on the nature of the deposition process and resulting film characteristics.

As mentioned in Chapter 2, one of the most commonly used methods for creating GO suspensions is the Hummer's method. The Hummer's method begins with the chemical oxidation of graphite powder (flakes). The graphite powder typically has a very broad particle size distribution, which in turn ultimately leads to a very broad distribution of GO particle sizes.[96,97] In various electro-deposition processes, which involve electrophoresis, this can lead to structural inconsistencies (such as porosity, film uniformity, etc.) in the film formed on a substrate. For suspensions with a broad particle size distribution, it has been shown to be advantageous to apply an alternating current (AC)-field during electrophoretic deposition of the films.[98–101] Indeed, separation of particles based on size and shape can be accomplished by tuning frequency and waveform. By extension, it then becomes possible to migrate and deposit particles of specific size on a substrate.[98–101]

The EC driven fabrication of GO films described in Chapter 3 is a very new technique. The effect of its processing parameters on film structure, composition, and deposition rate has not been extensively studied, and remains relatively unknown. The addition of Cu^{2+} to the suspension prior to electrocoagulation offers the opportunity of a pre-coagulation step, which would lead to the agglomeration of the GO particles. In addition, the abundant presence of copper in the suspension at the beginning of the deposition will affect the overall mechanism of the deposition, since there will be two competing processes: electrocoagulation and bulk coagulation.

This work explored the impact of particle aggregation (via a pre-coagulation step of the GO suspension) on the deposition process, in this case, focusing on the deposition rate. It also determined how the pre-coagulation step affected the concentration of copper ions incorporated in the GO film. Deposition involved both DC and AC fields. AC fields were applied during the

EC process with varying frequencies in an attempt to control the size of the GO particles involved in the deposition. The effect of frequency on the deposition rate and composition of the GO was also determined.

5.2 Experimental Methods

5.2.1 Material Synthesis

A GO suspension was created through the modified Hummers' method described in the Experimental Methods section of Chapter 3. The primary suspension had a GO concentration of approximately 8 mg/mL, a pH of 2, and a conductivity of 5.1 mS/cm. Copper sulfate pentahydrate ($CuSO_4.5H_2O$, Acros Organics, $\geq$ 99%) was added progressively to the primary suspension and changes in the pH value, conductivity, and stability were noted. Films were then deposited on copper substrates by several variations (listed below) of EC-assisted deposition.

Constant Potential (DC) Electrocoagulation with Primary Suspension:

GO films were deposited from the primary suspension onto copper foils (0.127 mm thick, annealed, 99.9%) with the same copper sample preparation and EC experimental setup techniques as those in Chapter 3 and Chapter 4. A 5V deposition voltage (field strength of approximately 3V/cm) was used and deposition times ranged from 10 to 90 seconds. Longer deposition times were used than the previous studies in order to gain insight into the mechanisms affecting deposition rate.

Constant Potential (DC) Electrocoagulation with Pre-coagulated Suspension:

Copper sulfate pentahydrate ($CuSO_4.5H_2O$, Acros Organics, ≥ 99%) was added to DI water at a concentration of approximately 0.122 g/mL (solution pH of 3.7) and stirred for 30 minutes. One milliliter of the copper sulfate solution was then added to the primary GO suspension (30 mL), which allowed the resulting mixture to contain 1000ppm of Cu^{2+} ions. The resulting "pre-coagulated" GO suspension was then stirred for 30 minutes. The addition of Cu^{2+} to the suspension should lead to the agglomeration of GO particles and increase the average particle size.[21] Films were formed from the pre-coagulated suspension using the same experimental conditions as the films formed from the primary suspension (0ppm of Cu^{2+}).

Alternating Current (AC) Field Electrocoagulation with Primary and Pre-coagulated Suspensions:

GO films were deposited onto copper foils (0.127 mm thick, annealed, 99.9%) with the same copper sample preparation as those in Chapter 3 and Chapter 4. The copper substrate was used as the working electrode in the electrochemical cell, while platinum served as the counter electrode. The distance between the both electrodes was fixed at 0.015 m. Electrocoagulation was performed by applying an AC field across the electrodes using a 60 MHz dual function/arbitrary waveform generator (BK Precision 4055B). The AC field had an amplitude value of 5V, frequencies ranging from 5 Hz to 100 kHz, and deposition times ranging from 10 to 60 seconds. The duty cycles used were 50% and 75%. Fig. 5.2.1 depicts the waveforms corresponding to each duty cycle. The AC field was applied to both the primary and pre-coagulated suspensions.

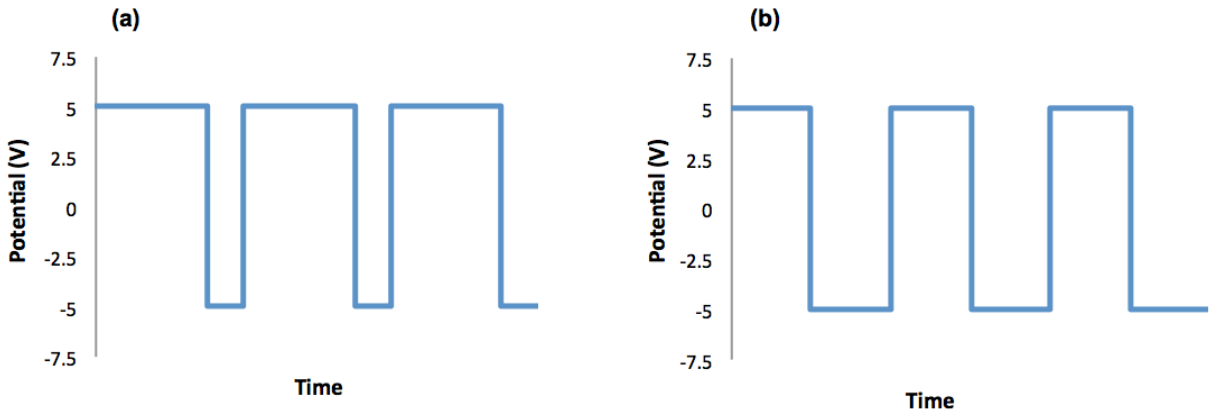

Fig. 5.2.1- AC waveform used in experiments: (a) 75% duty cycle, and (b) 50% duty cycle

5.2.2 Material Characterization

Profilometry

All the resulting GO films formed on the anodes were removed from the deposition bath, rinsed immediately with DI water, and dried on a hot plate at 65 °C under flowing nitrogen (2 psi). The thickness of the films was measured with a profilometer (Dektak 6M, Veeco). A diamond stylus was moved vertically into in contact with the sample and then moved laterally across the sample for a specified distance of 2000 microns and specified contact force of 3 mg. The thickness was measured at 5 to 10 different locations on a given sample, then averaged. The thickness measurements were repeated on samples formed under identical conditions to verify the consistency of the results.

Inductively Coupled Plasma Mass Spectroscopy

For ICP analysis, sections of GO films formed by the deposition methods described in Section 5.2.1 went through identical delamination and washing processes as the films mentioned in Chapter 3. Prior to ICP-MS analysis, the delaminated films were bleached in nitric acid for

metal dissolution and stabilization. An Agilent 7700x ICP-MS was used to determine the effect of AC frequency, time, and pre-coagulation on the concentration of copper incorporated in the film. The ICP-MS employed an RF power of 1550W, a plasma gas flow of 15 L/min, a carrier gas flow of 0.85 L/min, and a makeup gas flow of 0.15 L/min.

Raman Spectroscopy

The theoretical basis for Raman Spectroscopy was described in the experimental methods section of Chapter 3. A Jobin–Yvon Horiba Lab-Ram HR800 micro-Raman spectrometer was used with an Argon ion laser (514.5 nm) to determine the effect of pre-coagulation of the suspension on the resulting GO film structure through an examination of primary vibrational resonances described in Section 3.2. The beam was focused with a 100x microscope objective with a corresponding a 10μm spot size and a 100 mW incident power at the sample surface. Stokes-scattered spectra were collected over a spectral range of 1000-3000 cm^{-1} (5 cm^{-1} resolution). The spectra were collected with a thermoelectrically cooled CCD array using an integration time of 20s and signal averaging over 10 scans.

5.3 Results and Discussion

5.3.1 Suspension Characterization

To confirm that the addition of copper ions to GO suspensions (pH of 2) in the absence of an electric field would cause bulk coagulation of GO particles, copper ions were added to solution in the form of copper sulfate salt at increasing concentrations. When the solution concentration of copper reached approximately 2000 ppm, the GO suspensions became unstable. Further increase of copper concentration to approximately 3000 ppm, created a gel-like structure.

Also, the color of the GO suspension progressively changed from black to brown as copper was added (evident in Fig. 5.3.1).

Table 5.3.1 shows the changes in conductivity and pH as a function of added Cu^{2+} to the primary suspension. The pH remained unchanged as the copper was added; however the conductivity progressively increased. For the pre-coagulated depositions, a concentration between 0 and 2000 ppm of Cu^{2+} was required, since the stability of the suspension was necessary for EC to occur. An EC-driven deposition of a GO film onto a copper substrate from a suspension with 2000 ppm of Cu^{2+} added was attempted. However, the deposition was unsuccessful due to the highly viscous nature of the suspension. A concentration of 1000 ppm of Cu^{2+} was chosen for this reason for all subsequent experiments.

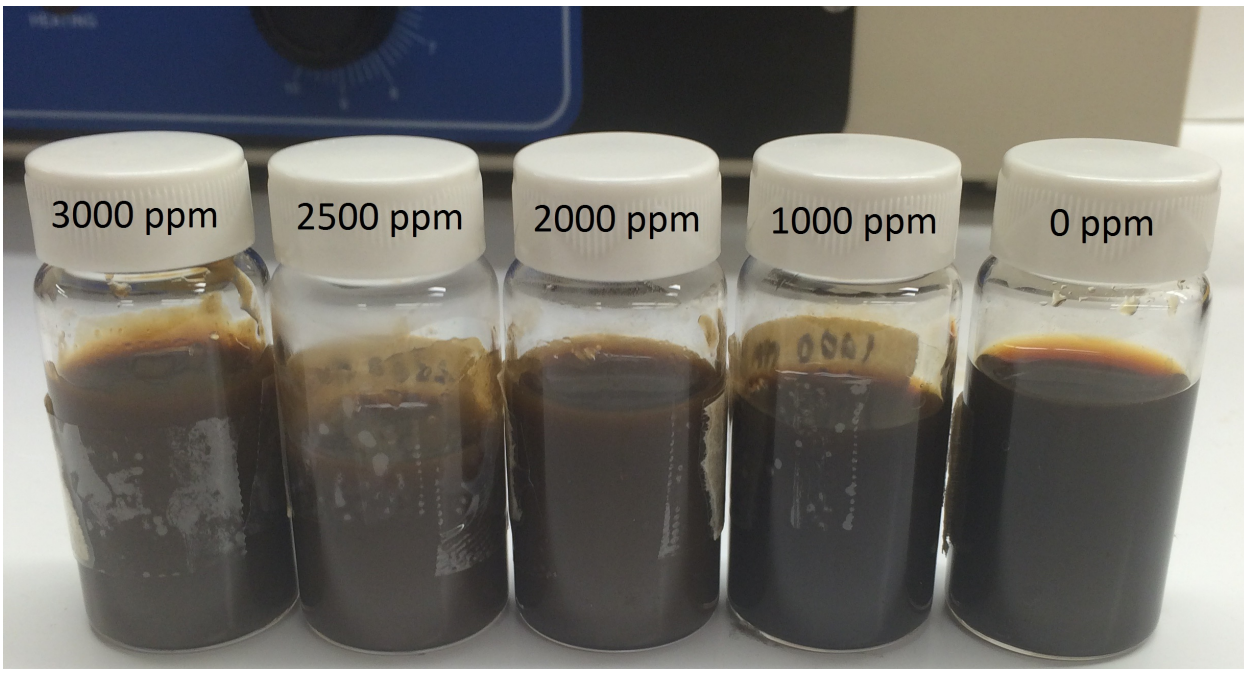

Fig. 5.3.1- Appearance of GO suspensions with different concentrations (in ppm) of added Cu^{2+}.

Table 5.3.1 –pH and conductivity of GO suspensions as function of added Cu^{2+} ions to the suspensions

Concentration of Cu^{2+} added to primary GO suspension	pH of suspension	Conductivity of suspension (mS/cm)
0 ppm	2	5.1
1000 ppm	2	6.3
2000 ppm	2	7.6
2500 ppm	2	8
3000 ppm	2	8.3

5.3.2 Film Characterization

Films deposited in DC Field:

Fig. 5.3.2 compares the deposition thickness over time for the EC-driven deposition of the primary suspension (0ppm) and the pre-coagulated (1000ppm) suspension in the presence of a DC field. For the deposition of the primary suspension, the thickness increases rapidly over the first 30 seconds. After 30 seconds, the deposition rate decreases and the thickness seems to plateau. The decrease in the deposition rate at constant voltage over longer times can be attributed to the decrease in the current over time as shown in Fig. 5.3.3. This phenomenon is in good agreement with the similar process of electrophoretic deposition (EPD).[102] At constant voltage, the potential difference between the electrodes is constant, but the electric field influencing electrophoresis decreases with deposition time because of the formation of an insulating layer (in this case GO) on the electrode surface.[102]

For the deposition of the pre-coagulated suspension, the film thickness is on par with that of the primary suspension over the first 20 seconds of the deposition. However, after 20 seconds,

the thickness and deposition rate are significantly lower compared to that of the primary suspension. This deviation is plausibly caused by the increase in particle size compared to that of the primary suspension. Larger particles tend to settle due to gravitational effects.[102] For electrophoretic migration to occur, the contribution of gravity to the mobility of particles must be less than the contribution of electrophoresis.[102] In addition, an increase in the particle size would lead to in an increase in the drag (proportional to surface area of particle) within the fluid, which would decrease the velocity of the particles migrating towards the electrode.[103] Larger particles would be less affected by the electric field, which would result in fewer GO particles being near the copper anode over longer periods of time.

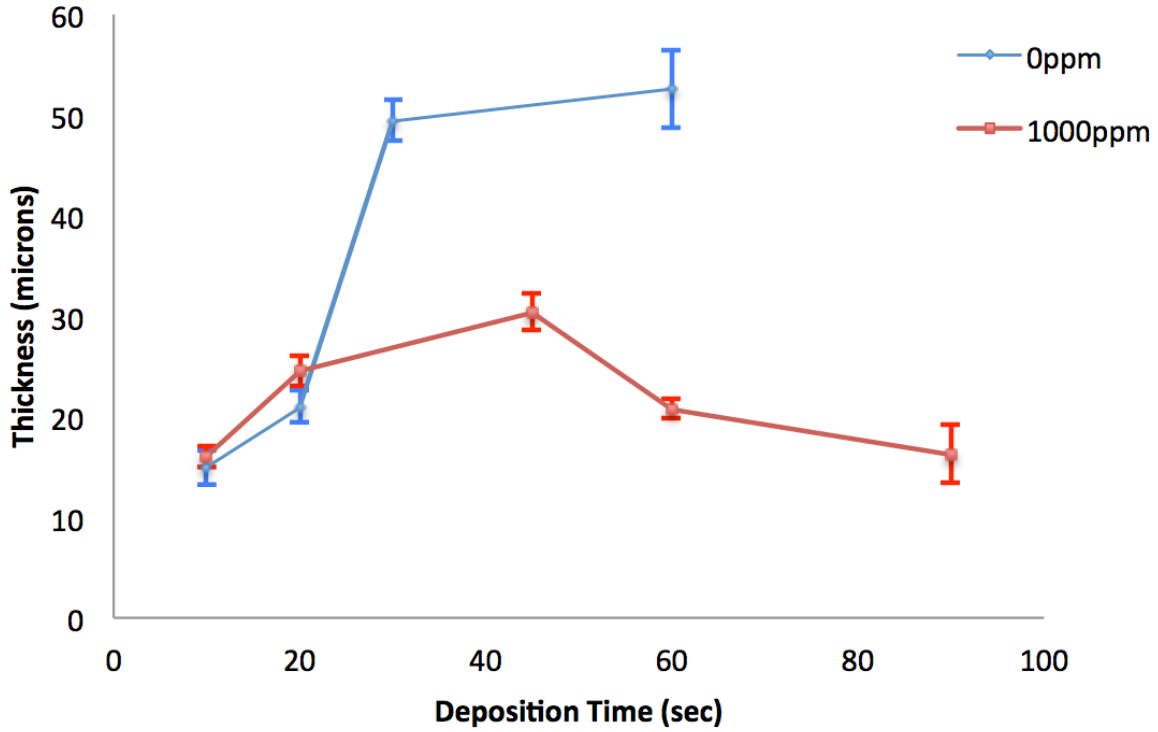

Fig. 5.3.2- Film thickness as a function of time during EC-driven deposition in a DC field in the presence (1000ppm) and absence (0ppm) of added copper.

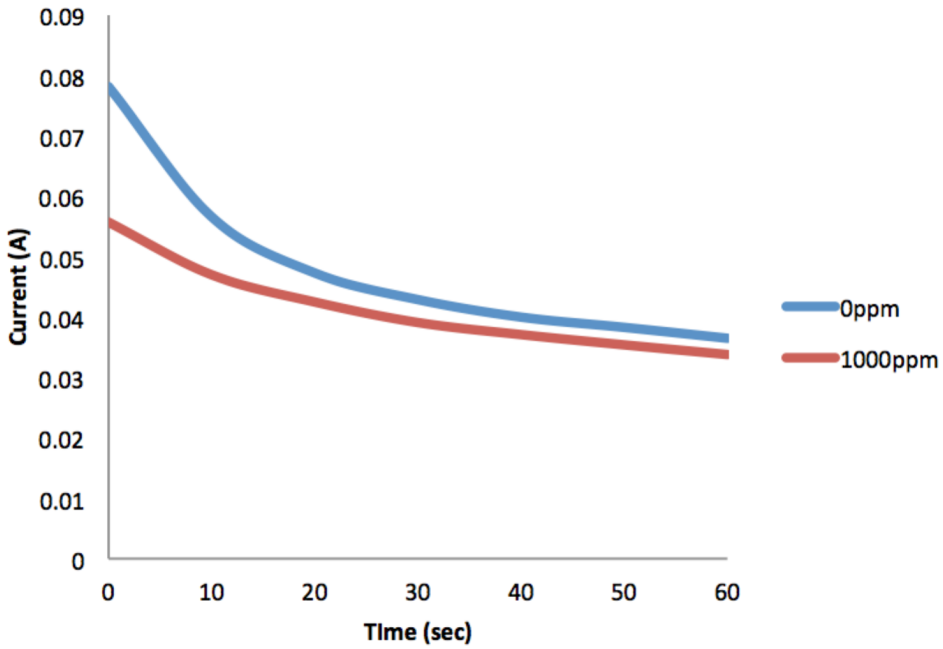

Fig. 5.3.3- Current as a function of time during EC-driven deposition in a DC field in the absence (0ppm) and presence (1000ppm) of added copper (deposition surface area on copper substrate was 1cm^2).

The thickness of the films formed from the pre-coagulated suspension actually begins to decrease after a deposition time of 45 seconds. Although the GO particles in contact with the copper electrode may be well adhered to the electrode, it is plausible that the GO particles farther away (exposed to pre-coagulated suspension) are weakly adhered. Visually, the films from the pre-coagulated suspension appear less compact (prior to drying) on the copper electrode than the films from the primary suspension. Over short deposition times, if the substrate is removed the GO particles may all still be adhered. However, it is possible that over longer deposition times, the GO particles on the outer surface of the film could be detached due to gravitational effects during removal from the suspension. A method to confirm this theory would be to perform all thickness measurements in-situ.

The extent of incorporation of copper ions in the films was characterized using ICP-MS. The ICP-MS analysis was carried out on several sets of films. Films for the analysis were

delaminated from the substrate and thoroughly washed in DI water and IPA. Sections of the films were digested in nitric acid prior to ICP- MS analysis. In terms of DC deposition from the primary suspension, two films were prepared under different conditions, namely 5V for 10s and 5V for 60s. The copper concentration was found to be approximately 92 mg/g for the 5V 10s film and 41 mg/g for the 5V 60s film, indicating a strong correlation between the deposition time and concentration of incorporated copper ions in the deposited material. The decrease in the concentration of copper incorporation with the increase in deposition time/thickness is in good agreement with ICP-MS analysis from Chapter 3 as well as the EDS analysis in Chapter 4, which demonstrated that the copper incorporation is gradually larger near the copper substrate.

In addition, the concentration of copper in the DC deposited GO film from the primary suspension and from the pre-coagulated suspension (1000ppm) was compared at 5V 60s. The copper concentration was found to be approximately 55 mg/g for the film deposited from the pre-coagulated suspension (34% increase compared to the one from primary suspension). The increased concentration of copper can be expected in the case of the pre-coagulated suspension since copper is incorporated through two pathways: Electrochemical oxidation of the sacrificial copper electrode and Cu^{2+} ions already present in the bulk suspension.

Films deposited in AC field:

EC-driven deposition in an AC field of the primary suspension (0ppm) and the pre-coagulated (1000ppm) suspension was attempted at a duty cycle of 50% and 75%. At a duty cycle 50%, the deposition was unsuccessful, while at 75% deposition occurred. In Chapter 3, it was shown that the GO particles exhibited a negative zeta potential at a pH of 2. Therefore, in the negative 5V regime the GO particles are repelled by the copper electrode and attracted to the

platinum counter electrode. The GO particles spent more time in the negative regime for the 50% duty cycle waveform than for the 75% percent duty cycle waveform. This would explain why only the 75% duty cycle waveform led to a successful deposition on the copper substrate. The 75% waveform is an asymmetric AC field with an induced DC component. This leads to a net drift of the negatively charged GO particles towards the copper electrode.

Fig. 5.3.4 compares the deposition thickness over time for the 75% duty cycle EC- driven deposition in an AC field of the primary suspension and the pre-coagulated suspension. Frequencies were varied from 5 Hz to 100 kHz and a constant deposition time of 60 seconds was applied. For both suspensions, initially an increase in frequency led to an increase in the film thickness. This is most certainly due to the fact that at higher frequencies, the GO particles spend less time in the negative regime of the waveform during a cycle.

However, for both suspensions, increasing the frequency leads to a decrease in the thickness after a certain frequency threshold (after 5000Hz for 0ppm and after 500 Hz for 1000ppm). During the application of an AC field, particles migrate in opposite directions at each half cycle. At the end of each half cycle, time is needed for the particles to change direction and accelerate from zero. Raissi et al.[101] rationalized that larger particles require more time to change the direction of electrophoretic migration than smaller particles due to higher inertia. At very high frequencies, larger particles are no longer able to keep pace with the AC field and only smaller average particle sizes and distributions electrophoretically migrate.[101] This would imply that the thickness of the GO films is decreased after threshold frequencies because larger particles are no longer able to keep up with the AC field and only smaller particles are capable of being deposited on the copper electrode. This would also explain why the pre-coagulated

suspension, which is expected to have on average larger GO particles, has a significantly lower threshold frequency than the primary suspension.

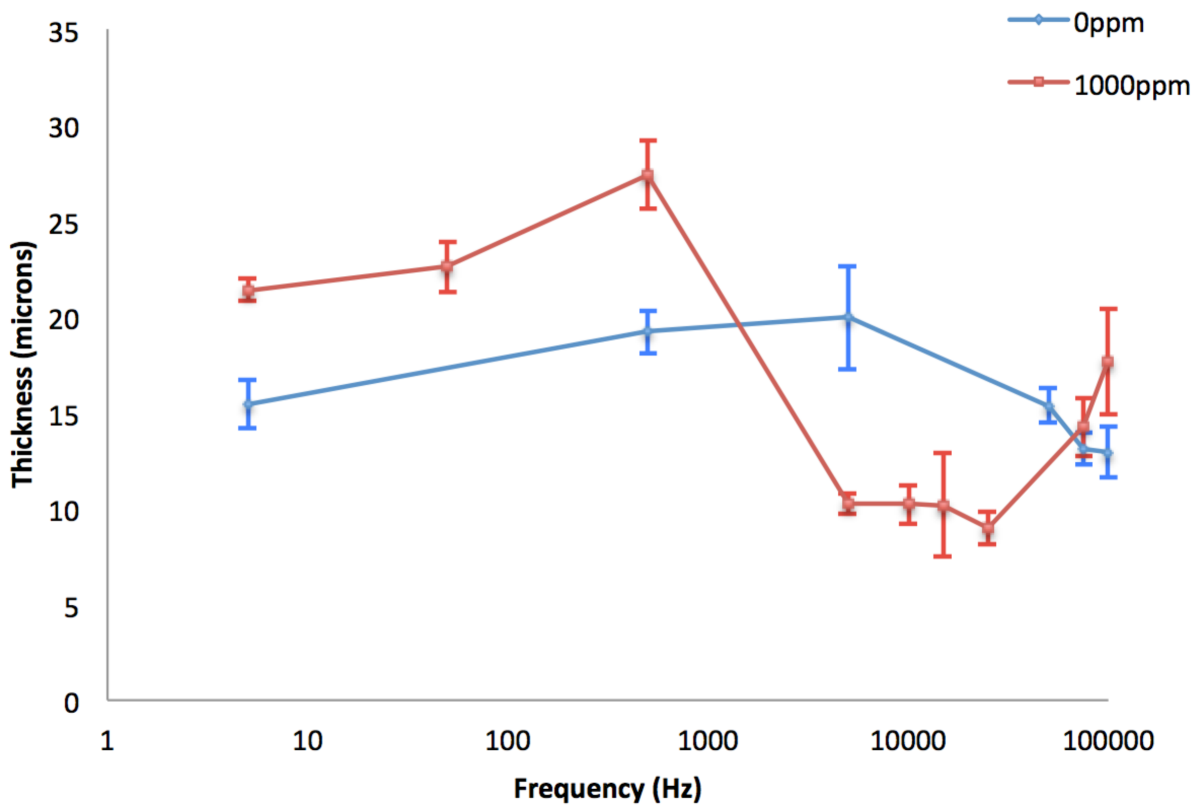

Fig. 5.3.4- Film thickness vs. frequency for 75% duty cycle AC EC-driven deposition with 0ppm and 1000ppm of Cu^{2+} pre-coagulant added to primary suspension over 60 seconds.

For the pre-coagulated suspension, it is very interesting to note that the thickness increases again with increasing frequency after 25 kHz. Copper ions were incorporated in the bulk suspension prior to the AC field. The copper ions and GO surfaces are oppositely charged, meaning they would be attracted to opposite electrodes. At frequencies above 25 kHz, it is possible that larger GO particles would be unable to migrate, while the copper ions bound to them would be capable of doing so. This opposition could lead to a rupture of the larger GO particles into smaller ones, which would then be capable of migrating and depositing on the

copper electrode. To confirm this theory, a future more detailed study on the particle size distribution as well as an ICP-MS analysis of the suspension would be necessary.

The ICP-MS analysis was also carried out on several sets of films formed by EC-driven deposition in an AC field. Films were prepared in a similar manner to those formed by DC EC-driven deposition. The effect of deposition time at constant frequency on the concentration of copper incorporated in the GO films from the primary suspension was studied.

Fig. 5.3.5 illustrates the concentration of copper incorporated in the films over time under the application of a 5kHz AC field. In a similar manner to that of the DC deposition, there is strong correlation between the deposition time and concentration of incorporated copper ions in the deposited material. As in the DC case, it can be assumed that the concentration of copper decreases as the distance from copper substrate increases. In addition, depositions from the pre-coagulated suspension followed the same trend. An ICP-MS analysis was performed on a 5 Hz and 500 Hz AC deposited film over 60 seconds from the pre-coagulated suspension. The concentration of copper incorporated in the deposited material was 57mg/g for 5Hz and 60s and 48mg/g for 500Hz 60s, indicating a decrease in the concentration with increasing thickness.

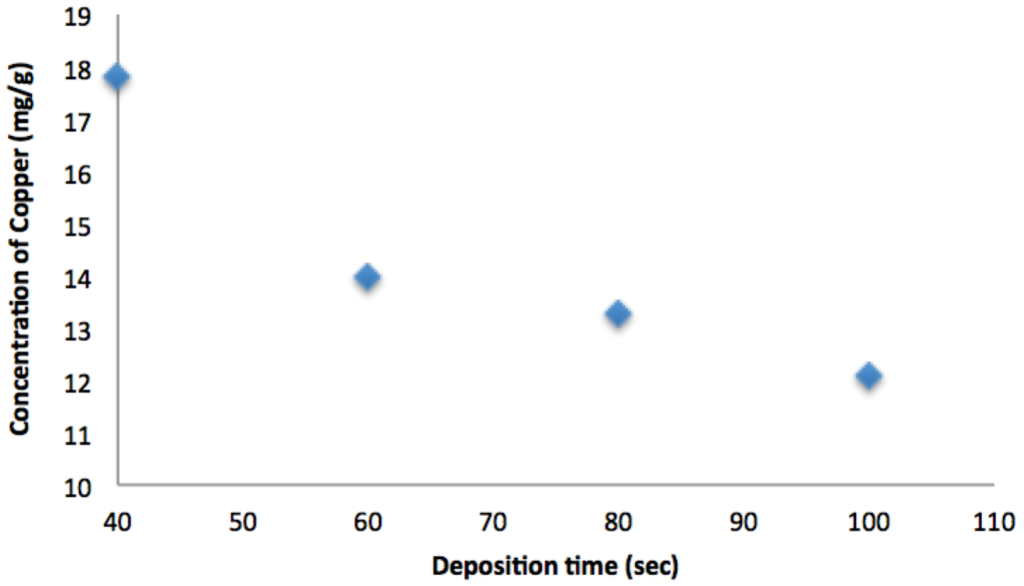

Fig. 5.3.5- Concentration of copper incorporated in GO film from primary suspension with 5V AC field at 75% duty and 5000 Hz vs. time.

Comparison of film characteristics between AC and DC fields:

It is important to note that at the same deposition time of 60 seconds from the primary suspension, all the AC deposited films in this study (regardless of frequency) had a lower thickness than the DC deposited films. The film deposited at 5kHz, which had the greatest thickness of the AC deposited films, had a thickness approximately 30μm lower (i.e. 61% decrease) than that of the DC deposited film. In addition, the concentration of copper incorporated in the deposited material was significantly lower in the case of the 5 kHz AC deposit (14 mg/g) than the DC deposit (41 mg/g). It can be anticipated that over 60 seconds, the copper substrate undergoes less electrochemical oxidation in the AC scenario than in the DC field (based on duty cycle). This would imply that less copper is introduced to the system to enhance the coagulation rate of GO. By extension, the relative contribution of EC is decreased in

the AC deposition, which in turn leads to the formation of thinner GO films with a lower concentration of copper ions incorporated compared to the DC deposition.

In the case of the deposition from the pre-coagulated system, it is reasonable to expect that the copper electrode would also undergo less electrochemical oxidation in AC than in DC over 60 seconds. If EC were the only contributing process to the film deposition, a similar trend to the deposition from the primary suspension would be anticipated. However, both AC (5Hz) and DC fields led to the deposition of films with similar thickness at the same deposition time of 60 seconds. If compared, it can be seen that the concentration of copper incorporated in the films are nearly identical (55 mg/g for DC deposit and 57 mg/g for AC deposit). The deposition from the pre-coagulated suspension therefore does not follow the same trend as the deposition from the primary suspension, where the application of an AC field led to the formation of thinner GO films with a lower copper ion concentration. The 1000ppm of copper, which was added to the bulk suspension to enhance coagulation of the GO particles, must contribute to the deposition rate and extent of copper. This would imply that there are two contributing mechanisms to the deposition: electrocoagulation and bulk coagulation.

In addition, the kinetics of the copper ions becomes more complex with the AC field than with the DC field for the pre-coagulated suspension. During the positive regime of the AC waveform, copper ions already present in the suspension migrate towards the platinum counter electrode. During the negative regime, the ions migrate towards the copper substrate. There are no visible signs of copper electroplating on the GO film formed on the copper electrode. However, the platinum electrode is visibly coated with copper. At deposition times of at least 60 seconds, EC-driven co-deposition of GO films on the platinum counter electrode is observed.

5.4 Conclusions

The EC driven fabrication of GO films is a novel technique that has not been extensively studied. This work, for the first time, showed the effect of tuning the EC processing parameters on film structure and composition. In the case of DC deposition, the particle aggregation had an effect on the deposition rate of both suspensions (primary and pre-coagulated) due to gravitational forces and drag within the fluid. Over a deposition time of 20 seconds, the pre-coagulated suspension led to the formation of GO films significantly thinner than that from the primary suspension.

The use of an AC field with varying frequency and duty cycle was also shown to have a direct effect on the deposition rate. A duty cycle over at least 50% was necessary to ensure that deposition could occur. AC depositions also have a threshold frequency above which the thickness of the deposited films begins to decrease. The threshold frequency was shown to decrease by an order of magnitude if the suspension underwent a pre-coagulation step. In the case of a non pre-coagulated suspension, the AC field leads to the formation of a thinner GO film with a lower concentration of copper ions incorporated. The same cannot be said for a pre-coagulated suspension, since there are multiple mechanisms at play during the deposition: electrocoagulation and bulk coagulation. In the case of the AC deposit from the pre-coagulated suspension, an EC-driven co-deposition of GO films on the platinum counter electrode was also observed.

An improved understanding of the process parameters established through this work opens new avenues for tailoring the deposited GO films for specific applications such as filtration membrane materials or supercapacitors.

Chapter 6: Conclusions

Graphene represents an attractive and important material from both a scientific and a technological perspective due to its unique properties (i.e. high thermal and electrical conductivity, excellent mechanical strength). However, additional research is yet required to refine material synthesis and processing to enhance properties while providing scalable fabrication. In this regard, the reduction of GO has become an important route to obtain chemically modified graphene platelets (also referred to as reduced graphene oxide (rGO)) in large scale and low cost.

The first phase of this dissertation focused on developing a new and improved method for the formation of GO films from solution. The distinguishing feature of this work as compared to previous efforts is the utilization of electrocoagulation (EC) as the driver for rapidly depositing GO films on conductive substrates such as copper. It has been shown that the incorporation of metal ions into the GO matrix provides significant mechanical and structural stability of GO films. However, in prior studies, the metal ions were usually incorporated in an uncontrolled manner. In contrast, this EC-driven formation technique allowed the controlled incorporation of metal ions into the GO films.

In the current work, Cu^{2+}-ion-containing GO films were deposited onto copper substrates from GO dispersions at ambient pressure and temperature. Further and equally importantly, the thickness and the rate of deposition of the GO films can be suitably controlled by adjusting applied voltage, deposition time and the concentration of GO particles in the suspension. It was found that the concentration of copper ions incorporated in the films had a strong correlation with deposition time and applied voltage used during the deposition process. This facile formation approach enabled the deposition of GO films ranging in thickness from a few microns

to above 100 microns, all within a minute, demonstrating its scalability. While this study focused on the use of a copper substrate, it can also be extended to other conductive substrates that can generate higher-valent cations (such as aluminum and stainless steel). The findings of this work open up new avenues for employing GO as filtration membranes and anti-corrosion coatings with remarkable mechanical and structural stability.

GO films are inherently an insulating material due to their oxygen functionalities. For GO to be used in applications where high conductivity is needed and where pristine graphene can be used (such as biosensors, supercapacitors, photovoltaics, etc.) a reduction step is necessary. Although, the conductivity of typical GO is enhanced upon reduction, it still does not reach the levels of pristine graphene. The second phase of the dissertation focused on this issue, i.e. the preparation of EC-GO/Cu(II) films for applications where a high conductivity is needed. In addition, an examination of the conductivity of the reduced EC-GO/Cu(II) films relative to tradition rGO films was of interest.

The films were electrochemically reduced through two routes. Cyclic voltammetry (CV) was first used to survey reduction processes present in the EC-GO/Cu(II) material. The reduction of Cu^{2+} and GO was shown to occur at two distinct redox potentials (-0.2V and -0.6V respectively). A negative constant potential (-0.9V), whose magnitude was greater than the redox potentials found in the CV scans, was then applied to EC-GO/Cu(II) films over the course of several hours. Both constituents of the GO/Cu(II) films were reduced throughout the entirety of film as confirmed by XPS, Raman spectroscopy, and 4-point probe measurements. Sheet resistances as low as 22 Ω/□ were measured when both constituents were reduced, demonstrating efficient electron transport in the material. This corresponded to an average conductivity, of approximately 3000 S/m, that was greater than traditional rGO films reduced by

hydrazine (20% increase), L-ascorbic acid (275% increase), thermal exfoliation (30% increase), microwave (1400% increase), and Al/HCl (43% increase). The findings of this work expose new possibilities for the EC-GO/Cu(II) films to be used as binder-free electrodes in supercapacitors, photovoltaic devices, batteries, and as sensors with enhanced conductivity relative to traditional rGO films.

The third dissertation phase examined the effect of EC processing parameters on film composition and deposition rate. Specifically, the effect of particle aggregation and the nature of the electric field were studied. Here, aggregation was accomplished via a pre-coagulation step and depositions were performed under both DC and AC fields. In the case of deposition under a constant applied voltage, particle aggregation had an effect on the deposition rate. Indeed, over a deposition time of 20 seconds, the GO film thicknesses from the pre-coagulated suspension were significantly less than that from the primary suspension. The use of an AC field with varying frequency and duty cycle was also shown to have a direct effect on the deposition rate. A duty cycle over 50% was necessary to ensure that deposition could occur. AC depositions also exhibited a threshold frequency above which the thickness of the deposited films began to decrease. The threshold frequency was shown to decrease by an order of magnitude when the suspension was pre-coagulated. In the case of a non pre-coagulated suspension, the AC field led to the formation of a thinner GO film with a lower concentration of copper ions incorporated. The same could not be said for a pre-coagulated suspension, since there were multiple mechanisms at play during the deposition: electrocoagulation and bulk coagulation. The tuning of process parameters such as GO particle aggregation and electric field opens new avenues for tailoring the deposited GO films for specific applications such as anti-corrosion coatings or supercapacitors.

In conclusion, EC-driven fabrication of metal-ion-containing GO films is a low cost and a very rapid process, whose deposition characteristics such as deposition rate and metal ion incorporation, can be tuned by control of process parameters (applied voltage, deposition time, GO suspension concentration, GO particle aggregation, electric field). The films created are beneficial to applications, such as filtration membranes and anticorrosion coatings, where enhanced mechanical stability in a variety of liquid environments is required.

Subsequent electrochemical reduction of the EC-GO/Cu(II) films leads to the formation of chemically converted graphene with enhanced conductivity relative to traditional rGO films. This transition from an insulating material to a conducting material allows for the scope of applications to be expanded to energy storage, sensors, photoelectric, and semiconductor devices. The electrochemical reduction processing is not only directly compatible with the EC technique, but it is also low cost, environmentally benign, and an established industrial approach. The combination of the rapid EC-technique and subsequent electrochemical reduction therefore represents a highly scalable process, which could eventually lead to the commercialization of graphene-based films.

Chapter 7: Future Work

The work in this dissertation explored the electrical properties of the rGO films produced by EC deposition and subsequent electrochemical reduction. The films exhibited high electrical conductivities, which is essential for the operation of supercapacitors. A suggestion for future work includes the use of the films as an electrode in supercapacitors. As previously mentioned, graphene-based materials are also known to exhibit excellent mechanical (high strength) and thermal (high conductivity) properties. Other suggestions for future work include the mechanical and thermal characterization of the EC deposited films. These characterizations would be particularly valuable towards the use of the films in semiconductor packaging (for example: thermal interface materials TIMs), where high strength and high thermal conductivities are needed.

The three phases of the dissertation focused on incorporating Cu^{2+} ions from a copper substrate into a GO matrix. Diverse metal ions can be incorporated through the use of other substrates (such as aluminum and stainless steel). Preliminary studies have been performed on the EC-driven deposition of GO on stainless steel 304. XPS analysis confirmed the presence of Fe^{3+} ions in the GO films. Nickel and chromium ions were additionally incorporated from the stainless steel. The incorporation of diverse metal ions would affect the overall mechanical, electrical, optical, and thermal properties of the films. A detailed study on the correlation between metal ions and the intrinsic properties of the films would be beneficial to the materials community. Indeed, the incorporation of a specific metal ion into the GO film might be necessary or advantageous for reaching ideal operating conditions in a particular application. For example, organic photovoltaic devices typically use an aluminum cathode; therefore an Al^{3+}-ion-

containing GO film on an aluminum substrate could act as an efficient electrode/photoactive layer interface.

The second project showed that the GO films fabricated by the EC technique were efficient salt (i.e. sodium chloride) absorbents. The salt particles were incorporated into the GO matrix by filling all the voids and fissures present in the film. Therefore, by tuning the density and the size of the voids present throughout the film, there would be the opportunity of varying the amount of salt being incorporated into the films. A detailed study on the effect of varying the EC process parameters (GO particle size, GO suspension concentration, electrical field, applied voltage, etc.) on the microstructure of the resulting films (specifically the void density and size) would be beneficial to the materials and environmental science communities. If the void density and size is tunable by varying the process parameters, then the film could be used as filtration membranes with strong promise towards water desalination or purification.

For other applications, the incorporation of NaCl into the film might be disadvantageous. Future work could include using diverse electrolytes (such as copper sulfate based electrolytes) during electrochemical reduction of the EC-GO/Cu(II) films. This could allow the voids to be filled with copper metal instead of sodium chloride, thereby adding an existing constituent to the film instead of adding a new constituent. The incorporation of sodium chloride could also be avoided if by tuning the process parameters, the film contains no voids. In addition, the initial substrate surface conditions play an important role in the microstructure formation of the resulting film. For example, preliminary results show that an electropolished copper surface leads to a dramatically different surface morphology than a rough copper surface. A constructive future study would be the use of surface functionalization as a means to influence film deposition and structure.

Through electrochemical processing, the Cu^{2+} ions were reduced and the presence of copper seems to be associated with oxygen and chlorine. However, it is not clear if the copper is in the form of Cu(s) coated with oxygen and chlorine atoms or in the form of Cu^{+} bonded with those atoms. Electron energy loss spectroscopy (EELS) would be helpful in determining the oxidation state information of the copper at atomic resolution. However, EELS would have to be coupled to an STEM with a lower acceleration voltage than 60kV. At 60kV, the GO film disintegrates at the higher magnifications needed for the EELS analysis.

Performing the EC-driven deposition in which copper ions are complexed by citrate/citric acid would also be valuable. The complexes are large in size and may provide information on what happens when the coagulating power of Cu^{2+} is reduced by complexation. It would also provide insight into the role of copper ions in the GO structure, i.e. are they intercalated or chemically bound in the GO films. Copper complexation occurs at pH ranges greater than 3.[104] The citric acid would therefore need to be introduced into GO suspensions at a higher pH than those described in this work (pH 2). Varying the pH would effect the adsorption rate of copper on GO[86], the zeta potential of the suspension[86], and the electrochemical oxidation rate of copper ions. Another suggestion for future work would be to study the effect of pH on the deposition characteristics.

Preliminary results have shown that the EC-driven deposition of GO on insulating substrates is possible if the substrates had been coated with Cu prior. An insulating substrate could then be patterned with Cu (or other metallic) films to spatially define GO deposition (bottom-up patterning). The GO could then be reduced to lead to the formation of rGO conductive pathways. This patterning would be very relevant to the construction of semiconductor and photovoltaic devices.

Finally, an interesting study would be the potential to form Cu nanoparticles during EC deposition with an AC field or subsequently during reduction for access to tunable plasmonic effects within GO or rGO. This would be applicable to plasmonic solar cells where electrically tunable absorption could lead to higher efficiencies. For this type of application, much thinner films (<100nm) than the ones fabricated in this study (micron to 100 micron range) would be necessary. Future work would also explore the ability to develop much finer control over film growth.

Appendix A: Additional STEM Images of EC-GO/Cu(II) Film under Annular Dark Field and Bright Field Modes

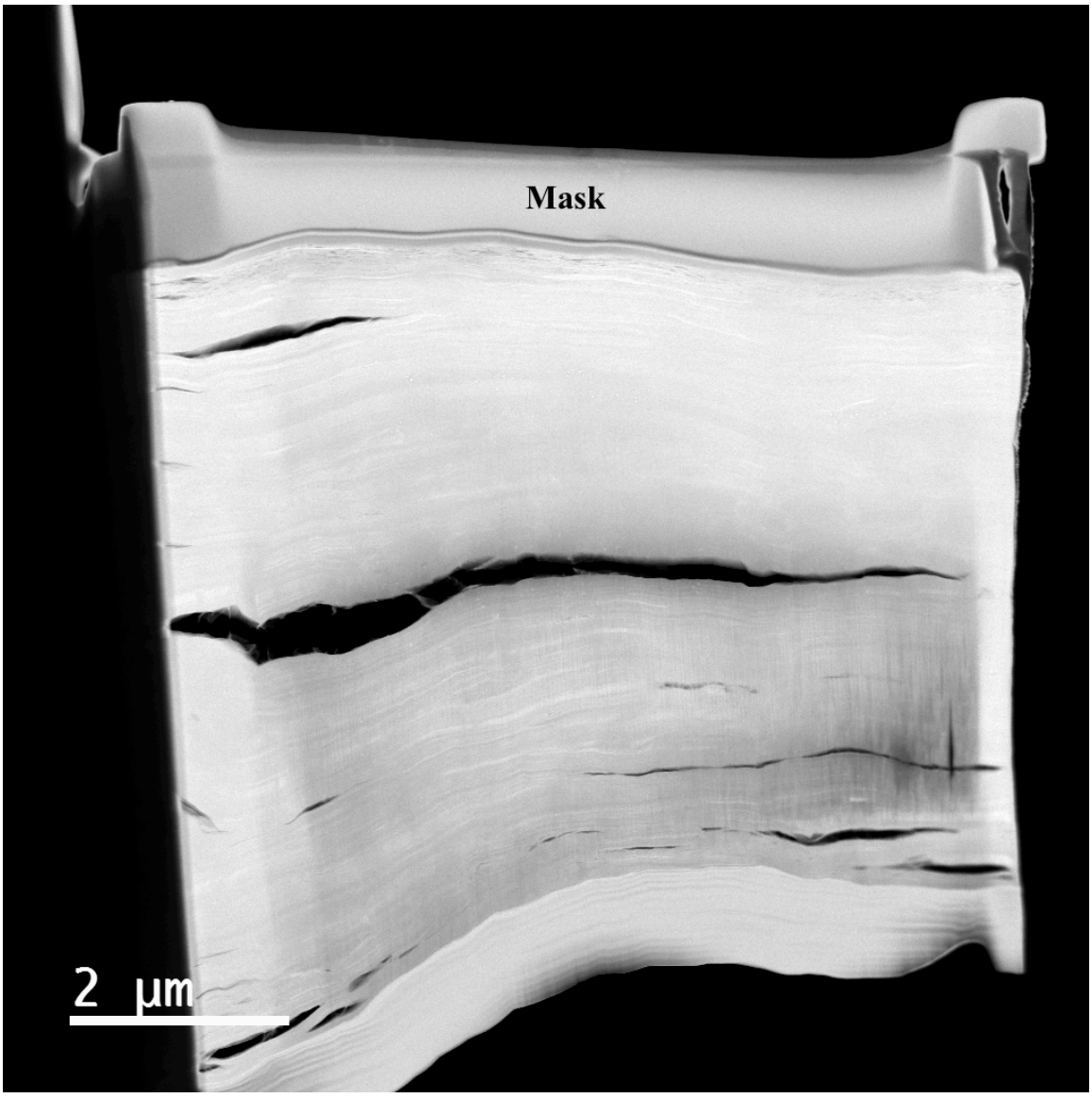

Fig. A.1- Cross-sectional STEM image of EC GO/Cu(II) under annular dark field (ADF) mode. The surface of GO in contact with the mask was GO surface in contact with the copper electrode before delamination. Towards bottom of image (lighter area) there is re-deposition from the ion beam. (2000x magnification)

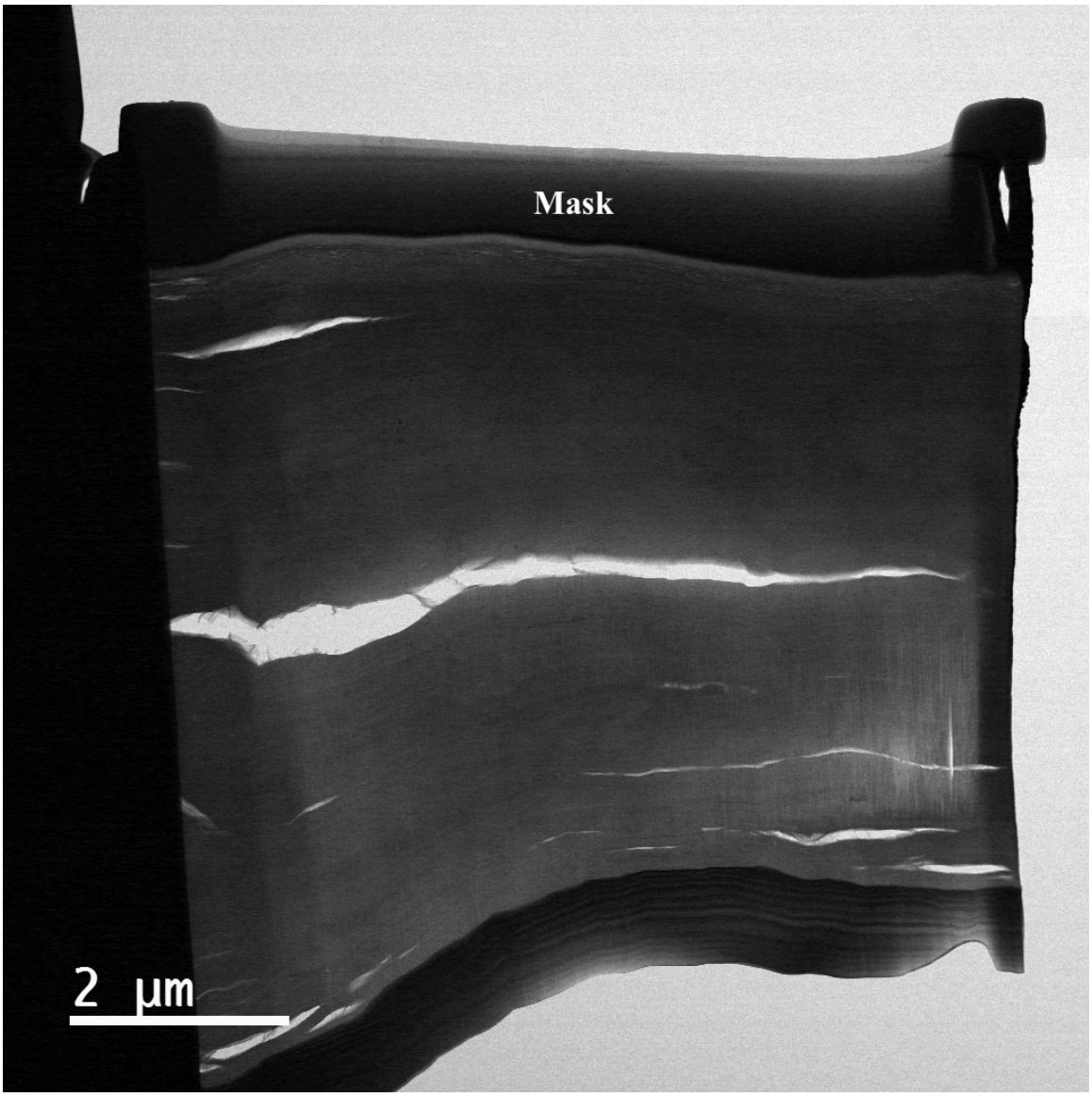

Fig. A.2- Cross-sectional STEM image of EC GO/Cu(II) under bright field (BF) mode. The surface of GO in contact with the mask was GO surface in contact with the copper electrode before delamination. Towards bottom of image (darker area) there is re-deposition from the ion beam. (2000x magnification)

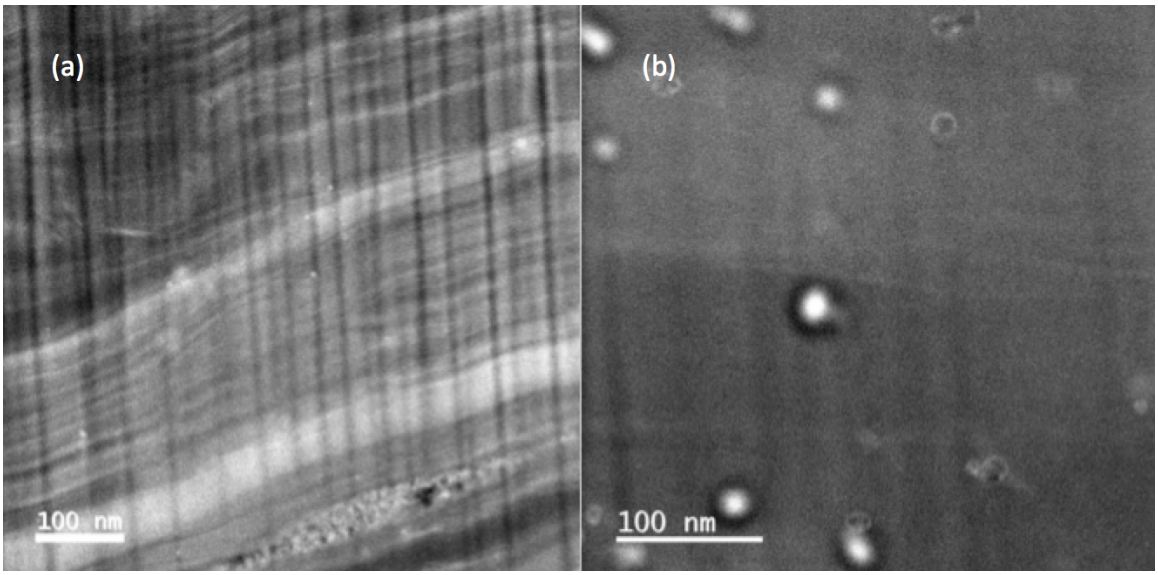

Fig. A.3- STEM in ADF mode: (a) higher magnification (30kx) image of crevices present throughout film. (b) higher magnification (50kx) image of copper oxide particles present throughout film.

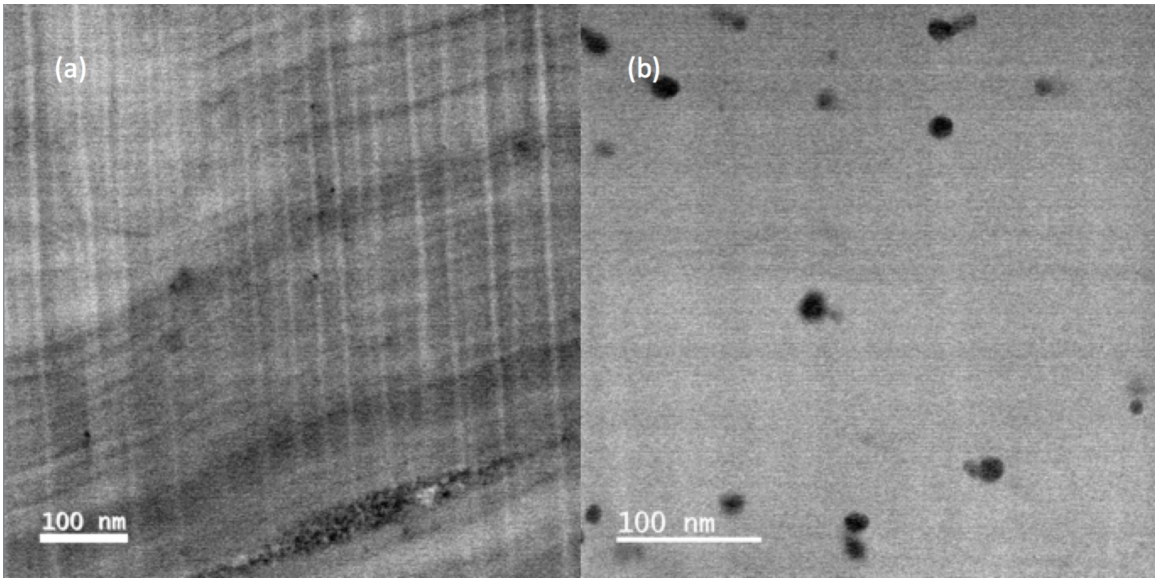

Fig. A.4- STEM in BF mode: (a) higher magnification (30kx) image of crevices present throughout film. (b) higher magnification (50kx) image of copper oxide particles present throughout film.

Appendix B: Additional STEM Images of Reduced EC-GO/Cu(II) Film

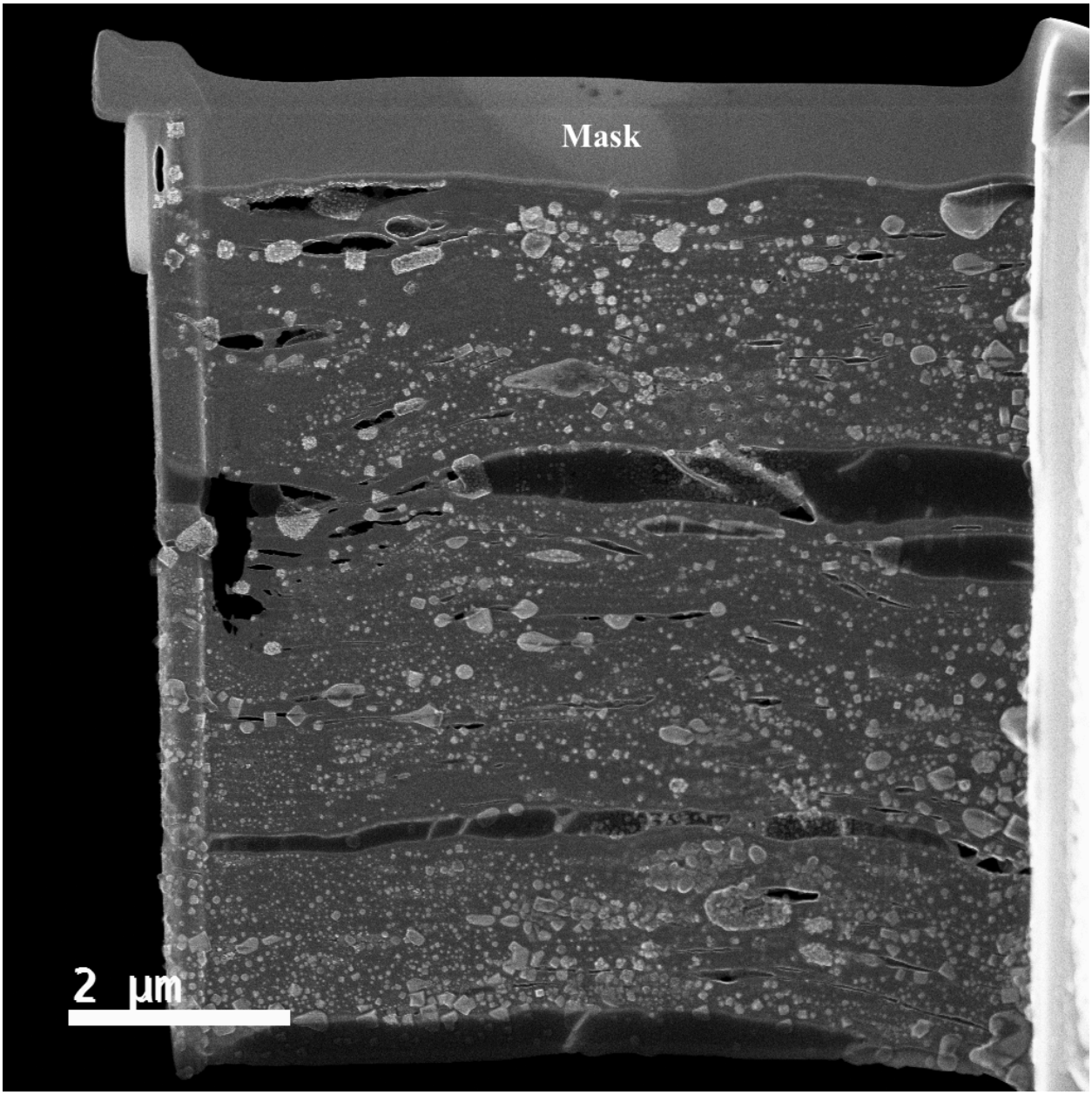

Fig. B.1- Cross-sectional STEM image of reduced EC GO/Cu(II) film under secondary electron (SE) mode. The surface of film in contact with the mask was GO surface in contact with the copper electrode before delamination. NaCl incorporation also shown. (2000x magnification)

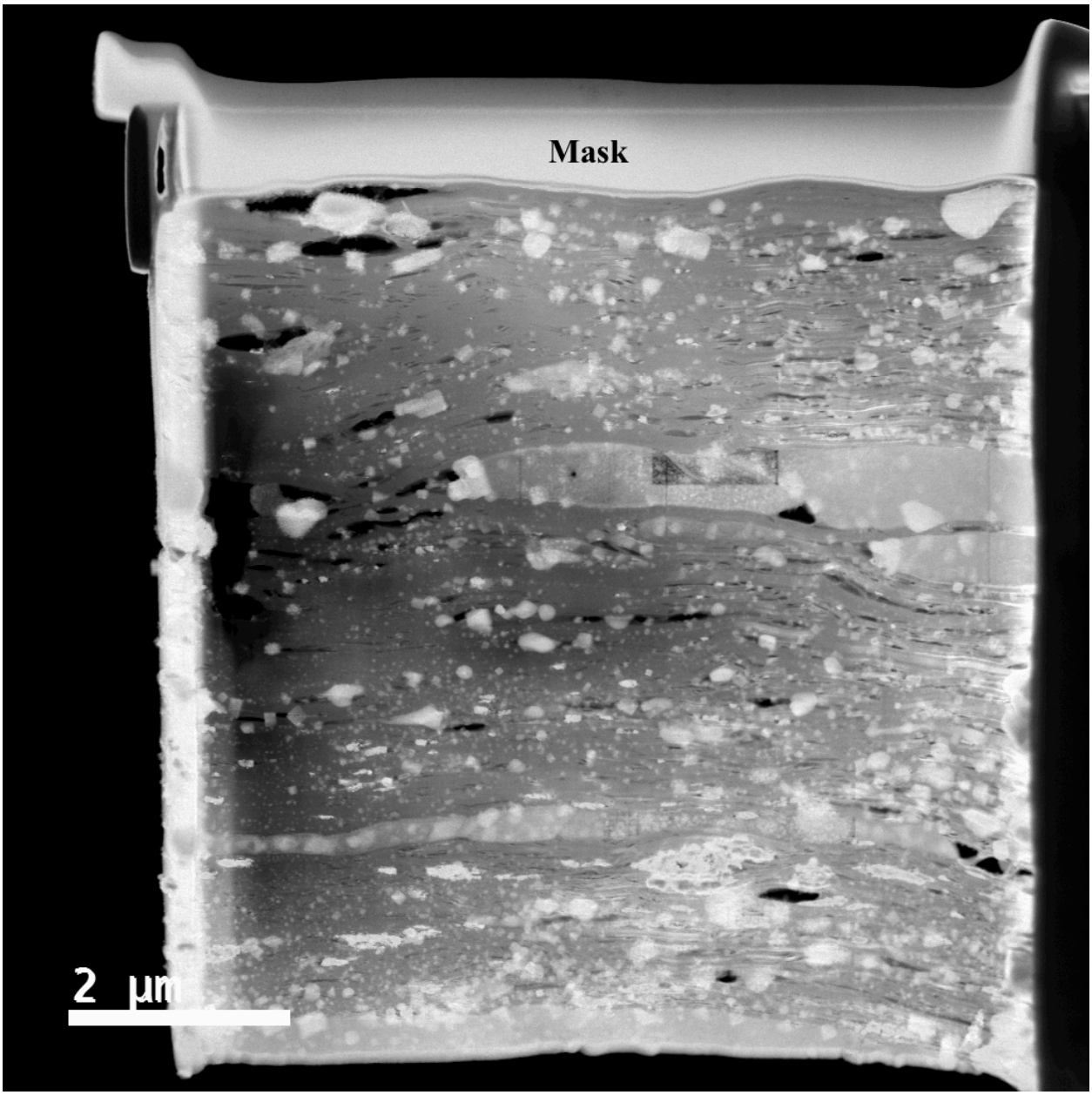

Fig. B.2- Cross-sectional STEM image of reduced EC GO/Cu(II) film under annular dark field (ADF) mode. The surface of film in contact with the mask was GO surface in contact with the copper electrode before delamination. NaCl incorporation also shown. (2000x magnification)

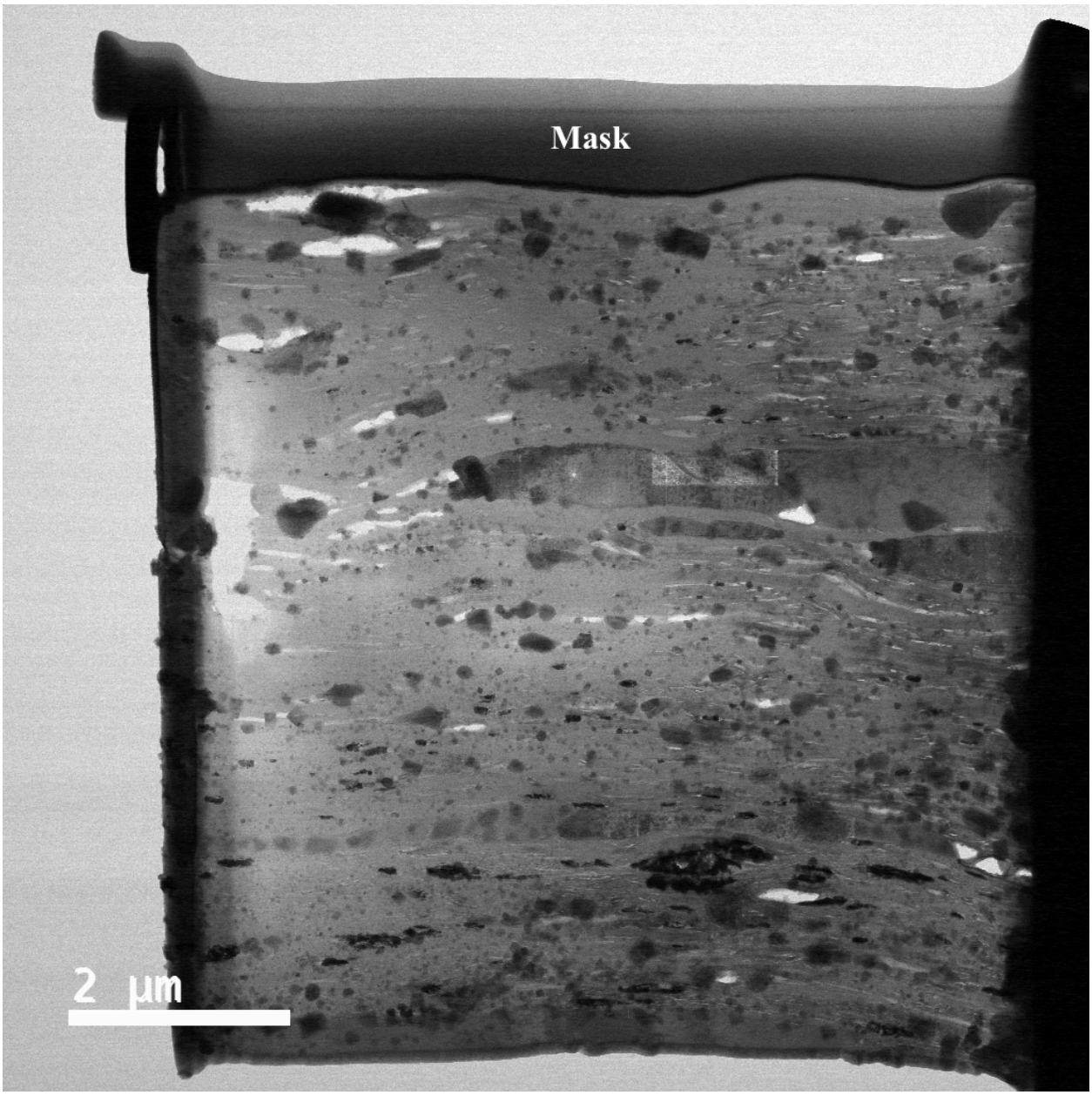

Fig. B.3- Cross-sectional STEM image of reduced EC GO/Cu(II) film under bright field (BF) mode. The surface of film in contact with the mask was GO surface in contact with the copper electrode before delamination. NaCl incorporation also shown. (2000x magnification)

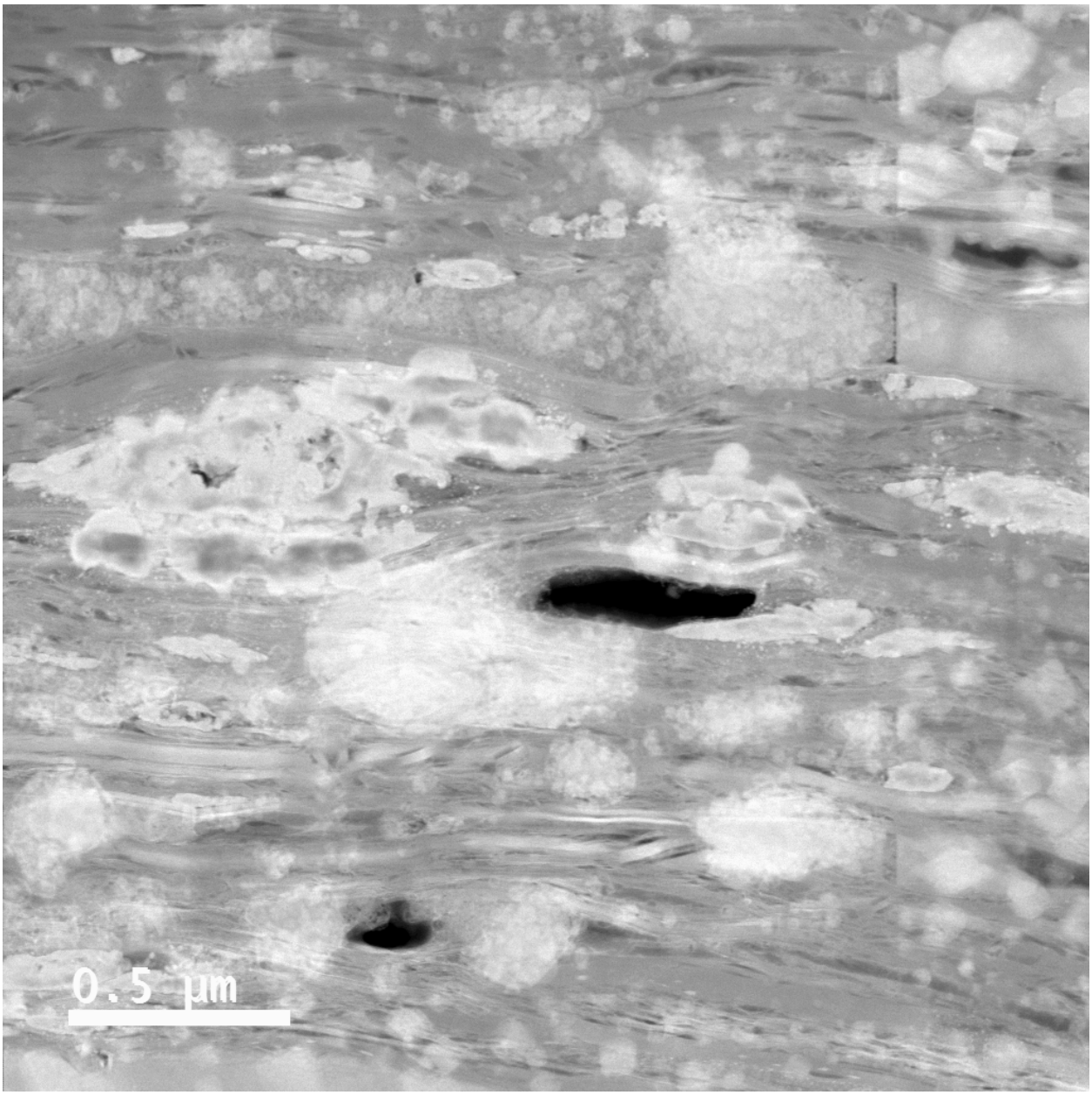

Fig. B.4- Higher magnification (8000x) STEM image in ADF mode of location on reduced EC GO/Cu(II) film where copper is present.

Fig. B.5- Higher magnification (8000x) STEM image in BF mode of location on reduced EC GO/Cu(II) film where copper is present.

References

1. Ping, J., Wang, Y., Fan, K., Wu, J. & Ying, Y. Direct electrochemical reduction of graphene oxide on ionic liquid doped screen-printed electrode and its electrochemical biosensing application. *Biosens. Bioelectron.* **28,** 204–209 (2011).
2. Chen, J., Yao, B., Li, C. & Shi, G. An improved Hummers method for eco-friendly synthesis of graphene oxide. *Carbon N. Y.* **64,** 225–229 (2013).
3. Dreyer, D. R., Park, S., Bielawski, C. W. & Ruoff, R. S. Graphite oxide. *Chem. Soc. Rev.* **39,** 228–240 (2010).
4. Bhuyan, M. S. A., Uddin, M. N., Islam, M. M., Bipasha, F. A. & Hossain, S. S. Synthesis of graphene. *Int. Nano Lett.* **6,** 65–83 (2016).
5. Murray, I. P. *et al.* Graphene oxide interlayers for robust, high-efficiency organic photovoltaics. *J. Phys. Chem. Lett.* **2,** 3006–3012 (2011).
6. Chen, Y., Zhang, X., Zhang, D., Yu, P. & Ma, Y. High performance supercapacitors based on reduced graphene oxide in aqueous and ionic liquid electrolytes. *Carbon N. Y.* **49,** 573–580 (2011).
7. Shahil, K. M. F. & Balandin, A. A. Graphene-multilayer graphene nanocomposites as highly efficient thermal interface materials. *Nano Lett.* **12,** 861–867 (2012).
8. Novoselov, K. S. *et al.* Electric field effect in atomically thin carbon films. *Science* **306,** 666–9 (2004).
9. Li, X. *et al.* Large-area synthesis of high-quality and uniform graphene films on copper foils. *Science (80-.).* **324,** 1312–1314 (2009).
10. de Heer, W. A. *et al.* Epitaxial graphene. *Solid State Commun.* **143,** 92–100 (2007).
11. Park, S. *et al.* Hydrazine-reduction of graphite- and graphene oxide. *Carbon N. Y.* **49,** 3019–3023 (2011).
12. Pei, S. & Cheng, H. M. The reduction of graphene oxide. *Carbon N. Y.* **50,** 3210–3228 (2012).
13. Stankovich, S. *et al.* Synthesis of graphene-based nanosheets via chemical reduction of exfoliated graphite oxide. *Carbon N. Y.* **45,** 1558–1565 (2007).
14. Toh, S. Y., Loh, K. S., Kamarudin, S. K. & Daud, W. R. W. Graphene production via electrochemical reduction of graphene oxide: Synthesis and characterisation. *Chemical Engineering Journal* **251,** 422–434 (2014).
15. Zhang, J. *et al.* Reduction of graphene oxide via L-ascorbic acid. *Chem. Commun. (Camb).* **46,** 1112–4 (2010).
16. De Silva, K. K. H., Huang, H.-H., Joshi, R. K. & Yoshimura, M. Chemical reduction of graphene oxide using green reductants. *Carbon N. Y.* **119,** 190–199 (2017).
17. He, W. *et al.* Electrophoretic deposition of graphene oxide as a corrosion inhibitor for sintered NdFeB. *Appl. Surf. Sci.* **279,** 416–423 (2013).

18. Yeh, C.-N., Raidongia, K., Shao, J., Yang, Q.-H. & Huang, J. On the origin of the stability of graphene oxide membranes in water. *Nat. Chem.* **7,** 166–70 (2014).

19. Sitko, R. *et al.* Adsorption of divalent metal ions from aqueous solutions using graphene oxide. *Dalt. Trans.* **42,** 5682 (2013).

20. Sitko, R., Zawisza, B. & Malicka, E. Graphene as a new sorbent in analytical chemistry. *TrAC - Trends Anal. Chem.* **51,** 33–43 (2013).

21. Yang, S. T. *et al.* Folding/aggregation of graphene oxide and its application in Cu2+removal. *J. Colloid Interface Sci.* **351,** 122–127 (2010).

22. Wu, W. *et al.* Highly Efficient Removal of Cu(II) from Aqueous Solution by Using Graphene Oxide. *Water, Air, Soil Pollut.* **224,** 1372 (2013).

23. Deng, X., Lü, L., Li, H. & Luo, F. The adsorption properties of Pb(II) and Cd(II) on functionalized graphene prepared by electrolysis method. *J. Hazard. Mater.* **183,** 923–930 (2010).

24. Dreyer, D. R., Todd, A. D. & Bielawski, C. W. Harnessing the chemistry of graphene oxide. *Chem. Soc. Rev.* **43,** 5288 (2014).

25. Gao, W. The chemistry of graphene oxide. *Graphene Oxide Reduct. Recipes, Spectrosc. Appl.* 61–95 (2015). doi:10.1007/978-3-319-15500-5_3

26. Singh, R. K., Kumar, R. & Singh, D. P. Graphene oxide: strategies for synthesis, reduction and frontier applications. *RSC Adv.* **6,** 64993–65011 (2016).

27. Chua, C. K. & Pumera, M. Chemical reduction of graphene oxide: a synthetic chemistry viewpoint. *Chem. Soc. Rev.* **43,** 291–312 (2014).

28. Zhang, Y. *et al.* Direct imprinting of microcircuits on graphene oxides film by femtosecond laser reduction. *Nano Today* **5,** 15–20 (2010).

29. Ramesha, G. K. & Sampath, S. Electrochemical Reduction of Oriented Graphene Oxide Films: An in Situ Raman Spectroelectrochemical Study. *J. Phys. Chem. C* **113,** 7985–7989 (2009).

30. Wang, D., Yan, W., Vijapur, S. H. & Botte, G. G. Electrochemically reduced graphene oxide-nickel nanocomposites for urea electrolysis. *Electrochim. Acta* **89,** 732–736 (2013).

31. Weisbart, C., Raghavan, S., Muralidharan, K. & Potter, B. G. Electrocoagulation driven fabrication of graphene oxide films. *Carbon N. Y.* **116,** (2017).

32. Chung, D. D. L. Review: Graphite. *Journal of Materials Science* **37,** 1475–1489 (2002).

33. Li, F., Jiang, X., Zhao, J. & Zhang, S. Graphene oxide: A promising nanomaterial for energy and environmental applications. *Nano Energy* **16,** 488–515 (2015).

34. Eng, A. Y. S. *et al.* Unusual inherent electrochemistry of graphene oxides prepared using permanganate oxidants. *Chem. - A Eur. J.* **19,** 12673–12683 (2013).

35. Chen, D., Feng, H. & Li, J. Graphene oxide: Preparation, functionalization, and electrochemical applications. *Chemical Reviews* **112,** 6027–6053 (2012).

36. Zhu, Y. *et al.* Graphene and graphene oxide: Synthesis, properties, and applications. *Adv. Mater.* **22,** 3906–3924 (2010).

37. Hummers, W. S. & Offeman, R. E. Preparation of Graphitic Oxide. *J. Am. Chem. Soc.* **80,** 1339 (1958).

38. Zaaba, N. I. *et al.* Synthesis of Graphene Oxide using Modified Hummers Method: Solvent Influence. *Procedia Eng.* **184,** 469–477 (2017).

39. Chen, J., Li, Y., Huang, L., Li, C. & Shi, G. High-yield preparation of graphene oxide from small graphite flakes via an improved Hummers method with a simple purification process. *Carbon N. Y.* **81,** 826–834 (2015).

40. Alam, S. N., Sharma, N. & Kumar, L. Synthesis of Graphene Oxide (GO) by Modified Hummers Method and Its Thermal Reduction to Obtain Reduced Graphene Oxide (rGO)*. *Graphene* **6,** 1–18 (2017).

41. Yu, H., Zhang, B., Bulin, C., Li, R. & Xing, R. High-efficient Synthesis of Graphene Oxide Based on Improved Hummers Method. *Sci. Rep.* **6,** 1–7 (2016).

42. Cote, L. J., Cruz-Silva, R. & Huang, J. Flash reduction and patterning of graphite oxide and its polymer composite. *J. Am. Chem. Soc.* **131,** 11027–11032 (2009).

43. Kauppila, J., Kunnas, P., Damlin, P., Viinikanoja, A. & Kvarnström, C. Electrochemical reduction of graphene oxide films in aqueous and organic solutions. *Electrochim. Acta* **89,** 84–89 (2013).

44. Deng, K.-Q., Zhou, J. & Li, X.-F. Direct electrochemical reduction of graphene oxide and its application to determination of L-tryptophan and L-tyrosine. *Colloids Surf. B. Biointerfaces* **101,** 183–8 (2013).

45. Wang, Z., Zhou, X., Zhang, J., Boey, F. & Zhang, H. Direct Electrochemical Reduction of Single-Layer Graphene Oxide and Subsequent Functionalization with Glucose Oxidase. *J. Phys. Chem. C* **113,** 14071–14075 (2009).

46. Zhou, M. *et al.* Controlled synthesis of large-area and patterned electrochemically reduced graphene oxide films. *Chem. - A Eur. J.* **15,** 6116–6120 (2009).

47. Nicholson, R. S. Theory and Application of Cyclic Voltammetry f m Measurement of Electrode Reaction Kinetics. *Anal. Chem.* **37,** 1351–1355 (1965).

48. Kirby, B. J. & Hasselbrink, E. F. Zeta potential of microfluidic substrates: 1. Theory, experimental techniques, and effects on separations. *Electrophoresis* **25,** 187–202 (2004).

49. Moussa, D. T., El-Naas, M. H., Nasser, M. & Al-Marri, M. J. A comprehensive review of electrocoagulation for water treatment: Potentials and challenges. *Journal of Environmental Management* **186,** 24–41 (2017).

50. Hunter, R. J. *Zeta potential in colloid science: principles and applications*. *Colloid science CN - QD549 .H95 1981* (1981). doi:http://dx.doi.org/10.1016/B978-0-12-361961-7.50004-3

51. Freire, J. M. *et al.* Using zeta-potential measurements to quantify peptide partition to lipid membranes. *Eur. Biophys. J.* **40,** 481–487 (2011).

52. Hermansson, M. The DLVO theory in microbial adhesion. *Colloids and Surfaces B: Biointerfaces* **14,** 105–119 (1999).

53. Mollah, M. Y., Schennach, R., Parga, J. R. & Cocke, D. L. Electrocoagulation (EC)--

Science and Applications. *J. Hazard. Mater.* **84,** 29–41 (2001).

54. Mollah, M. Y. A. *et al.* Fundamentals, present and future perspectives of electrocoagulation. *J. Hazard. Mater.* **114,** 199–210 (2004).

55. Hakizimana, J. N. *et al.* Electrocoagulation process in water treatment: A review of electrocoagulation modeling approaches. *Desalination* **404,** 1–21 (2017).

56. Rizzo, L. in *The Role of Colloidal Systems in Environmental Protection* 219–238 (2014). doi:10.1016/B978-0-444-63283-8.00009-0

57. Vincent, B. Early (pre-DLVO) studies of particle aggregation. *Advances in Colloid and Interface Science* **170,** 56–67 (2012).

58. Oncsik, T., Trefalt, G., Csendes, Z., Szilagyi, I. & Borkovec, M. Aggregation of negatively charged colloidal particles in the presence of multivalent cations. *Langmuir* **30,** 733–741 (2014).

59. Wang, L. *et al.* Layered assembly of graphene oxide and Co–Al layered double hydroxide nanosheets as electrode materials for supercapacitors. *Chem. Commun.* **47,** 3556 (2011).

60. Chavez-Valdez, A., Shaffer, M. S. P. & Boccaccini, A. R. Applications of graphene electrophoretic deposition. A review. *Journal of Physical Chemistry B* **117,** 1502–1515 (2013).

61. Xu, B. *et al.* What is the choice for supercapacitors: graphene or graphene oxide? *Energy Environ. Sci.* **4,** 2826 (2011).

62. Li, P. *et al.* Tunable Lyotropic Photonic Liquid Crystal Based on Graphene Oxide. *ACS Photonics* **1,** 79–86 (2014).

63. Kang, D. *et al.* Oxidation resistance of iron and copper foils coated with reduced graphene oxide multilayers. *ACS Nano* **6,** 7763–7769 (2012).

64. Park, J. H. & Park, J. M. Electrophoretic deposition of graphene oxide on mild carbon steel for anti-corrosion application. *Surf. Coatings Technol.* **254,** 167–174 (2014).

65. Meunier, N. *et al.* Comparison between electrocoagulation and chemical precipitation for metals removal from acidic soil leachate. *J. Hazard. Mater.* **137,** 581–590 (2006).

66. Akbal, F. & Camcidotless, S. Copper, chromium and nickel removal from metal plating wastewater by electrocoagulation. *Desalination* **269,** 214–222 (2011).

67. Belongia, B. M. Treatment of Alumina and Silica Chemical Mechanical Polishing Waste by Electrodecantation and Electrocoagulation. *J. Electrochem. Soc.* **146,** 4124 (1999).

68. Kin, K. T., Tang, H. S., Chan, S. F., Raghavan, S. & Martinez, S. Treatment of chemical-mechanical planarization wastes by electrocoagulation/electro-fenton method. *IEEE Trans. Semicond. Manuf.* **19,** 208–215 (2006).

69. Janković, A. *et al.* Graphene-based antibacterial composite coatings electrodeposited on titanium for biomedical applications. *Prog. Org. Coatings* **83,** 1–10 (2015).

70. Hasan, S. A. *et al.* Transferable graphene oxide films with tunable microstructures. *ACS Nano* **4,** 7367–7372 (2010).

71. An, S. J. *et al.* Thin film fabrication and simultaneous anodic reduction of deposited

graphene oxide platelets by electrophoretic deposition. *J. Phys. Chem. Lett.* **1,** 1259–1263 (2010).

72. Beverskog, B. Revised Pourbaix Diagrams for Copper at 25 to 300°C. *J. Electrochem. Soc.* **144,** 3476 (1997).

73. Hollander, J. M. & Jolly, W. L. X-Ray Photoelectron Spectroscopy. *Acc. Chem. Res.* **3,** 193–200 (1970).

74. Saha, N. C. & Tompkins, H. G. Titanium nitride oxidation chemistry: An x-ray photoelectron spectroscopy study. *J. Appl. Phys.* **72,** 3072–3079 (1992).

75. Bumbrah, G. S. & Sharma, R. M. Raman spectroscopy – Basic principle, instrumentation and selected applications for the characterization of drugs of abuse. *Egyptian Journal of Forensic Sciences* **6,** 209–215 (2016).

76. File:Ramanscattering.svg - Wikimedia Commons. Available at: https://commons.wikimedia.org/wiki/File:Ramanscattering.svg. (Accessed: 16th May 2018)

77. Callister, W. D. Materials science and engineering: An introduction (2nd edition). *Mater. Des.* **12,** 59 (1991).

78. File:Bragg diffraction 2.svg - Wikimedia Commons. Available at: https://commons.wikimedia.org/wiki/File:Bragg_diffraction_2.svg. (Accessed: 16th May 2018)

79. Instruments, M. Measuring Zeta Potential – Laser Doppler Electrophoresis. *Malvern Guid.* 1–2 (2015).

80. Goldburg, W. I. Dynamic light scattering. *Am. J. Phys.* **67,** 1152–1160 (1999).

81. Uzgiris, E. E. Laser Doppler methods in electrophoresis. *Prog. Surf. Sci.* **10,** 53–164 (1981).

82. Montaser, A. Inductively Coupled Plasma Mass Spectrometry. *Anal. Chem.* **82,** 4786–4810 (2010).

83. Zhou, W., Apkarian, R. P. & Wang, Z. L. Fundamentals of Scanning Electron Microscopy. *Scanning Microsc. Nanotechnol.* 1–40 (2007). doi:10.1007/978-0-387-39620-0_1

84. Zeng, C., Tang, Z., Guo, B. & Zhang, L. Supramolecular ionic liquid based on graphene oxide. *Phys. Chem. Chem. Phys.* **14,** 9838 (2012).

85. Johra, F. T., Lee, J. W. & Jung, W. G. Facile and safe graphene preparation on solution based platform. *J. Ind. Eng. Chem.* **20,** 2883–2887 (2014).

86. Cote, L. J. *et al.* Graphene oxide as surfactant sheets. *Pure Appl. Chem.* **83,** (2010).

87. Shen, X., Lin, X., Yousefi, N., Jia, J. & Kim, J. K. Wrinkling in graphene sheets and graphene oxide papers. *Carbon N. Y.* **66,** 84–92 (2014).

88. Swartzendruber, L. J. Four-point probe measurement of non-uniformities in semiconductor sheet resistivity. *Solid State Electron.* **7,** 413–422 (1964).

89. Giannuzzi, L. A. & Stevie, F. A. A review of focused ion beam milling techniques for

TEM specimen preparation. *Micron* **30,** 197–204 (1999).

90. Williams, D. B. & Carter, C. B. in *Transmission Electron Microscopy* 3–17 (1996). doi:10.1007/978-1-4757-2519-3_1

91. Nellist, P. D. in *Scanning Transmission Electron Microscopy* 91–115 (2011). doi:10.1007/978-1-4419-7200-2_2

92. Shindo, D. & Oikawa, T. in *Analytical Electron Microscopy for Materials Science* 81–102 (2002). doi:10.1007/978-4-431-66988-3_4

93. Fan, Z. *et al.* An environmentally friendly and efficient route for the reduction of graphene oxide by aluminum powder. *Carbon* **48,** 1686–1689 (2010).

94. Schniepp, H. C. *et al.* Functionalized single graphene sheets derived from splitting graphite oxide. *J. Phys. Chem. B* **110,** 8535–8539 (2006).

95. Fritz, J. J. Chloride complexes of copper(I) chloride in aqueous solution. *J. Phys. Chem.* **84,** 2241–2246 (1980).

96. Ahmad, R. T. M. *et al.* Guided Electro-Optical Switching of Small Graphene Oxide Particles by Larger Ones in Aqueous Dispersion. *Langmuir* **32,** 13458–13463 (2016).

97. Shojaeenezhad, S. S., Farbod, M. & Kazeminezhad, I. Effect of initial graphite particle size and shape on oxidation time in graphene oxide prepared by Hummers' method. *J. Sci. Adv. Mater. Devices* (2017). doi:10.1016/j.jsamd.2017.09.003

98. Neirinck, B., Van Der Biest, O. & Vleugels, J. A current opinion on electrophoretic deposition in pulsed and alternating fields. *Journal of Physical Chemistry B* **117,** 1516–1526 (2013).

99. Ozhukil Kollath, V. *et al.* AC vs. DC electrophoretic deposition of hydroxyapatite on titanium. *J. Eur. Ceram. Soc.* **33,** 2715–2721 (2013).

100. Chávez-Valdez, A. & Boccaccini, A. R. Innovations in electrophoretic deposition: Alternating current and pulsed direct current methods. *Electrochimica Acta* **65,** 70–89 (2012).

101. Raissi, B., Marzbanrad, E. & Gardeshzadeh, A. R. Particle size separation by alternating electrophoretic deposition. *J. Eur. Ceram. Soc.* **29,** 3289–3291 (2009).

102. Besra, L. & Liu, M. A review on fundamentals and applications of electrophoretic deposition (EPD). *Progress in Materials Science* **52,** 1–61 (2007).

103. Van der Biest, O. O. & Vandeperre, L. J. ELECTROPHORETIC DEPOSITION OF MATERIALS. *Annu. Rev. Mater. Sci.* **29,** 327–352 (1999).

104. Tamilmani, S., Huang, W., Raghavan, S. & Small, R. Potential-pH Diagrams of Interest to Chemical Mechanical Planarization of Copper. *J. Electrochem. Soc.* **149,** G638 (2002).